

2004

Effect of geometry on solder joint reliability of leadless leadframe package

Hsiu-hsin Chung
San Jose State University

Follow this and additional works at: https://scholarworks.sjsu.edu/etd_theses

Recommended Citation

Chung, Hsiu-hsin, "Effect of geometry on solder joint reliability of leadless leadframe package" (2004). *Master's Theses*. 2696.
DOI: <https://doi.org/10.31979/etd.hm3x-v3j2>
https://scholarworks.sjsu.edu/etd_theses/2696

This Thesis is brought to you for free and open access by the Master's Theses and Graduate Research at SJSU ScholarWorks. It has been accepted for inclusion in Master's Theses by an authorized administrator of SJSU ScholarWorks. For more information, please contact scholarworks@sjsu.edu.

NOTE TO USERS

This reproduction is the best copy available.

UMI[®]

**EFFECT OF GEOMETRY ON SOLDER JOINT RELIABILITY
OF LEADLESS LEADFRAME PACKAGE**

A Thesis

Presented to

The Faculty of the Department of Materials Engineering

San Jose State University

In Partial Fulfillment

of the Requirements for the Degree

Master of Science

by

Hsiu-hsin Chung

December 2004

UMI Number: 1425498

INFORMATION TO USERS

The quality of this reproduction is dependent upon the quality of the copy submitted. Broken or indistinct print, colored or poor quality illustrations and photographs, print bleed-through, substandard margins, and improper alignment can adversely affect reproduction.

In the unlikely event that the author did not send a complete manuscript and there are missing pages, these will be noted. Also, if unauthorized copyright material had to be removed, a note will indicate the deletion.

UMI[®]

UMI Microform 1425498

Copyright 2005 by ProQuest Information and Learning Company.

All rights reserved. This microform edition is protected against unauthorized copying under Title 17, United States Code.

ProQuest Information and Learning Company
300 North Zeeb Road
P.O. Box 1346
Ann Arbor, MI 48106-1346

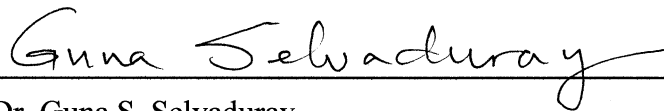
© 2004

Hsiu-hsin Chung

ALL RIGHTS RESERVED

APPROVED FOR

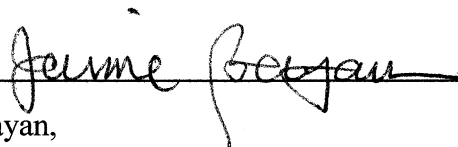
THE DEPARTMENT OF MATERIALS ENGINEERING



Dr. Guna S. Selvaduray,
Department of Chemical and Materials Engineering

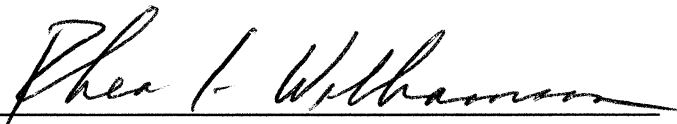


Dr. Fred Barez,
Department of Mechanical Engineering



Mr. Jaime Bayan,
National Semiconductor Corporation

APPROVED FOR THE UNIVERSITY



ABSTRACT

EFFECT OF GEOMETRY ON SOLDER JOINT RELIABILITY OF LEADLESS LEADFRAME PACKAGE

By Hsiu-hsin Chung

The objective of this investigation was to determine and understand the relationship between solder joint reliability and geometry factors of the solder joints since the geometry factors can directly affect the design rules of packaging. A Leadless Leadframe Package (LLP) was used in this investigation.

Two different land sizes and three different Die Attach Pad (DAP) sizes, which resulted in 6 solder joint configurations, were tested. The solder joint shear forces were measured after surface mount process and the solder joint resistance were monitored at 100 cycle intervals during temperature cycling for a total of 6 designs. The predominant failure mode during shear was shearing through the solder joint. Voids were mainly caused by flux entrapment. LLPs with DAP soldered down performed better than those without the DAP soldered down. LLPs with larger land area were better than those with small land area.

ACKNOWLEDGEMENTS

The author wishes to thank her thesis advisor, Dr. Guna Selvaduray, Professor, Department of Chemical and Materials Engineering, San Jose State University, for his guidance, encouragement, and perseverance in seeing this project to its completion.

Thanks are also due to Dr. Fred Barez, Professor, Department of Mechanical Engineering, San Jose State University, for his valuable advice and for being the author's thesis committee chair.

The author is grateful to Mr. Jaime Bayan, Senior Engineer, National Semiconductor Package Technology Group, for his technical guidance and editorial comments during the writing of this thesis. A special thank you is due to Mr. Steve Lee, Engineering Manager of National Semiconductor Package Technology Group, for his support and help with the experimental equipment. The author is also indebted to National Semiconductor Package Technology Group, which sponsored this project.

The author wishes to specially thank her wonderful parents, Qun-yu Chung and Zih-ying Pan Chung, her sister, Yuch-tsen Juliette Chung, and her husband and best friend, Yusuf Yildiz, for their encouragement and support through the entire process.

TABLE OF CONTENTS

	Page
ABSTRACT	iv
ACKNOWLEDGEMENTS	v
LIST OF FIGURES	x
LIST OF TABLES	xiv
CHAPTER 1. INTRODUCTION	1
1.1 What Is A Microelectronic Package?	1
1.2 Chip Scale Packages	4
1.3 Leadless Leadframe Package (LLP)	5
1.3.1 Advantages of LLP	6
1.3.2 Limitations and Problems of LLP	7
1.4 Potential Reliability Issues Related to LLP	8
1.5 Solder Joint Reliability	9
1.5.1 Significance of Solder Joint Reliability	9
1.5.2 Factors That Affect Solder Joint Reliability	9
CHAPTER 2. LITERATURE REVIEW	11
2.1 Effect of Solder Joint Geometry	11
2.1.1 Solder Joint Profile	12
2.1.2 Solder Joint Thickness	13
2.1.3 Ds/Dp Ratio	14
2.2 Effect of PCB Solder Pad Composition	17

2.3	Effect of Reflow Process	19
2.3.1	Reflow Environment (IR-reflow)	19
2.3.2	Reflow Profile	20
2.4	Voiding Initiation Mechanism in Surface Mount Process	21
2.4.1	Flux Entrapment	21
2.4.1.1	Materials	21
2.4.1.2	Reflow Environment	28
2.4.1.3	Geometry Factor	30
2.4.2	Dissolved Gas in Raw Material	31
2.4.3	Solidification Shrinkage	33
2.5	Summary of Literature Review	33
	CHAPTER 3. EXPERIMENTAL OBJECTIVE AND APPROACH	35
3.1	Experimental Objective	35
3.2	Experimental Parameters and Level Determination	36
3.3	Design of Experiment	38
3.4	Experiment Flow	38
3.4.1	Leadframe Design	40
3.4.2	PCB Design – Parts Distribution for Surface Mount	41
3.4.3	Parts Assembly	45
3.4.4	Surface Mount	46
3.4.4.1	Solder Paste	46
3.4.4.2	Stencil	46

3.4.4.3	IR-reflow Profile	47
3.4.4.4	Flow Chart of Surface Mount	48
3.4.5	Inspection	48
3.4.5.1	Solder Joint Thickness Measurement	49
3.4.5.2	X-ray Examination	49
3.4.6	Test Method	50
3.4.6.1	Shear Test	50
3.4.6.2	Temperature Cycle Test	53
3.4.7	Data Analysis	55
3.4.7.1	Weibull Distribution	55
3.4.7.2	One-way Analysis of Variance (One-way ANOVA)	57
3.4.8	Failure Analysis	58
3.5	Number of Parts and PCBs Needed for Experiment	58
CHAPTER 4. RESULT AND DISCUSSION		60
4.1	Solder Joint Thickness	60
4.2	Shear Test	60
4.3	Temperature Cycling Test	65
CHAPTER 5. CONCLUSION		83
CHAPTER 6. FUTURE WORK		84
REFERENCES		85
APPENDIX A. Moisture Sensitivity Levels		87
APPENDIX B. Solder Joint Thickness Measurement and Statistical Values		88

APPENDIX C. Shear Force Measurement and Shear Strength Determinations	89
APPENDIX C-1. Records of Shear Force Measurement for Designs A to F	90
APPENDIX C-2. Shear Strength Determinations	91
APPENDIX C-3. Nominal Solder Joint Area for Designs A to F	92
APPENDIX C-4. Shear Strengths Converted from Shear Forces for Designs A to F	93
APPENDIX D. Failure Modes for Design A to F	94
APPENDIX E. Shear Strength Data and ANOVA	95
APPENDIX E-1. Shear Strength Data for Designs A to F	96
APPENDIX E-2. ANOVA – Single Factor for Shear Strength Data	97
APPENDIX F. Loop Resistance of PCB # 5 ~ # 8 from 0 cycle to 3003 cycles	98
APPENDIX G. Calculation of Weibull Distribution	122

LIST OF FIGURES

	Page
Figure 1. Schematic diagram showing an encapsulated conventional SOP package	2
Figure 2. Different types of microelectronic packages	3
Figure 3. Top view and bottom view of LLP	5
Figure 4. Cross section of LLP	6
Figure 5. Schematic drawing of solder joint between LLP and PCB	8
Figure 6. Schematic drawing of D_s and D_p	11
Figure 7. Fatigue life of different solder joint profile	12
Figure 8. Schematic drawing of D_s/D_p ratio	14
Figure 9. Shear strength and the height of solder joint as a function of D_s/D_p	15
Figure 10. Thermal fatigue test results of PBGA assemblies	16
Figure 11. Weibull plot for Cu-Ni-Au at 80% & 95% statistical confidence interval (20 °C)	17
Figure 12. Comparison of Weibull plots for samples A (Cu-Ni-Sn pads) and B (Cu-Ni-Au pads)	18
Figure 13. Comparison of Weibull plots for samples B (Cu-Ni-Au pads) and C (SMOBC pads)	19
Figure 14. Schematic drawing of IR-reflow profile	20
Figure 15. Relationship between activator content and flux activity (wetting time)	22
Figure 16. Relationship between flux activity and void content – line A	23
Figure 17. Relationship between flux activity and voiding in BGA joints	24
Figure 18. Effect of solvent boiling point on the voiding of BGA joints using solder pastes or fluxes only	24

	Page
Figure 19. Effect of Sn63 (-325/+500 mesh) metal content on voiding of BGA joints	27
Figure 20. Relationship between powder size and voiding of BGA joints	28
Figure 21. Effect of reflow temperature on the voiding of BGA joints soldered with A3-B1-M3-90 solder paste under air atmosphere	29
Figure 22. Relation between flux activity voiding in BGA joints	30
Figure 23. Effect of paste coverage area on voiding of paste B-3-90	31
Figure 24. Land and DAP of a 12L LLP	36
Figure 25. Investigation flow chart	39
Figure 26. Sample drawing of leadframe design (Large land area)	40
Figure 27. Parts distribution on testing PCB	41
Figure 28. Top layer of PCB (Top view)	43
Figure 29. Bottom layer of PCB (Top view)	44
Figure 30. Schematic daisy chain wire bonding diagram for 44L LLP	45
Figure 31. IR-reflow profile for the soldering process	47
Figure 32. Flow char of surface mount process	48
Figure 33. X-ray photograph of a LLP of design F	50
Figure 34. Instron Universal Test Instrument Model 1122	51
Figure 35. Schematic drawing of relationships between shear head, shear direction, specimen, and fixture	51
Figure 36. Schematic drawing of the solder joint geometry of design A to F	52
Figure 37. Failure modes of shear test	53
Figure 38. Schematic drawing of temperature cycle profile	54

	Page
Figure 39. Probability density function $f(t)$	56
Figure 40. Cumulative distribution function $F(t)$	56
Figure 41. Cracks at the interface between Cu-pad and solder	58
Figure 42. Sheared surface of solder joints of a 44L LLP	61
Figure 43. Sheared surfaces of solder joints on PCB and package sides	61
Figure 44. Unknown liquid inside the void of solder joint at DAP area	64
Figure 45. Tacky material inside the void of solder joint at DAP area for a four-month-old unit	65
Figure 46. Indication of first failed pins for Board # 5	68
Figure 47. Indication of first failed pins for Board # 6	69
Figure 48. Indication of first failed pins for Board # 7	70
Figure 49. Indication of first failed pins for Board # 8	71
Figure 50. Indication of top and bottom rows of the pins	72
Figure 51. Schematic drawing of Scooping Effect	73
Figure 52. Weibull plots of the designs A to F	75
Figure 53. Indication of the cross-section pictures	76
Figure 54. Solder joints cross-section of design A	76
Figure 55. Solder joints cross-section of design B	77
Figure 56. Solder joints cross-section of design C	78
Figure 57. Solder joints cross-section of design D	79
Figure 58. Solder joints cross-section of design E	80
Figure 59. Solder joints cross-section of design F	80

Figure 60. Stress raisers of a LLP solder joint

81

LIST OF TABLES

	Page
Table 1. Effect of Predrying and Solvent Boiling Point on Voiding	25
Table 2. Correlation between Mesh Number and Particle Size	28
Table 3. Experimental Factors and Levels	37
Table 4. Factors Combination Table for Full Factorial DOE	38
Table 5. Number of Parts and PCBs Needed in Experiment	59
Table 6. Predominant Failure Mode of Designs A to F	62
Table 7. Number of Failure Cycles of Each Board and Each Unit	66
Table 8. Number of Failures Per Design at 3003 Cycles	67

CHAPTER 1

INTRODUCTION

A Leadless Leadframe Package (LLP) is a leadframe-type Chip Scale Package (CSP), which provides the advantage of being small, light-weight, and suitable for portable microelectronic packaging requirements. The convenience and protection of a traditional package combined with the small size, low weight, and high performance of a bare die are present in the CSP. Though the CSP has several distinct advantages, there are also limitations and reliability problems. A brief introduction to the LLP CSP and its advantages and limitations are presented in this chapter. In addition, the concerns of reliability as they pertain to solder joint are also discussed.

1.1 What Is A Microelectronic Package?

The major functions of a microelectronic package are power distribution, signal distribution, protection, and heat dissipation. A microelectronic package is a set of materials that provides the above functions to the integrated circuit (IC).

Leadframe/substrate selection, die bonding, wire bonding, and package encapsulation are the four main procedures in package assembly. A cross-section of a conventional small-outline-package (SOP) is shown in Figure 1. The leadframe provides the electrical interconnections and mechanical support to the IC chip. The die attach is an adhesive that provides adhesion between the leadframe and the chip, providing mechanical

continuity. The wires connect the chip and the leadframe electrically. The encapsulation provides protection from the environment and also mechanically supports the IC chip.

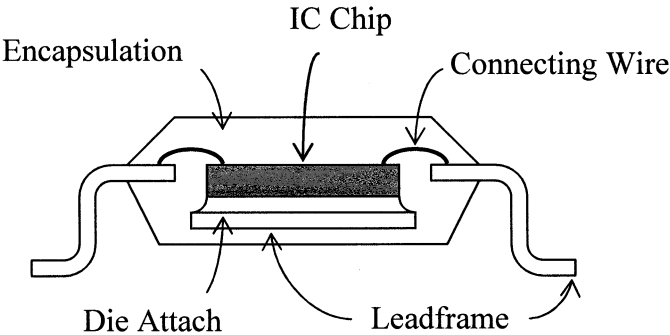


Figure 1. Schematic diagram showing an encapsulated conventional SOP package.

Because the bare chip is fragile, it is not easy to handle, test, rework or use on its own. An interconnection from the miniscule chip to the macroscopic world for power and signal distribution needs to be established. Microelectronic packages are constructed to meet these functions. Furthermore, because the circuit elements on a bare chip are much smaller than a whisker (0.18 micron to 1 micron), they are very susceptible to any damage and contamination on the chip's surface. Packages protect the IC chip from mechanical and environmental damage. When the IC chip is functioning, heat will be generated. If the device cannot dissipate its heat, failures can occur. For some thermally-enhanced package types, embedded heat spreaders or exposed heat slugs help the heat dissipate from the surface of the IC chip.

There are hundreds of package designs, including conventional and advanced types. Six types of packages are shown in Figure 2. The dual-in-line package (DIP), small outline package (SOP), and quad flat package (QFP) are conventional type of packages while the ball grid array (BGA), peripheral lead chip-scale package (Peripheral Lead CSP), and flip chip package (FCP) are advanced ones.

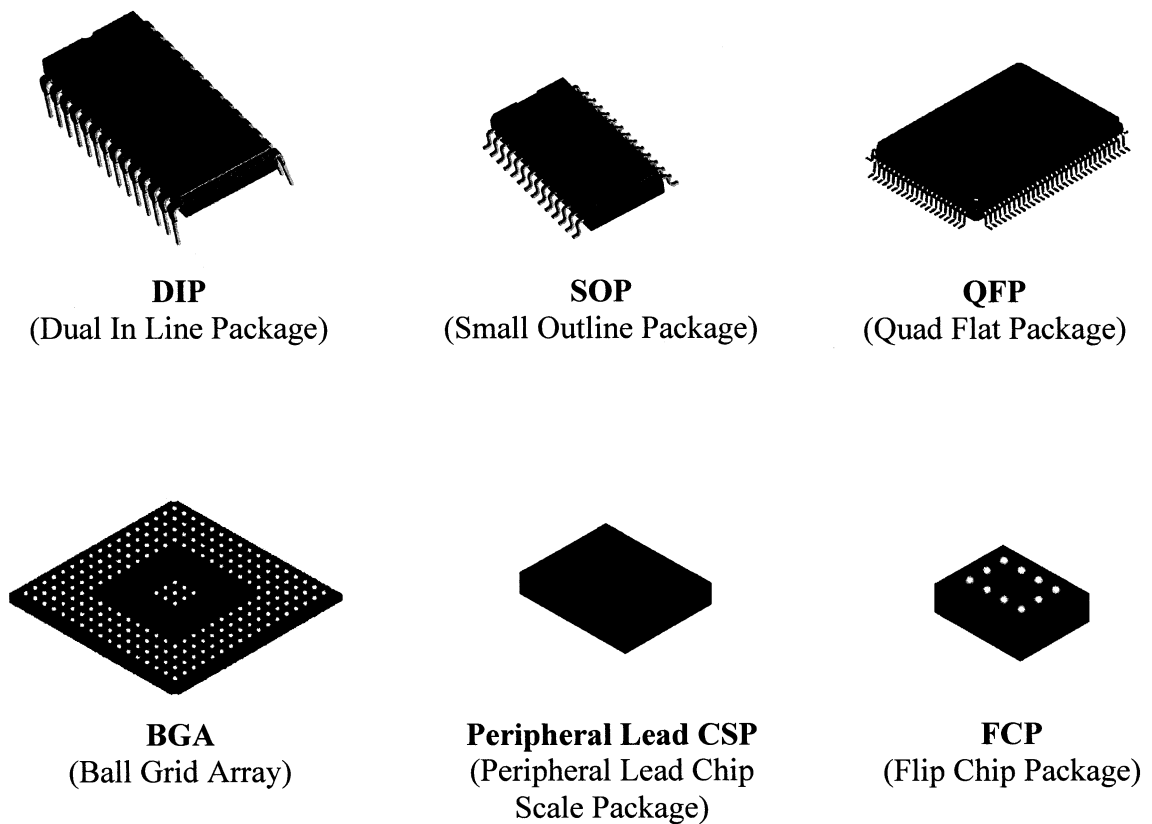


Figure 2. Different types of microelectronic packages.
(source: <http://ptg.nsc.com/cgi-in.mktlist>)

1.2 Chip Scale Packages

What is a chip-scale package (CSP)? According to the meaning of the words, the package size is very close to the chip size. By definition, the ratio of the chip area to the package area has to be greater than 0.8. In other words, the ratio of the package size to the chip area is smaller than 1.2 [1]. The driving force for developing CSPs was to meet the needs of portable products, with increased functionality and speed and smaller dimensions. We can divide CSPs into three categories: array CSPs, peripheral lead CSPs, and wafer level CSPs [2]. The significant advantages of CSPs over other package types are the reduction of area, volume, weight and system cost along with the improvement in electrical and thermal performance. Despite its advantages, CSPs do have limitations. CSPs assembled with laminated substrates (either array type or peripheral type) have poor resistance to moisture absorption. This is because the materials used in laminated substrates are polymeric materials that are prone to moisture absorption. The general moisture resistance ability for laminated CSPs is Moisture Level 3*. That means packages can still pass the test requirements after being soaked in a 30°C/60% RH moisture chamber for 192 hours. Another limitation is the lead count capability. 20 ~ 100 is the most common lead count range for peripheral lead CSPs. When the lead count exceeds 100, array CSPs or fine-pitch BGAs are preferred. In the case of wafer level CSPs, the limitation is that they are unforgiving of assembly errors. Because they are processed as a whole wafer instead of individual units, a single assembly error can affect

* Moisture Level 3: 30°C/60%RH, 192 hours. Description of the moisture sensitivity levels is provided in Appendix A.

a large number of units. There are many other types of CSPs. All of them have advantages and limitations. These need to be considered before deciding which type to use for a particular application.

1.3 Leadless Leadframe Package (LLP)

LLP is a custom leadframe type of CSP. The singulation process of the leadframe CSP is different from the trimming/forming process for traditional leadframe packages. For leadframe CSP isolation, an entire matrix of units are encased with mold compound and then singulated with a diamond impregnated saw blade. This process is similar to the die sawing process. Once cut, picking and placing is the last step in the LLP assembly flow. Schematic drawings of the final package and the cross section of the LLP are shown in Figures 3 and 4, respectively.

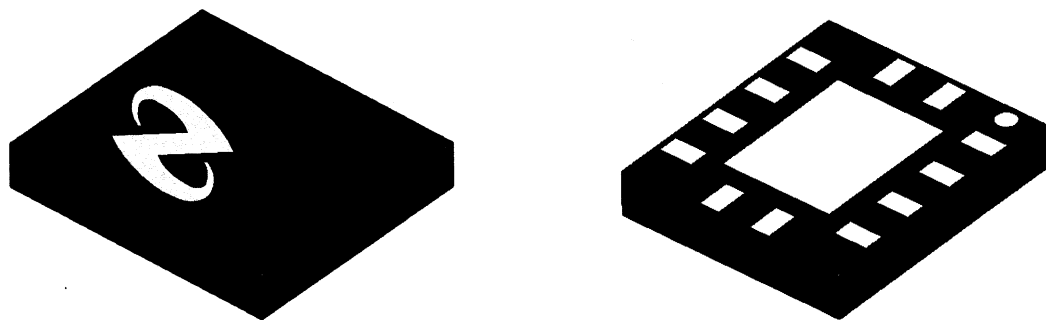


Figure 3. Top view and bottom view of LLP. (Source: presentation by National Semiconductor Corp., Feb. 7, 2000)

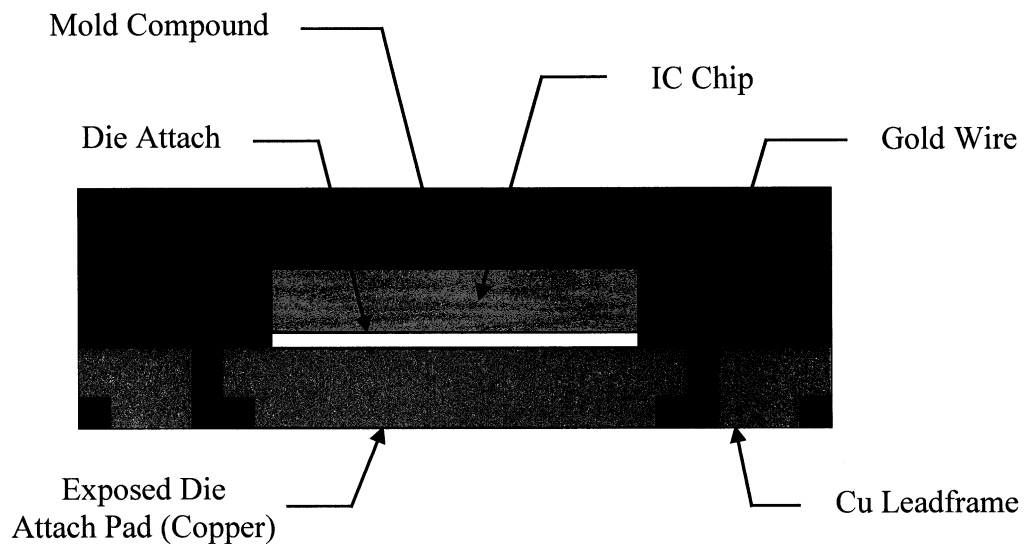


Figure 4. Cross section of LLP.

1.3.1 Advantages of LLP

What is the interest in LLPs? There are three distinct advantages of LLPs over other conventional leadframe packages or other CSPs. Better ability to dissipate heat is the primary advantage. As can be seen in Figure 4, the exposed die attach pad (DAP) of an LLP is the key to its thermal performance (heat dissipation). The exposed DAP acts like the heat slug of other advanced leadframe packages. Improved electrical performance is the second advantage of LLPs. Theoretically, electrical performance of an IC cannot be improved by any package. However, the electrical performance of the bare chip will degrade by any added routing, via traces, or connections. Since the LLPs have a relatively short path between the die and the system board, it can be expected to have inherently better electrical performance over other conventional packages. The

third advantage is that LLPs have been found to pass Moisture Level 1*. For most CSPs, Level 3 is the common rating for moisture sensitivity level. Moisture Sensitivity Level 1 indicates excellent resistance to moisture absorption. Moisture absorbed by the package can cause problems of corrosion, popcorning** and other malfunctions. In addition, LLPs provide a smaller footprint, a thinner package, and lower cost. A smaller footprint enables a higher component density on printed circuit boards (PCB). These advantages make LLPs attractive.

1.3.2 Limitations and Problems of LLP

LLPs belong to peripheral lead CSPs, and exhibit the same limitation of lead count capability. So far the range of lead count for LLPs is from 8 to 56 leads.

The first problem in developing LLPs was the singulation that involved cutting through the copper leadframe. Copper smears and burrs were observed after singulation. This problem has been solved by changing the design of the leadframe. The second problem encountered was manufacturing on large scale LLPs. The design of the leadframe becomes critical in the case of large scale LLPs due to the insufficient mechanical support provided by the leadframe. Since this package type is still relatively new, it was not yet ready for production at the time of this investigation (2000-2001). In addition, because of its construction, visual inspection of the part is not possible after it is mounted onto a PCB.

* Moisture Level 1: 85oC/85% RH, 168 hours. Detailed description of the moisture sensitivity levels is provided in Appendix A.

** Popcorning: the trapped moisture inside a plastic package will vaporize and expand during the IR reflow process. The expanded moisture causes encapsulation deformation, such as popping bumps and cracks.

1.4 Potential Reliability Issues Related to LLP

To make sure that LLPs can maintain their normal functions over the lifetime of the IC device, there are several potential reliability issues that need to be resolved, the solder joint being perhaps the biggest potential reliability problem. This is the subject of this investigation. The solder joint between the LLP and the PCB is shown in Figure 5.

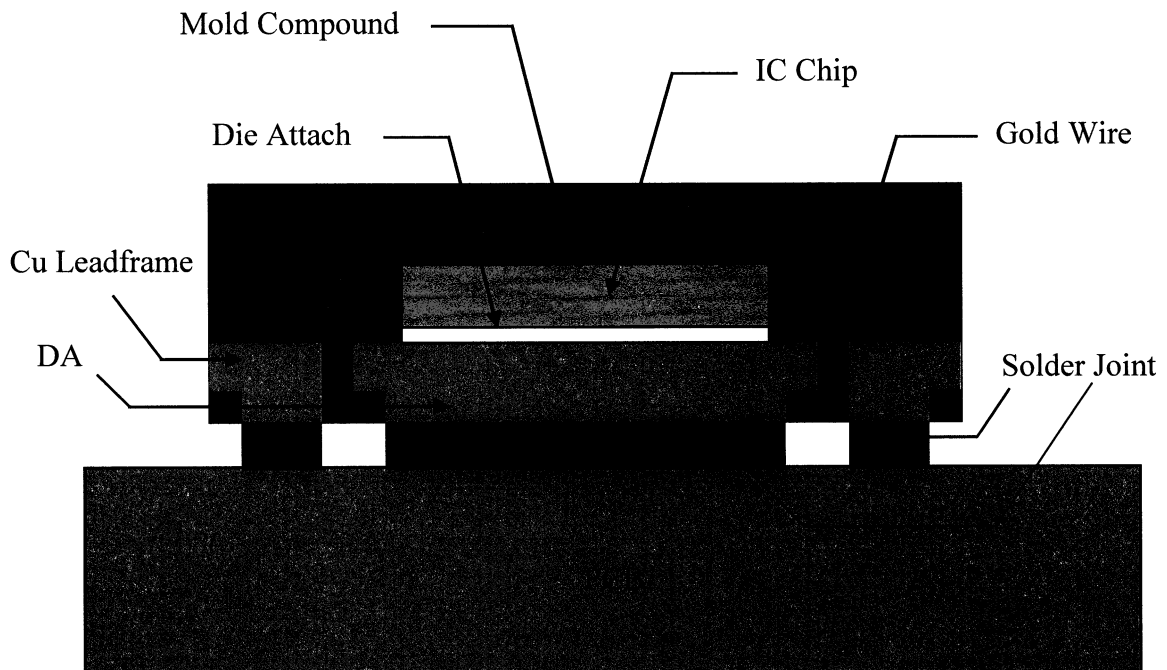


Figure 5. Schematic drawing of solder joint between LLP and PCB.

Moisture resistance was another potential reliability issue of LLPs. However, since LLPs have been shown to pass Moisture Level 1 [3], this is no longer an issue. The third potential reliability issue is leadframe corrosion because the lead finish is lead-tin plated.

This electroplated layer is anodic with respect to the lead base metal [4]. Leadframe corrosion may be initiated by any cracks or scratches in the presence of moisture and contamination. The fourth reliability concern with LLPs is electrostatic discharge (ESD^{*}) [5], which can occur during manufacturing, handling, or service. Since the circuit is so tiny, even the slightest discharge may damage the circuit. The last potential reliability issue is the manufacturing process itself. Since LLPs are still new to the assembly process, any improper stress applied during processing can cause reliability problems later. For example, improper force and power in the wire bonding process may cause the bond to lift after temperature cycling.

1.5 Solder Joint Reliability

1.5.1 Significance of Solder Joint Reliability

The purpose of the solder joint is to provide the electrical and mechanical interconnection between the microelectronic package and the PCB. Structural and electrical integrity needs to be maintained over the lifetime of the IC device. The general failure mechanisms of the solder joint are creep, fatigue, and fracture. A more detailed discussion of this topic is presented in Chapter 2.

1.5.2 Factors That Affect Solder Joint Reliability

Factors affecting solder joint reliability can be divided into four categories: design parameters, material properties, manufacturing process, and service conditions. At the

* ESD: the transfer of electrical charge between two bodies at different potentials, either through direct contact or through an induced electrical field.

design stage, solder joint reliability can be affected by thermal stresses due to coefficient of thermal expansion (CTE) mismatches between the component and the PCB. Failures can also occur due to accumulated fatigue damage. Besides the CTE mismatch, solder joint reliability can also be affected by solder joint geometry. The level of stress endurance may be improved by using a larger contact area or less sharp corners of the solder joints. The reliability performance of the solder joint can be improved by using a package design with a small CTE mismatch and the proper solder joint geometry. For material properties, the solder joint reliability is directly affected by the strength of the solder itself. Higher strength solders generally exhibit better solder joint reliability. For the manufacturing process, the solder joint reliability is affected by pre-assembly surface conditions and the IR reflow profile. These are important parameters for obtaining good solder joints. If there is any contamination on the contact area before soldering, the solder joint's reliability may be compromised. Further, if the IR reflow profile is not proper, such as wrong peak temperature, improper ramp up rate, and improper cooling rate, solder joints lacking in reliability may also be formed. Finally, the device or package lifetime can be affected by various operating environments, such as atmospheric composition, service temperature, and temperature cycling frequency.

In Chapter 2, the background of solder joint reliability and a general overview of the current understanding of the factors which affect the reliability are presented. In Chapter 3, the experimental objective and approach are described and explained. Chapter 4 contains the results of the research and discussions of the results. Chapter 5 is conclusions. In Chapter 6, suggestions for future work are presented.

CHAPTER 2

LITERATURE REVIEW

The intent of this literature search was to determine what has already been determined and/or defined with regards to solder joint integrity as it relates to LLP design. This will allow narrowing the field of research, focus the investigation, and develop a definitive and effective design of experiment. The literature search covered the following: (a) solder joint geometry (b) solder pad composition (c) reflow process.

2.1 Effect of Solder Joint Geometry

Solder joint geometry can affect the reliability performance of microelectronic packages. A literature review regarding to the solder joint profile, solder joint thickness, and D_s/D_p ratio are presented in this section. D_s refers to solder ball diameter while D_p refers to PCB solder pad diameter as shown in Figure 6.

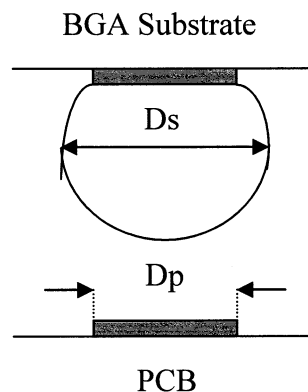


Figure 6. Schematic drawing of D_s and D_p .

2.1.1 Solder Joint Profile

The effect of the solder joint shape was addressed by John Lau in 1996 [6], who also summarized the results of solder joint reliability evaluations of Flip Chip Packages. 95wt%Pb/5%wtSn (high-Pb) solder bumps were used as electrical interconnections from the bare chip to the substrate. Thermal fatigue tests were performed to determine the reliability of the solder bumps. The range of temperature cycling was from -50°C to 150°C . Each cycle was 1 hour with a dwell time of 15 minutes. The results showed that hourglass-shaped bumps have a fatigue life that is 3 times longer than that for barrel-shaped ones. The shapes are shown in Figure 7. However, details of the sample size and failure criteria were not described in the publication. The reason cited for hourglass-shaped bumps exhibiting a longer fatigue life was that the maximum effective strain occurs near the neck area whereas the maximum effective strain for barrel-shaped bumps occurs near the silicon chip, where high stresses due to CTE mismatch occur.

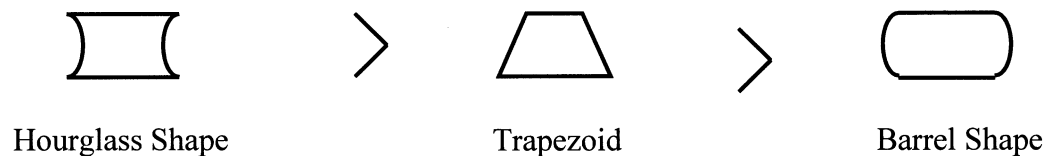


Figure 7. Fatigue life of different solder joint profile.

2.1.2 Solder Joint Thickness

The general procedures for the surface mount process are flux printing, solder paste printing, parts placing, and solder reflow. The solder paste is wet and will shrink after the reflow process. Even if the solder paste shrinks, thicker solder pastes can still result in a thicker solder joint. The relationship of solder paste thickness and thermal fatigue life was investigated by Krinke in his research in 1988 [7]. Eutectic solder paste (37wt%Pb/63wt%Sn) was used for the Leadless Chip Carrier (LCC) in this study. Just as in the solder joint profile study, thermal fatigue tests were employed to determine the reliability of solder joints. The range of temperature cycling was from -55°C to 100°C . Each cycle was 1.5 hours and the dwell time was 15 minutes. After assembly and thermal cycling, the solder joint shape and surface appearance were inspected using a 55X magnification optical microscope, followed by scanning electron microscope/energy dispersive X-ray (SEM/EDX) analysis to determine the effects of temperature cycling. The three stages of solder joint degradation were defined as stress mark, stress crack, and crack. The examinations were performed after 25, 50, 100, 150, 200, 250, and 300 cycles. Four thicknesses of solder pastes, namely, 16 mils, 14 mils, 12 mils and 10 mils, were tested in this study. After examining the stress mark, stress crack, and crack, 16 mil-thick solder paste was found to exhibit the longest fatigue life. The fatigue life decreased with decreasing solder paste thickness. Neither sample size nor profile of the solder joint was mentioned in the paper. The failure was determined only by visual inspection, which can result in large uncertainties. However, it can still be concluded that higher solder joint thickness provides better solder joint reliability.

2.1.3 Ds/Dp Ratio

The relationship between the Ds/Dp ratio and solder joint strength/reliability was investigated by Y.P. Wu et al for BGA packages [8]. Eutectic solder balls (37wt%Pb/63wt%Sn) were used in 169 pins and 255 pins BGAs. Two test methods were employed in this research: shear and thermal shock fatigue tests. The various Ds/Dp ratios, which were used in this experiment, are shown in Figure 8. Ds (solder ball diameter) was fixed at 0.76 mm. The Dp (solder pad diameter) values were 0.5 mm, 0.635 mm, 0.75 mm and 1.0 mm, resulting in Ds/Dp ratios of 1.32, 1.2, 1.02 and 0.76, respectively.

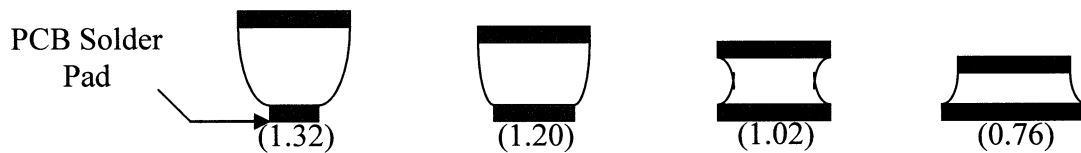


Figure 8. Schematic drawing of Ds/Dp ratio.

In the shear test, shear strength was obtained. For each Ds/Dp ratio, a total of 8 – 10 shear tests were performed and the average value was reported. The average standard deviation value for all readings was in the range of 20%. The data are shown in Figure 9. According to the results of the shear tests, when the Ds/Dp is equal to 1.2, the solder joints exhibit the highest shear strength.

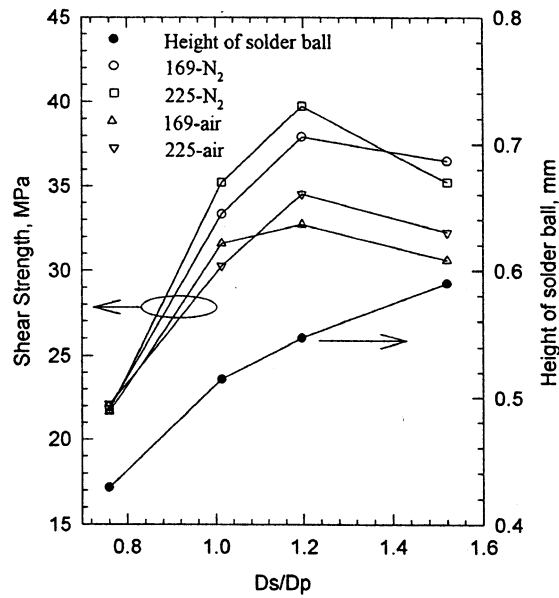


Figure 9. Shear strength and the height of solder joint as a function of D_s/D_p (Ref: [8]).

For thermal shock fatigue tests, the range of temperature cycling was from -35°C to 150°C and the dwell time was 15 minutes. To capture fatigue failure, the electrical resistance of the solder joint was monitored continuously by a computer. The sample size and failure criteria were not reported. The results of the thermal fatigue tests are shown in Figure 10. According to these results, when the $D_s/D_p = 1.0$ ($D_s = 0.76$ mm, $D_p = 0.635$ mm), the fatigue life of the solder joint is maximized.

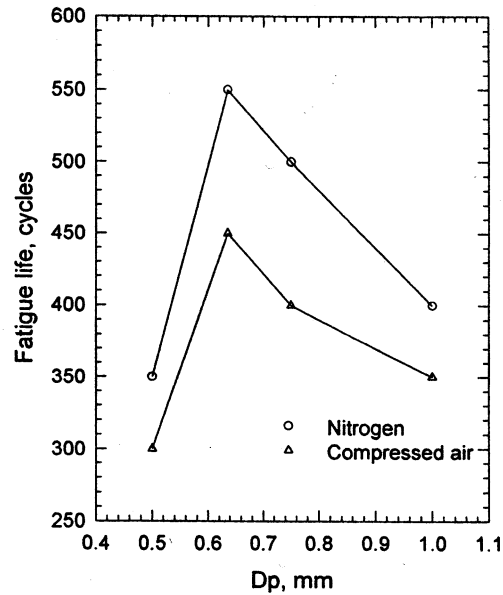


Figure 10. Thermal fatigue test results of PBGA assemblies (Ref:[8]).

For shear tests, the best results were obtained when $D_s/D_p = 1.2$ while for the thermal fatigue test, the longest fatigue life was when $D_s/D_p = 1.0$. When the pad size of the PCB is equal to the pad size of the package, the stresses at the package-to-solder interface and the PCB-to-solder interface are the same and will balance out. When the pads are not the same size, the smaller pad stresses a small cross section near the interface and acts like a stress concentrator, which leads to a shorter fatigue life. Thus fatigue life of the solder joints with $D_s/D_p = 1.0$ is better than for other D_s/D_p ratios. The D_s/D_p ratio is generally 1.0, which corresponds to these experimental results. These results were utilized in the design of the specimens for this investigation.

2.2 Effect of PCB Solder Pad Composition

Three different pad surface compositions, Cu-Ni-Au, Cu-Ni-Sn, and SMOBC/SSC (Solder Mask Over Bare Copper/Selective Solder Coating), were tested by John H. Lau et al [9]. Eutectic solder paste (37wt%Pb/63wt%Sn) was used. 4-point isothermal fatigue bending was employed to determine the mean life of the solder joints. The electrical resistance of the solder joints was monitored continuously by a computer in order to capture fatigue failure, which was defined as a 10% increase in the measured resistance. 10 units per surface composition were tested. 2-sided, 90%, symmetrical statistical-confidence interval was used to calculate the mean life to failure, which is shown in Figure 11, for various confidence levels.

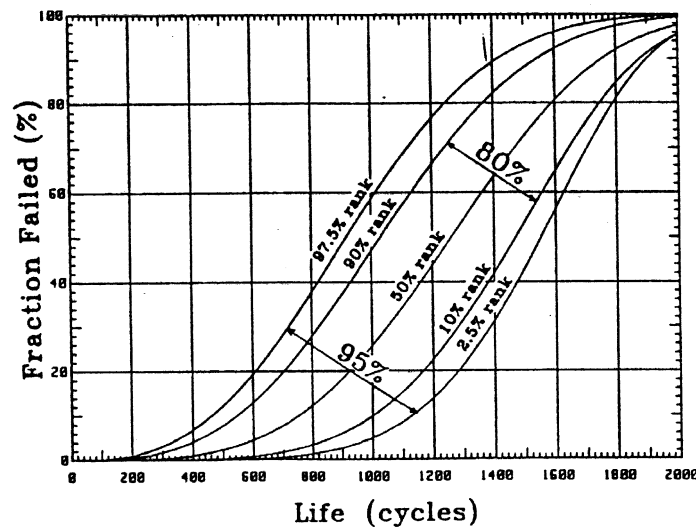


Figure 11. Weibull plot for Cu-Ni-Au at 80% & 95% statistical confidence interval (20°C) (Ref:[9]).

As can be seen in Figure 11, the same data will yield different results if a different confidence level is used in the calculation of the distribution function. Upon this basis, the mean life of solder joints attached to PCBs with a Cu-Ni-Au pad or a SMOBC is found to be better than those attached to PCBs with Cu-Ni-Sn pads. The mean life of solder joints attached to a Cu-Ni-Au PCB and a SMOBC PCB are about the same. The results are shown in Figure 12 and Figure 13. The A, B, and C curves shown in Figures 12 and 13 are the Weibull plots for the Cu-Ni-Sn, Cu-Ni-Au and SMOBC pads, respectively.

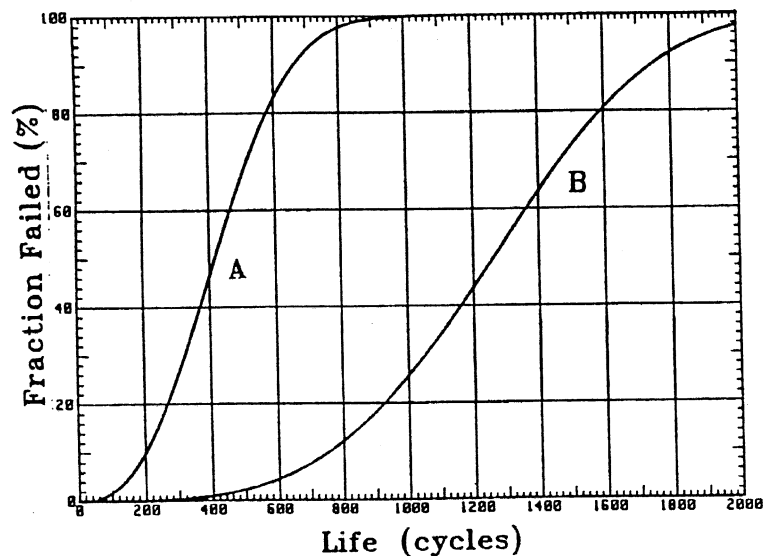


Figure 12. Comparison of Weibull plots of samples A (Cu-Ni-Sn pads) and B (Cu-Ni-Au pads) (Ref:[9]).

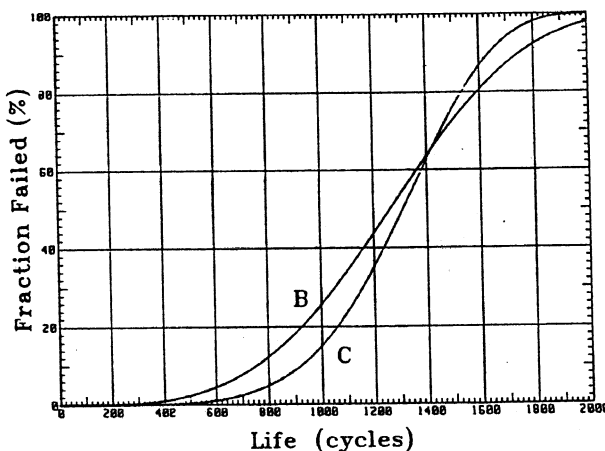


Figure 13. Comparison of Weibull plots of samples B (Cu-Ni-Au pads) and C (SMOBC pads) (Ref:[9]).

2.3 Effect of Reflow Process

The reflow soldering process consists of solder-paste application, component placement, preheating, slow heating, and melting/fillet formation [10]. The effect of the reflow process on solder joint reliability is reviewed here, with special emphasis on the reflow environments, reflow profile and their effects.

2.3.1 Reflow Environment (IR-reflow)

There are various types of reflow methods. The most common type is infrared (IR) reflow, which belongs to the radiative heat-transfer approach. The reflow environment can affect the solder joint reliability as well. This was investigated by Y.P. Wu for BGA packages [8]. Two reflow conditions, air and $N_2/50$ ppm O_2 , were studied. About 40 test data per reflow condition were tested. The results showed that reflow with $N_2/50$ ppm O_2 resulted in better shear strength and fatigue life than reflowing in air.

2.3.2 Reflow Profile

O'Hara et al [14] reported that a cooler reflow profile with 205°C peak temperature resulted in less voiding than the typical profile with 226°C peak temperature. Depending on the size and location of the voids inside the solder joints, the reliability of the solder joint can be lowered by these voids. A standard reflow profile has been developed by JEDEC and has been standardized as J-STD-020 [11]. The maximum ramp up rate for preheating is 3°C/sec. The temperature range is $125 \pm 25^\circ\text{C}$, and the maximum time for preheating is 120 seconds. For the slow heating region, the time interval for the temperature above the eutectic point (183°C) should be between 60 and 150 seconds. For the melting and fillet formation region, the temperature range is peak temperature $+5/-0^\circ\text{C}$. The time interval for the temperature above peak temperature should be between 10 and 20 seconds. For an individual package, the reflow profile can be fine-tuned to meet the special requirement. The schematic drawing of reflow profile is shown in Figure 14.

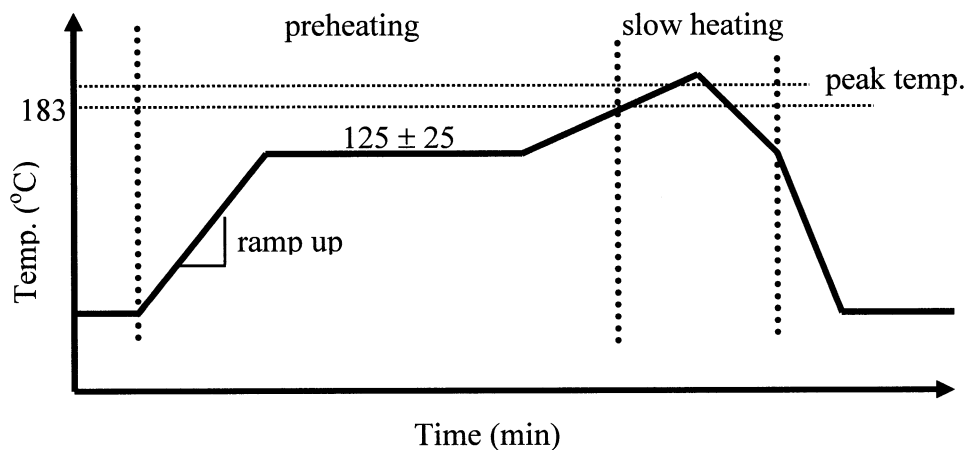


Figure 14. Schematic drawing of IR-reflow profile.

2.4 Voiding Initiation Mechanism in Surface Mount Process

When the microelectronic packages become smaller and smaller, the pitch for interconnections between the packages and the PCBs becomes narrower and narrower, which makes surface mount technology face the challenge of ultra-fine pitch product. When the solder joint dimensions become smaller, reliability concerns become more important because voids existing in the solder joints can affect the reliability of solder joints more seriously. This is the motivation for wanting to understand the initiation mechanism of voids during the surface mount process.

A review of the published literature indicates that there are three major factors which cause voids: flux entrapment, dissolved gas in raw materials, and solder shrinkage during solidification. Details of these factors are described below.

2.4.1 Flux Entrapment

The reasons for flux entrapment can be divided into three categories – materials, reflow environment, and geometry factor.

2.4.1.1 Materials

The materials used in the solder paste for surface mount process are solder flux and metallic solder. The flux system consists of rosin, activator, and solvent. Flux is very important to the soldering process due to its chemical, thermal, and physical functions. Chemically, flux helps to expose the clean surface by removing the surface oxides and sulfides. It also maintains a chemical blanket over the surface to prevent re-oxidation

during the soldering process. The flux also enhances heat transfer from molten solder to the joint area. Physically, the flux reduces the interfacial surface tension between the solder and the base metal [12]. Research papers on the relationship between the rosin content and void formation were not found. However, the relationships of activator content vs. void content and solvent content vs. void content have been studied.

A relationship of decreasing void content with increasing flux activity was reported by Hance, W.B. et al in 1992 [13]. Copper coupons were used in this study. The flux activity was regulated by varying the activator content, as shown in Figure 15.

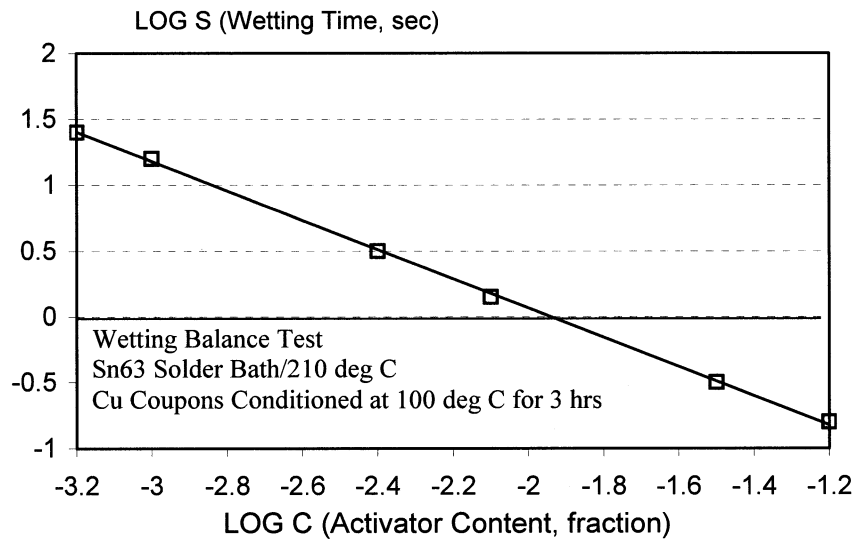


Figure 15. Relationship between activator content and flux activity (wetting time) (Ref: [13]).

The higher the activator content, the higher the flux activity and the shorter the wetting time, which results in a lower voiding content, as shown in Figure 16. This is because the higher activity flux usually eliminates the oxides more rapidly and completely, therefore reducing the possibility of void formation. However, a virtually negligible effect of flux activity on voiding was reported by O'Hara et al [14, 15], who used BGA components and PCBs instead of copper coupons. These results are shown in Figure 17. The difference between Figures 16 and 17 was expected by the authors since the soldering process for BGAs is not a wetting process but merely a coalescence process while for copper coupons it is a wetting process.

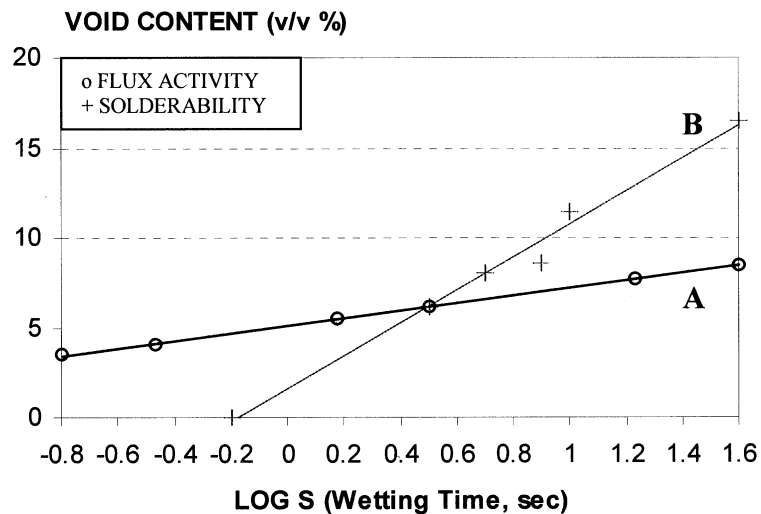


Figure 16. Relationship between flux activity (wetting time) and void content – line A (Ref: [13]).

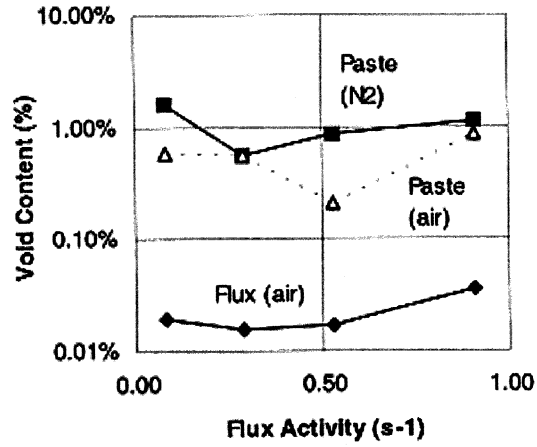


Figure 17. Relationship between flux activity and voiding in BGA joints (Ref: [14]).

The effect of the boiling point of the solvent on voiding was studied by W.B. O'Hara et al [13]. Their results showed that the higher the solvent's boiling point, the lower the void content, as shown in Figure 18.

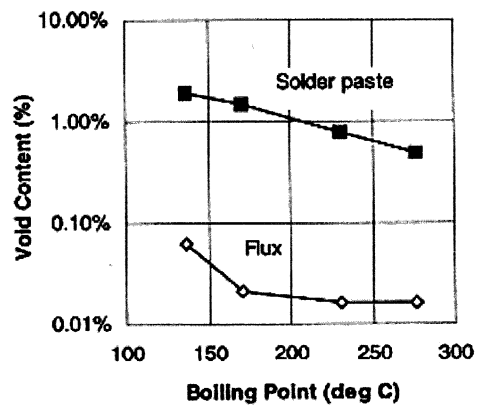


Figure 18. Effect of solvent boiling point on the voiding of BGA joints using solder pastes or fluxes only (Ref: [14]).

Based on the result shown in Figure 18, O’Hara et al proposed a “Flux-exclusion-rate Model”, according to which the higher the solvent volatility i.e., lower solvent boiling point, the greater the potential for flux remnant entrapment and void formation [14, 15]. O’Hara’s explanation and justification for the model is as follows: “The flux drying out readily will result in a flux remnant with a higher viscosity. This higher viscosity remnant will have a greater difficulty to be excluded from the interior of the molten solder, and therefore will have more chance to be entrapped in the molten solder and serve as an out-gassing source, hence contribute more to the voiding”. The higher boiling point solvents dry out slower and remain less viscous than lower boiling point solvent, thus resulting in a lower void content. However, a contradictory result was obtained by O’Hara et al in their earlier work in 1992 [13]. In that study, the void content was found to increase with an increase in the solvent’s boiling point, as shown in Table 1. The reflow temperature was 230°C.

Table 1. Effect of Predrying and Solvent Boiling Point on Voiding (Ref: [13]).

Flux Type	Predry	Void Content (v/v %)
B-2-90	Yes	6.40
B-2-90	No	0.44
B-3-90	No	0.26
BH-3-90	No	1.01

The two fluxes, B-3-90 and BH-3-90 have similar chemical constituents. Both have flux B, -325/+500 mesh powder (code 3), and 90% metal loading. The only difference is the boiling points of the solvents used for these two fluxes. The solvents' boiling points for B-3-90 and BH-3-90 were 230°C and 280°C, respectively. After sending an e-mail to O'Hara et al regarding to this contradiction, Dr. N.C. Lee, in 2000 [16], responded as follows: "Voiding is generated by outgassing. This is a sporadic phenomenon, bubbles generated then escaped quickly. Then, the next bubble generated then escaped. For high boiling point, if the process temperature is below the temperature where boiling occurs, the flux-exclusion-rate model will prevail. However, if the process temperature is around the boiling action temperature of the high boiling point solvent, the higher boiling can end up hurting the voiding performance. This is the difference in the results reported in the two papers".

A proportional relationship between metal loading and voiding was reported by O'Hara et al in 1992, 1996, and 1998 [13-15]. The higher the metal loading, the higher the void content. This trend is shown in Figure 19. However, due to insufficient data points, the trend-line can be either exponential or linear. The author assumed the trend is exponential. The proportional relationship can be attributed partly to an increase in the total oxide content in the metal powder surface, which increases the fluxing reaction, thus increasing the amount of outgassing. Another reason can be the greater difficulty for flux to escape due to tighter powder packing, therefore increasing the chance of forming more high viscosity metal salt. This is consistent with the flux-exclusion-rate model described above. But, if we take a closer look at the data points, it is impossible to have void

content when there is no metal loading. After excluding the 0% metal content data point, the remaining points indicated that void content varies independently of metal content. However, this problem in data interpretation has not been discussed with the authors. The relationship between metal content and void content, based on this study, is therefore inconclusive.

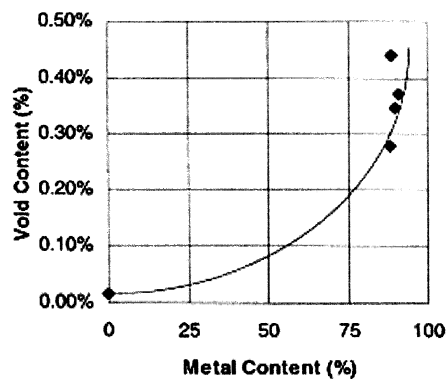


Figure 19. Effect of Sn63 (-325/+500 mesh) metal content on voiding of BGA joints (Ref: [14]) (0 % metal content means pure flux).

While the metal content can affect the void formation, the particle size of the metal load also plays an important role and affects voiding. O'Hara et al reported that a smaller powder size resulted in higher void contents [13-15]. Smaller powder size means more surface area per unit solder volume, or more solder oxide per unit solder volume. Voiding in a solder joint is mainly caused by outgassing. The greater the solder oxide content, the greater the fluxing reaction, and the higher the flux reaction product concentration. The reaction products include water, which will vaporize and contribute to outgassing. The results are shown in Figure 20. A correlation between mesh number and particle size is shown in Table 2.

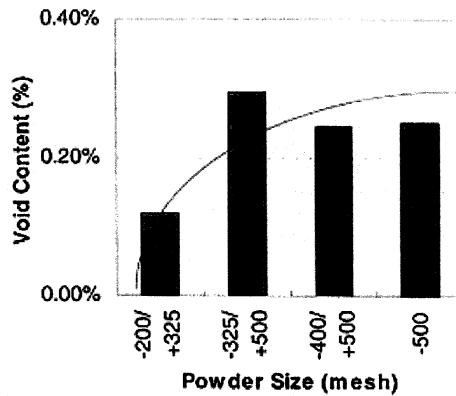


Figure 20. Relationship between powder size and voiding of BGA joints (Ref: [14]).

Table 2. Correlation between Mesh Number and Particle Size (Ref: [14]).

Mesh Number	Size (micron)
200	74
325	44
400	38
500	25

2.4.1.2 Reflow Environment

The reflow environment for the surface mount process is defined by the reflow profile and reflow atmosphere. The effect of the reflow profile on voiding was investigated by O'Hara et al in 1996 [14]. A cool reflow profile (peak temperature 205°C) resulted in less voiding than the typical profile (peak temperature 226°C), as shown in Figure 21. In addition, the difference in the voiding between the two reflow profiles decreased with increasing solvent boiling point.

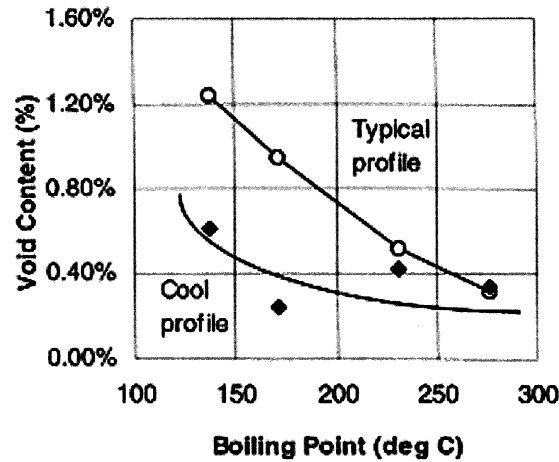


Figure 21. Effect of reflow temperature on the voiding of BGA joints soldered with A3-B1-M3-90 solder paste under air atmosphere (Ref: [14]).

This result also can be explained by the “flux-exclusion- rate model,” which was proposed by O’Hara et al. Presumably, the cool reflow temperature dried out the volatile solvent less readily than the typical profile did. The remaining un-dried solvent reduced the viscosity of the remnant flux, then enhanced the exclusion process of the flux from the molten solder, and consequently resulted in less voiding.

While the reflow profile plays an effective role on voiding, the reflow atmosphere was found to show no significant effect on void formation. This result was also reported by O’Hara et al [14]. The presence of oxygen during reflow usually promotes metal oxidation and results in poor solderability. Because the solderability of both BGA bumps and PCB pads is very good, the solder joints should not be sensitive to the reflow atmosphere. Within experimental error, the reflow atmosphere showed no effect on the voiding of BGA joints, as shown in Figure 22.

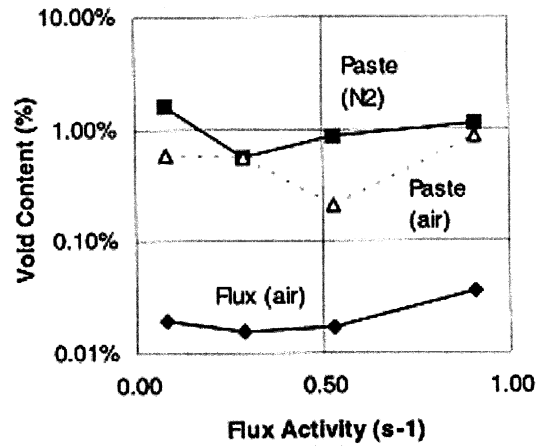


Figure 22. Relation between flux activity voiding in BGA joints (Ref: [14]).

2.4.1.3 Geometry Factor

Effect of coverage area of solder paste on voiding was investigated by O'Hara et al in 1992 [13]. The results are shown in Figure 23. However, only two data points are shown in Figure 23. No information on the number of specimens tested was provided. Hence it is not clear if the data points in Figure 23 represent average values, or if they are single data points. The author assumed a linear trend and concluded that voiding was found to decrease with decreasing coverage area (print width). If the print thickness and the final joint height remain constant, reducing the print width means increasing the surface exposed to air, thus enhancing the escaping of outgassed and entrapped flux.

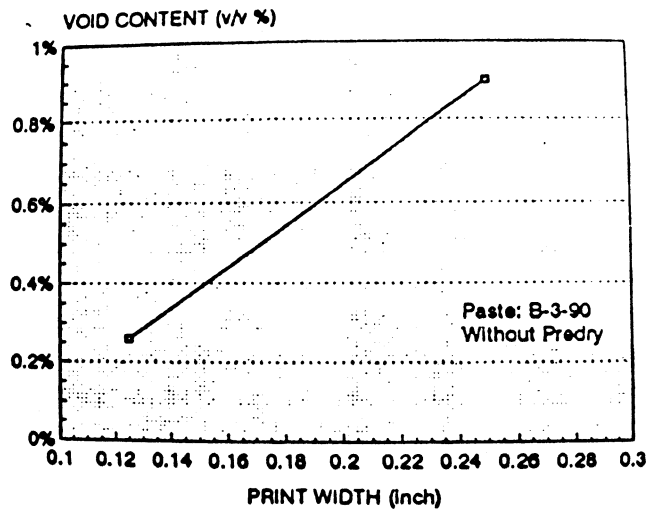
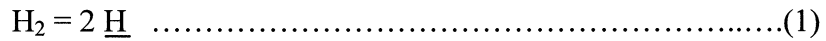


Figure 23. Effect of paste coverage area on voiding of paste B-3-90 (Ref: [13]).

2.4.2 Dissolved Gas in Raw Material

Though flux entrapment is the major reason for void initiation, dissolved gas in the raw material still plays an important role in voiding. The raw material referred to here is the tiny solder particles (metal load) in the solder paste or the solder balls. Gases, such as hydrogen and oxygen, can dissolve in the molten solder. After cooling down, the dissolved gases remain in the solid solder balls in monoatomic form, \underline{H} and \underline{O} . When the solder balls are brought to the eutectic temperature during the reflow process, the dissolved gas near the surface of molten solder can diffuse out, while those in the center coalesce into their molecular form, H_2 and O_2 , and are trapped. These trapped gases can also cause voiding. Sievert's Law [17] can be used to estimate the volume of trapped gases in liquid and solid metals. As an example, for hydrogen dissolves in molten copper, the H_2 gas dissociates into its monoatomic form \underline{H} , as shown in Equation (1):



The equilibrium constant (K_a) for Equation (1) is:

$$K_a = [\underline{\text{a}}_{\text{H}}]^2 / \underline{\text{a}}_{\text{H}_2(\text{g})} \dots\dots\dots(2)$$

Where $\underline{\text{a}}_{\text{H}}$ = activity of $\underline{\text{H}}$

$\underline{\text{a}}_{\text{H}_2}$ = activity of H_2

Since dissolved gases behave ideally in liquid metals

$$\underline{\text{a}}_{\text{H}} = [\underline{\text{H}}] \dots\dots\dots(3)$$

$$\underline{\text{a}}_{\text{H}_2(\text{g})} = P_{\text{H}_2} \dots\dots\dots(4)$$

Where $[\underline{\text{H}}]$ = concentration of dissolved hydrogen

P_{H_2} = partial pressure of $\text{H}_2(\text{g})$

By substituting Equations (3) and (4) into Equation (2), Equation (5) can be obtained:

$$[\underline{\text{H}}]^2 = K_a P_{\text{H}_2} \dots\dots\dots(5)$$

K_a can be obtained from Equation (6)

$$K_a = \exp(- \Delta G^0 / RT) \dots\dots\dots(6)$$

Where ΔG^0 = Standard Gibbs free energy change for the dissolution reaction

R = Universal gas constant

T = Reaction temperature (K)

From Equation (5), $[\underline{\text{H}}]$ (the solubility of H_2 in molten copper or other liquid metals) can be obtained. The solubility of hydrogen in molten copper has been estimated to be about $7.34 \text{ cm}^3/100\text{g}$ [17]. This value represents a large amount of trapped gases, which should not be ignored.

2.4.3 Solidification Shrinkage

The effect of solder solidification shrinkage on void formation was pointed out by P.W. Barnes [18]. During the reflow process, the solder in the molten state wets the contact surfaces of the package side and the PCB side. After cooling down, the solder solidifies, with volume shrinkage. If the wetting force between the solder and contacts is stronger than the shrinkage force due to solidification, cracks or a void may be initiated. No experimental data were reported to substantiate this postulate.

2.5 Summary of Literature Review

The literature search helped define the factors to be examined during this research. According to the literature review, there are several factors that can affect solder joint reliability. For solder joint geometry, an hourglass shaped solder joint exhibited the longest fatigue life when compared to trapezoid and barrel shaped solder joints. The solder joint thickness also played an important role in solder joint reliability. The thicker the solder joint, the better the reliability. The longest thermal fatigue life was expected when the D_s/D_p ratio equals to one. For PCB pad composition, similar performance for Cu-Ni-Au pad and SMOBC pad were reported. Both Cu-Ni-Au and SMOBC pads resulted in better solder joint reliability than with Cu-Ni-Sn pads. For reflow conditions, $N_2/50$ ppm O_2 resulted in higher shear strength and fatigue life than reflowing in air. In addition to the factors mentioned above, void formation also affects the solder joint reliability. Not only the materials, such as flux and solder paste, alter the void formation; the reflow environment, dissolved gas in raw material, and solder joint shrinkage during

solidification can also affect void formation. All these factors have to be controlled in the experiment in order to distinguish the effectiveness of the design factors.

CHAPTER 3

EXPERIMENTAL OBJECTIVE AND APPROACH

3.1 Experimental Objective

The overall objective of this investigation was to determine and understand the relationship between solder joint reliability and the following three factors: lead contact area, die attach pad (DAP) area, and solder joint thickness.

The lead contact area of an LLP was reduced in size to determine if the design would be able to pass the required reliability level. If the reduced lead area has no effect on the reliability, then more leads can be placed in the same package size, which would be a big benefit to the package design.

The die attach pad contact area was investigated to determine the effect of area on solder joint reliability. The weakest point of the solder joints in a package is always the corner lead, because the corner lead is furthest away from the center of the package. This is the situation when the DAP is not soldered. If the DAP of a package is soldered onto a PCB, will the new stress center shift to the corner of the DAP or will it remain in the center of the package? If the stress center shifts to the corner of DAP, then a new design rule can be set up without affecting the package size.

From the literature review, it was found that the thicker the solder joint, the better the reliability. So, the solder joint thickness was investigated in order to optimize it. Due to limitations of time and other constraints, only the DAP and land size were investigated. The other factors that affect the solder joint reliability, such as pad

compositions, reflow conditions, and soldering materials were controlled by the National Semiconductor Corporation's surface mount subcontractor and could not be varied without major disruptions to the production process. The surface mount process and materials employed were in accordance with National Semiconductor Corporation's standards.

3.2 Experimental Parameters and Level Determination

Two factors, the DAP and the Land soldered area, were investigated. The lands and DAP of a 12L LLP package are shown in Fig. 24.

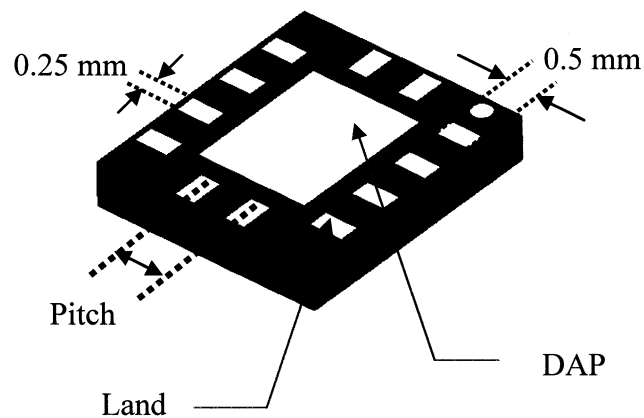


Figure 24. Land and DAP of a 12L LLP.

The existing package that was needed for this study was the 44L LLP. The body size of the 44L LLP is 7 x 7 mm. The first parameter was soldered land area. The existing design of the land area was 0.25 x 0.5 mm for 0.5 mm pitch. A smaller land area

– 0.25 x 0.3 mm – was tested to see if there was any possibility of reducing the land area while maintaining the same reliability level. If the land area could be made smaller, then the DAP size could be increased for larger silicon die. The second parameter was the die attach pad (DAP) soldered area. The design for the DAP area was “100% soldered” on to the testing PCB. Smaller DAP areas – 0% and 50% – were tested in an attempt to understand the shifting of the stress neutral point. From past research it has been established that thicker solder joints are more reliable. However, due to the limitations of fine pitch, solder joint thickness cannot be picked arbitrarily. In this investigation, the solder joint thickness was fixed at 2 mils, which is the thickness needed in current generation products. The experimental factors and levels are summarized in Table 3.

Table 3. Experimental Factors and Levels

Factor Level	Land Area	DAP Area	Nominal Solder Joint Thickness
1	0.25 x 0.3	0%	2 mils
2	0.25 x 0.5	50%	2 mils
3		100%	2 mils

3.3 Design of Experiment

A full factorial design was employed in this project. The combinations are shown in Table 4.

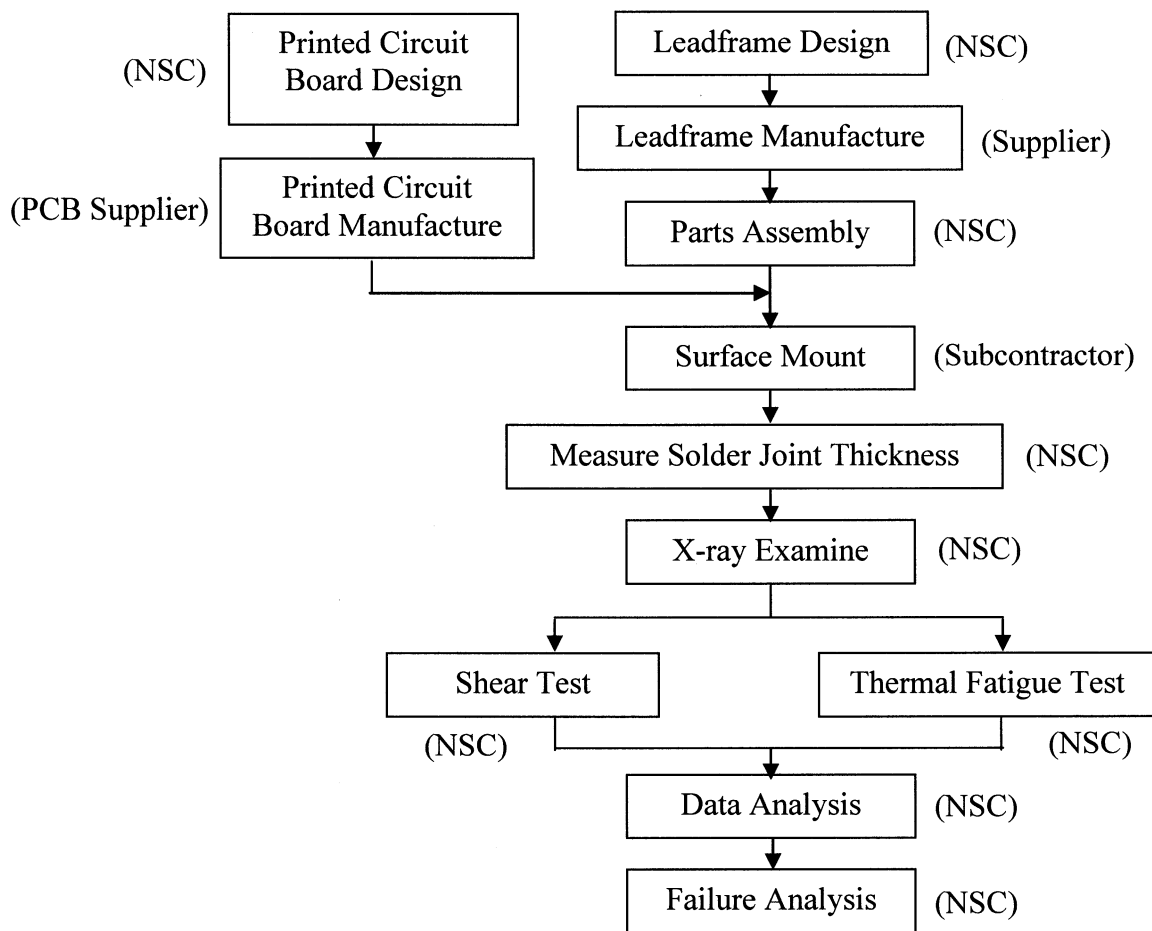
Table 4. Factors Combination Table for Full Factorial DOE

Design	Land Area	DAP Area
A	0.25 x 0.5 mm	0%
B		50%
C		100%
D	0.25 x 0.3 mm	0%
E		50%
F		100%

3.4 Experimental Process

The experimental process was divided into five steps. The first step was the preparation of materials, which included leadframe design, manufacture and testing, and the PCB design and manufacture. The second step was parts assembly and surface mount processing. The third step, inspection, included solder joint thickness measurements and X-ray examination. Since the solder joint thickness is controlled by several factors, such as stencil type, stencil opening and thickness, solder paste type, and printing process, etc, the actual solder joint thickness was measured after surface mounting. The purpose of X-ray inspection was to make sure the quality of the solder joints was good. In order to obtain sufficient evidence to distinguish between solder joint failures caused by geometry

design as opposed to voids, a void examination was performed prior to any further testing. The fourth step was testing, which included both shear tests and temperature cycle tests. The final step included data analysis and failure analysis. The flow chart of whole investigation is shown in Figure 25. The companies in charge of each step are shown in brackets.



NSC: National Semiconductor Corp.

Figure 25. Investigation flow chart.

3.4.1 Leadframe Design

In order to lower the cost for leadframe designing, various DAP sizes were designed in the same leadframe. There were two leadframe designs. One was with a small land area (0.25 x 0.3 mm), and the other was with a big land area (0.25 x 0.5 mm). For both, two different DAP sizes (50% and 100%) were designed in the same leadframe. The design for the leadframe with big land area is shown in Figure 26.

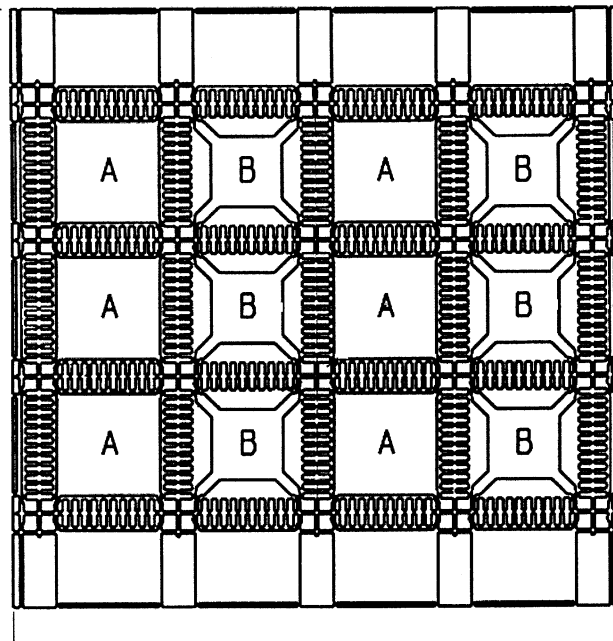
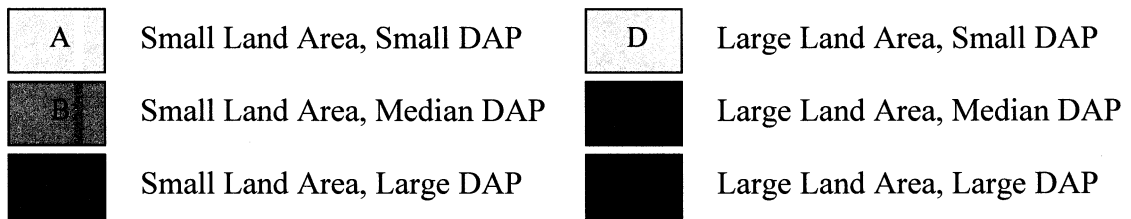
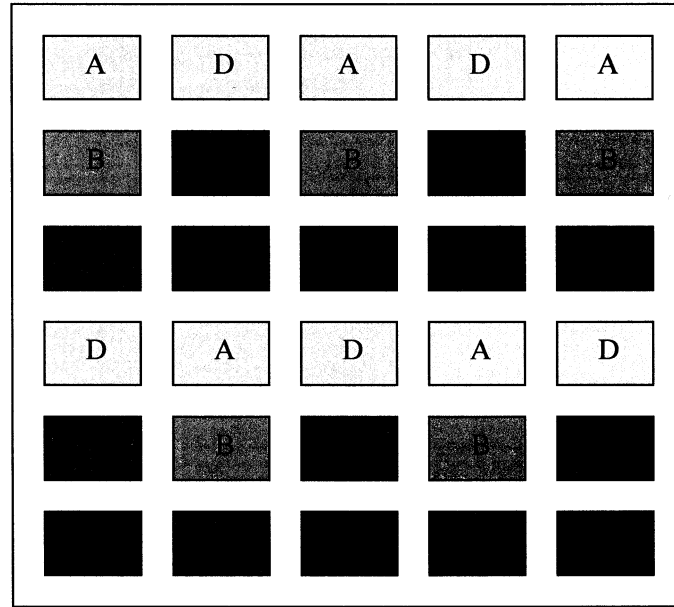


Figure 26. Sample drawing of leadframe design (large land area). A and B represent the large DAP (100%) and median DAP (50%) designs, respectively. (Source: NSC Leadframe drawing).

3.4.2 PCB Design – Parts Distribution for Surface Mount

After assembly, the LLPs were surface mounted on a printed circuit board (PCB).

In order to have balance and an even distribution, the distribution shown in Figure 27 was employed.



Small Land: 0.25 x 0.3 mm

Large Land: 0.25 x 0.5 mm

Small DAP: 0% DAP area

Median DAP: 50% DAP area

Large DAP: 100% DAP area

Figure 27. Parts distribution on testing PCB.

In this distribution, 5 units per design (A, B, C, D, E and F) were mounted on one PCB. Four such assemblies, as shown in Figure 26, were built for both shear and temperature cycle testing. The 5 units were distributed in the middle and at the corner of the PCB evenly. The purpose of this distribution was to minimize the corner effect due to CTE mismatch. Because the LLP at the corner of a PCB has a longer distance to the neutral point (DNP) than the one in the center, the stresses experienced by a corner LLP are greater than the one at the center. If the LLPs are not distributed evenly (corner position plus center positions), when a failure occurs, it would not be possible to unequivocally identify the cause, namely, due to design factors or the location variation.

The testing boards used were a 2-layer FR-4 PCB. In order to make electrical continuity measurements possible, a daisy chain design was employed for PCB routing and LLP wire bonding. A Schematic drawing of the top and bottom layers of the PCB are shown in Figures 28 and 29, respectively.

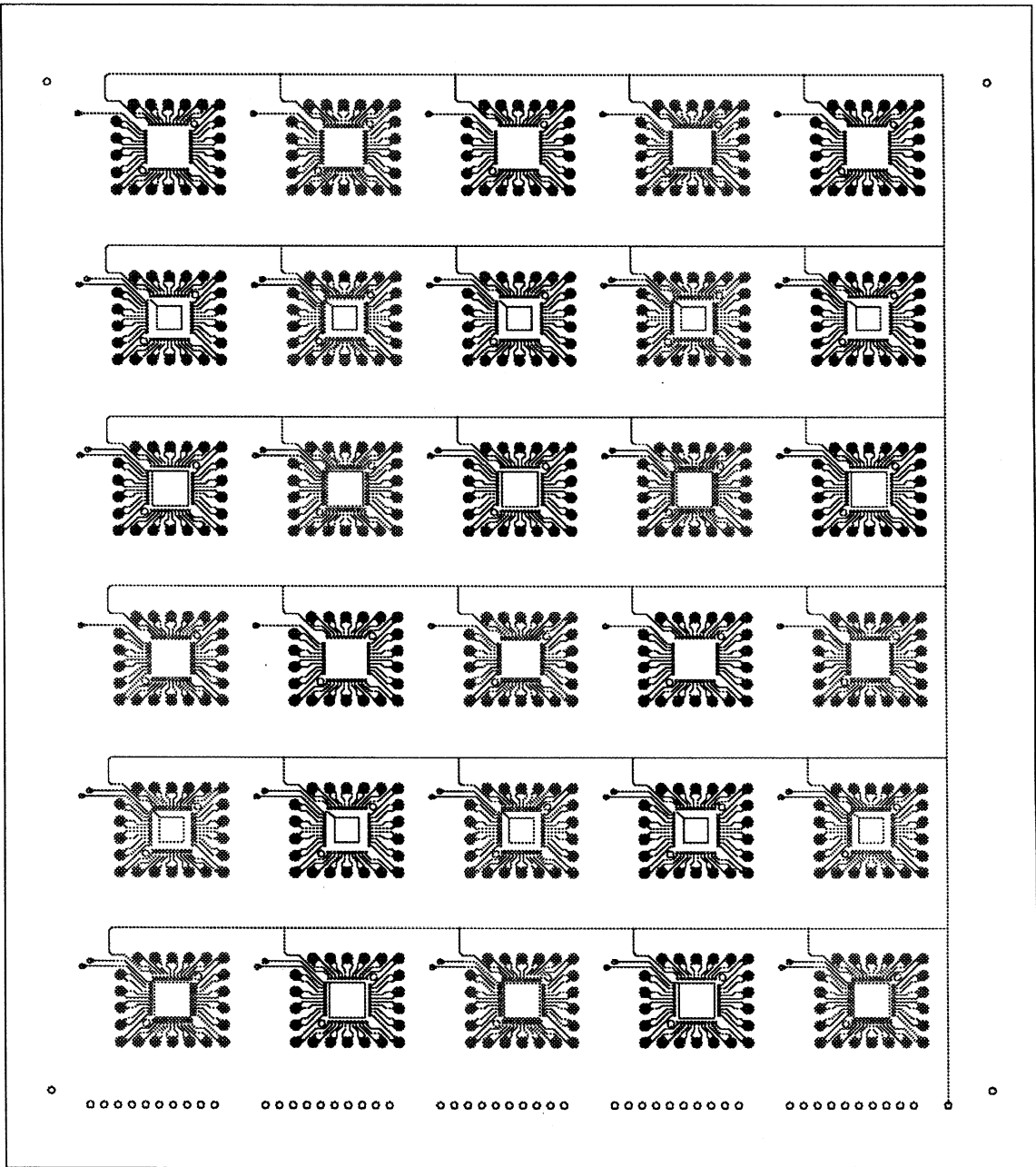


Figure 28. Top layer of PCB (Top view).

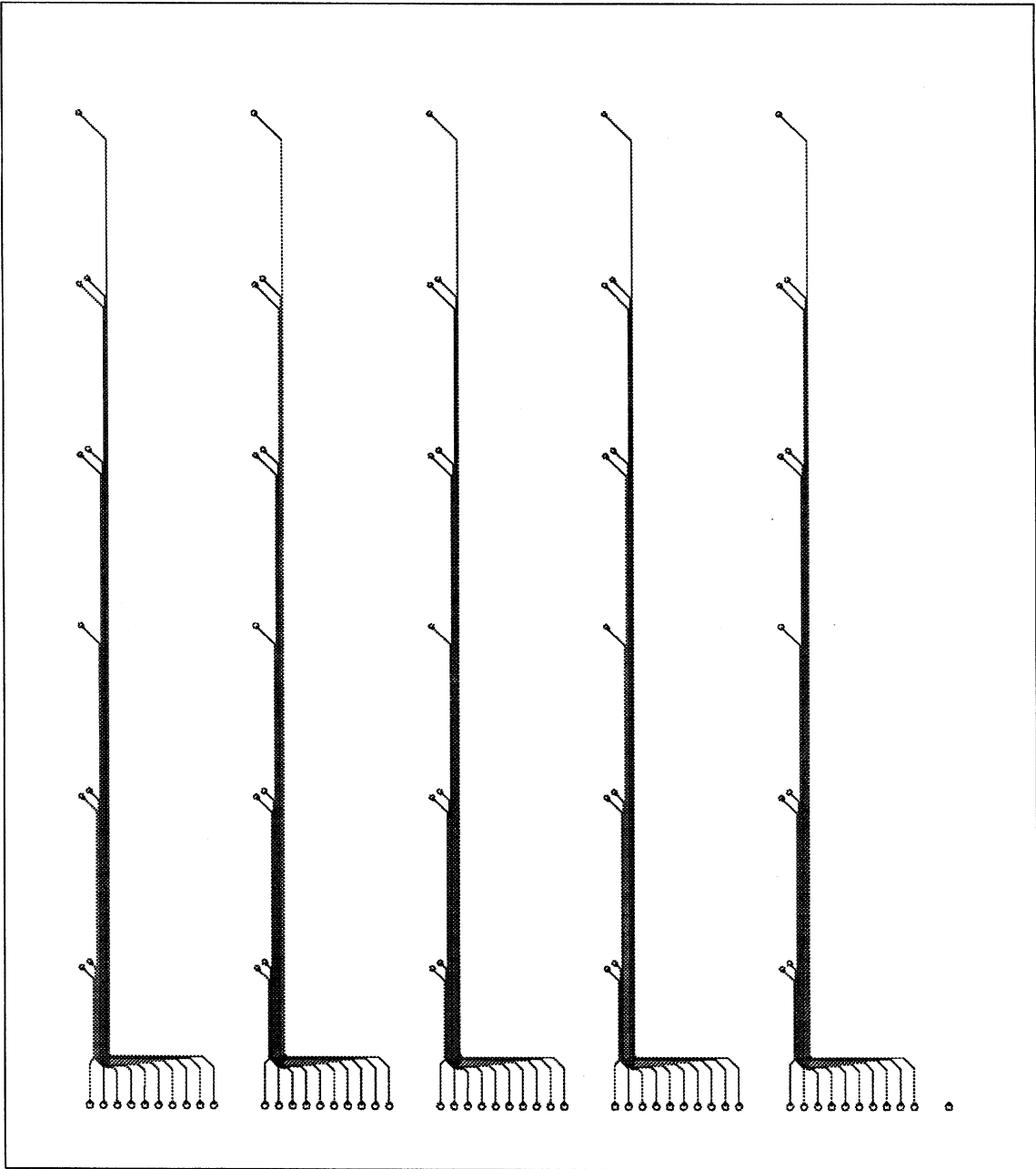


Figure 29. Bottom layer of PCB (Top view).

3.4.3 Parts Assembly

The materials used for the LLP assembly are listed below:

Die: Dummy Die
Wire: Gold (Diameter = 1.2 mils, purity: 99.99%)
Die Attach: Ablestik Ablebond 8360
Mold Compound: Sumitomo 7730

In order to make sure the loop circuit (Daisy Chain) was terminated by an open solder joint instead of a wire bond defect, double wirebonds were employed during the wire bonding process. The schematic wire bonding diagram is shown in Figure 30.

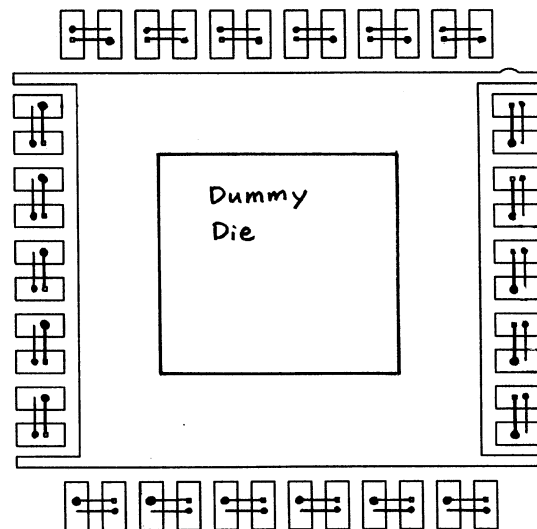


Figure 30. Schematic daisy chain wire bonding diagram for 44L LLP
(Source: NSC bonding diagram)

3.4.4 Surface Mount

The quality of the surface mounting process can be affected by a number of factors. The following describes the materials and parameters employed for this investigation, including the type of solder paste, stencil design, and the reflow profile. A flow chart of surface mount process is also presented.

3.4.4.1 Solder Paste

The solder paste used in this experiment was mesh Type III provided by Alpha Metals, Inc. (WS609, 90-3-M13). This solder paste consisted of two components – 88 ~ 90 wt% eutectic Pb-Sn solder (63Sn/37Pb) particles and 10 ~ 12 wt% water soluble flux.

3.4.4.2 Stencil

The stencil used in this experiment was laser cut followed by electropolishing. The ease of the dimension control is the major advantage of a laser cut stencil. However, the wall surface aperture is not smooth enough after laser cutting. Therefore the electropolishing, i.e., microetching, is necessary.

In order to have effective solder paste transfer, the aperture's aspect ratio, i.e., the aperture width divided by aperture height, has to be bigger than 1.5, based on previous working experience with surface mounting. The bigger the aperture's aspect ratio, the better the transfer efficiency.

3.4.4.3 IR-reflow Profile

The IR-reflow profile of the soldering process employed is shown in Figure 31. The average ramp up rate was 1~2 °C/sec, and maximum ramp up rate was 2.75°C/sec. The peak temperature was 235°C. The duration time above 183°C (eutectic temperature for Pb/Sn system) was 155 seconds. The maximum ramp down rate was 4.3°C/sec.

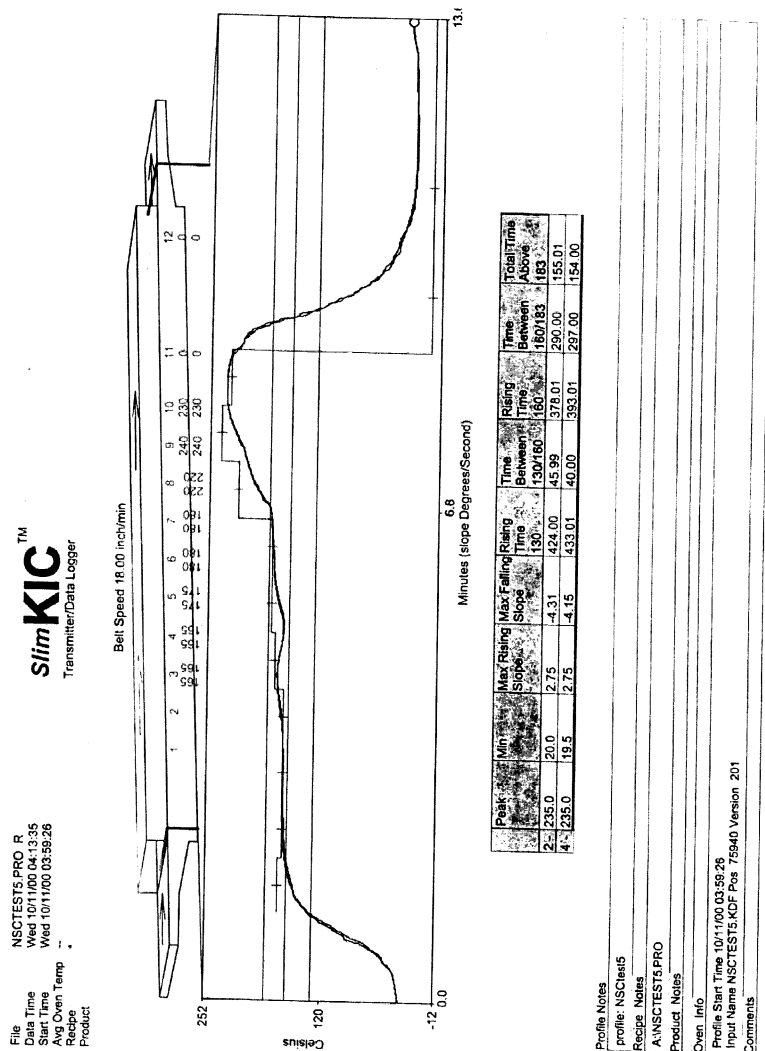


Figure 31. IR-reflow profile for the soldering process.

3.4.4.4 Flow Chart of Surface Mount

The flow chart of the surface mount process is shown in Figure 32.

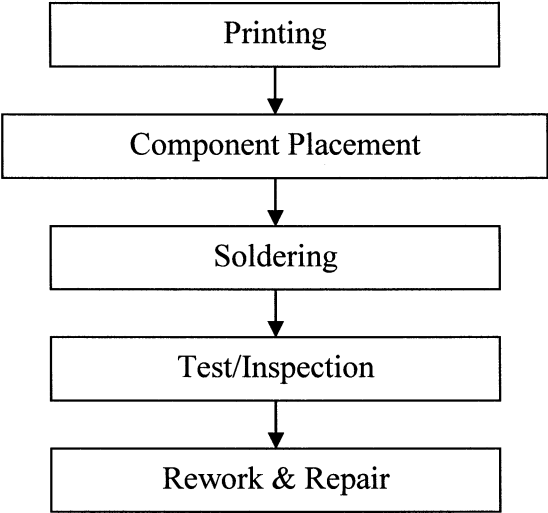


Figure 32. Flow chart of surface mount process.

3.4.5 Inspection

The third step, inspection, included solder joint thickness measurements and X-ray examination. After surface mounting, all the parts were inspected, before further testing, to identify the causes of failure. For solder joint thickness measurement, the sampling rate was 10%. For X-ray examination, the inspection rate was 100%. Those parts with insufficient soldered area (soldered area < 75%) were discarded and were replaced by new parts and PCBs.

3.4.5.1 Solder Joint Thickness Measurement

Since the solder joint thickness is controlled by several factors, such as stencil type, stencil opening and thickness, solder paste type, and printing process, etc, the actual solder joint thickness was measured after surface mounting. A 3-D optical microscope (OM), which can record the x, y, z moving distance, was used to measure the solder joint thickness. First, the OM focused on the top of PCB and the vertical meter was set to zero. Then, the turntable of OM was moved and the unit was brought under the objective lens. The OM was focused on the top corner of the package and the reading of the vertical meter was recorded. The recorded height included the package thickness, i.e., the stand of height, and the solder joint thickness. The solder joint thickness was obtained by subtracting the package thickness. The same process was repeated for the other three corners of the same package. The measurements from the four corners were then averaged and recorded as the solder joint thickness for the particular package. The data for the solder joint thickness measurements are shown in Appendix B.

3.4.5.2 X-ray Examination

The purpose of X-ray inspection was to make sure the quality of the solder joints was good prior to further testing. The size, location, and total volume percentage of voids within solder joints can greatly affect solder joint reliability. In order to obtain sufficient evidence to distinguish between solder joint failures caused by geometry design as opposed to voids, a void examination was performed prior to any further testing. The total void area had to be less than 25% of the total DAP area in order for the sample to

“pass” X-ray examination. The same criterion was used for coverage of the land area as well. A sample X-ray micrograph is shown as Figure 33. The light-color spots in Figure 33 are the voids inside the solder joints.

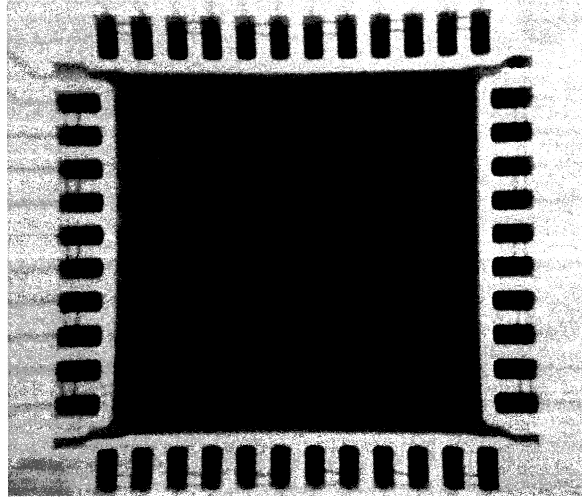


Figure 33. X-ray micrograph of a LLP of design F (large land area, large DAP area).

3.4.6 Test Method

Two test methods, shear tests and temperature cycle tests, were employed in evaluating the solder joint performance for LLPs. The following is a detailed description for both test methods.

3.4.6.1 Shear Test

The Instron Universal Test Instrument Model 1122 was used for shear test in the experiment. A photograph of an Instron 1122 is shown in Figure 34. The crosshead speed was 0.2 inch per second. The Shear Test was performed in a top-to-bottom direction, shown by an arrow in Figure 35.

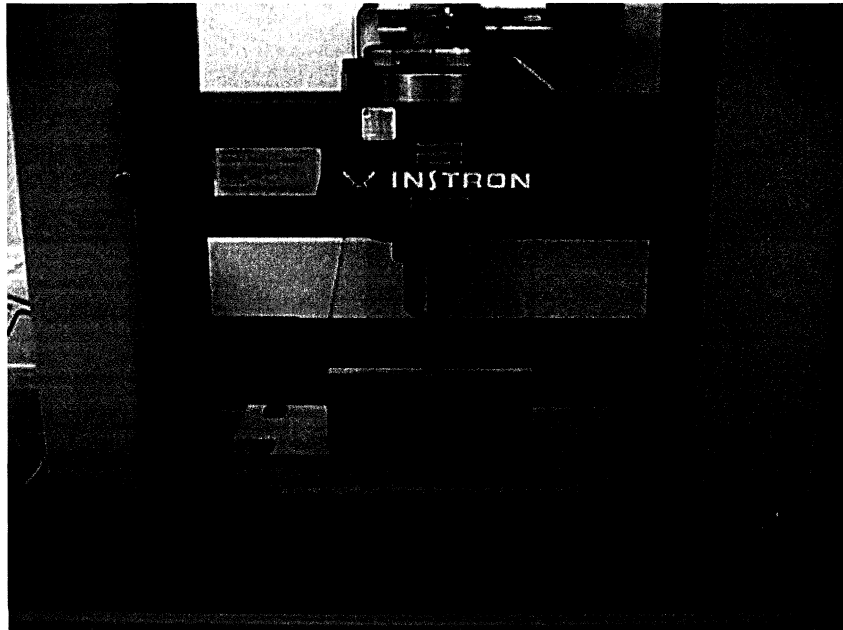


Figure 34. Instron Universal Test Instrument Model 1122
 (Source: Wayne Lee, Internal Packaging Engineering
 Report: Pull and Shear testing for the 16, 24, 28, 48L
 CSP & 64, 100L FBGA, June 16, 2000, p2).

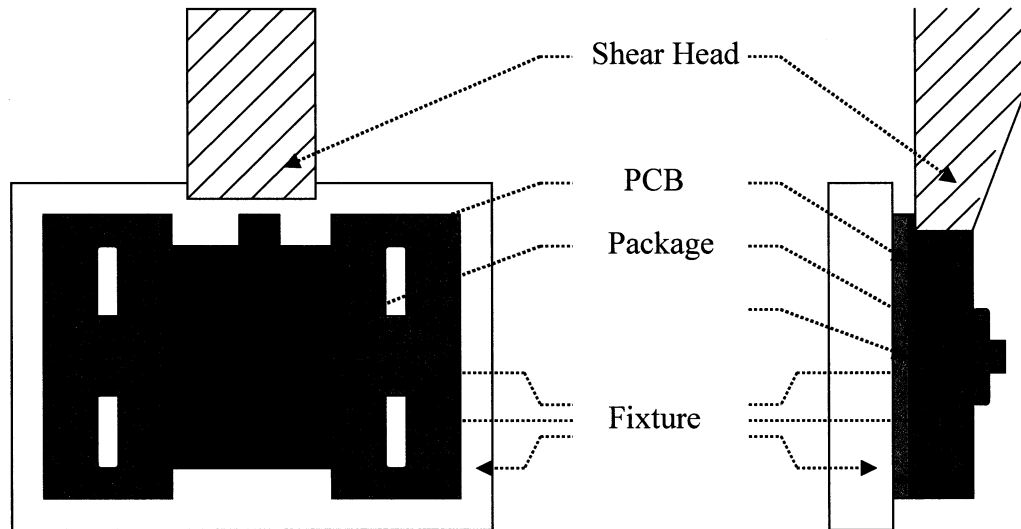


Figure 35. Schematic drawing of relationships between shear head, shear direction, specimen and fixture.

The schematic drawing of the solder joint geometry of design A to F is shown in Figure 36. The shear force was first measured from the shear tester. The shear force was then converted to shear strength by dividing the value of the shear force by the nominal solder joint area.

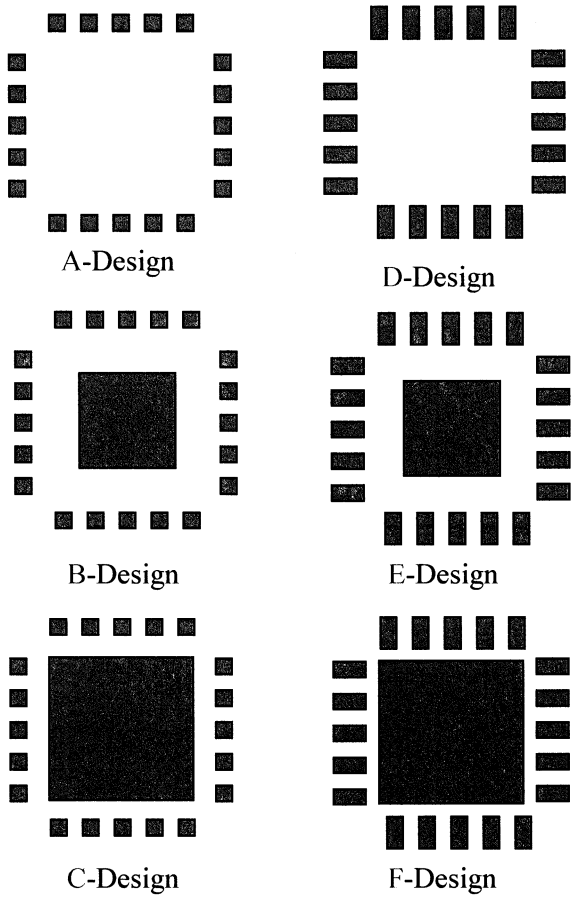


Figure 36. Schematic drawing of the solder joint geometry of designs A to F.

The solder joints of the LLP were sheared until all the solder joints broke. Information on the strengths of different solder joint geometry was provided by this test. The shear failure modes were divided into 5 categories as shown in Figure 37. The layer that had been sheared represents the weakest component in the system.

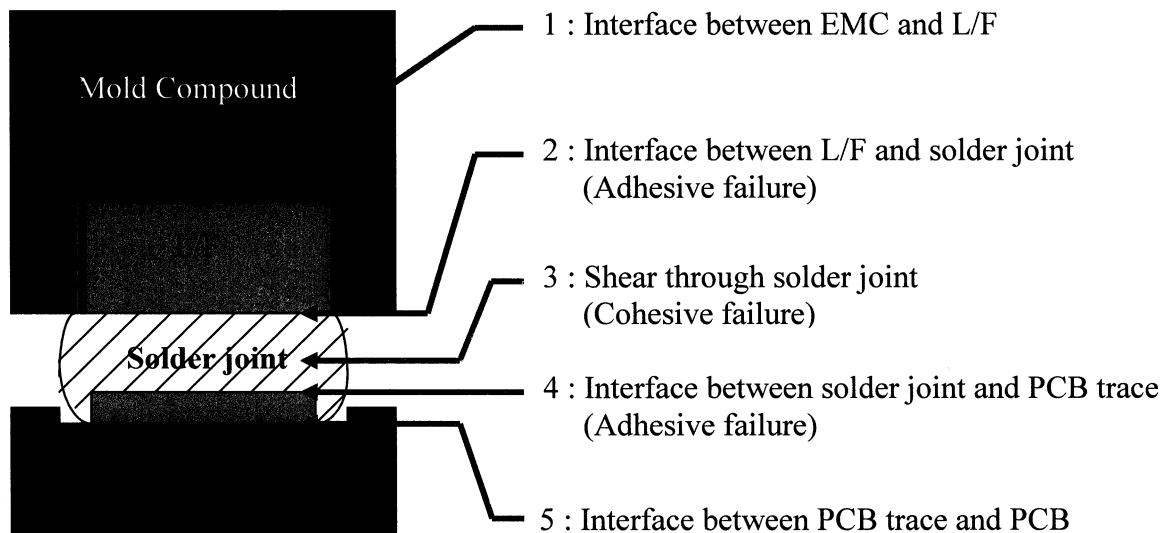


Figure 37. Failure modes of shear test.

3.4.6.2 Temperature Cycle Test

The parts were surface mounted on the Daisy-Chain-Design PCB and submitted for temperature cycle testing. 20 units per design were tested. Before submitting to the temperature cycle test, the loop resistance of each unit was measured at 0-hour to establish a basis for comparison. The test condition of the temperature cycle test was -40

to 125°C. Each cycle was 1-hour and the dwell time at each temperature was 15 minutes.

A schematic drawing of the temperature cycle profile is shown in Figure 38.

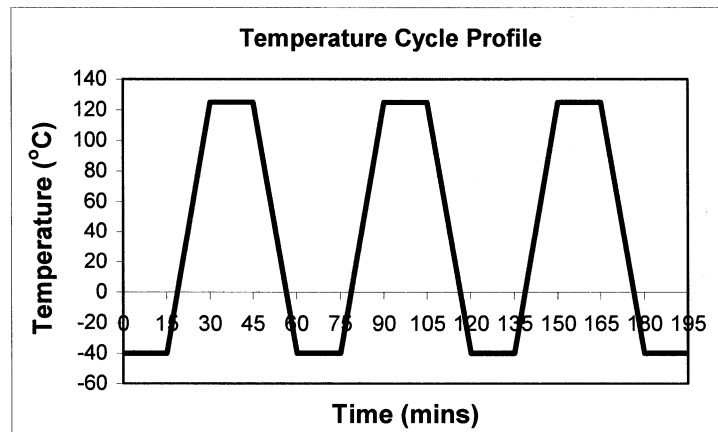


Figure 38. Schematic drawing of temperature cycle profile.

If there are cracks in the solder joints, the electrical resistance of solder joints will increase. This is a useful method to detect cracks in solder joints. The electrical resistance was monitored off-line at a frequency of once per 100 cycles in order to capture the failure of solder joints. The parts were extracted from the temperature cycling chamber and left in a room temperature environment to cool down. The electrical resistance was measured 15 minutes after removal from the chamber. The criterion of failure was a 10% increase in the loop resistance as defined in the IPC specification with specification number: IPC-SM-785 [19]. Because of time limitations, the test was stopped at 3003 cycles (about 4.5 months).

3.4.7 Data Analysis

For the temperature cycle test, the Weibull Distribution was employed to represent the effect of solder joint geometry on the reliability of the device, while the one-way ANOVA (Analysis of Variences) was employed to examine the statistical meaning of the data obtained from the shear tests.

3.4.7.1 Weibull Distribution

Weibull distribution applies to both decreasing and increasing failure rates. A decreasing failure rate generally represents the period of early failures while an increasing failure rate represents a longer period of time to wear out [20]. The Weibull Probability Density Function (PDF) and Cumulative Distribution Function (CDF) are given as follows:

PDF: $f(t) = (\beta/t)(t/\alpha)^\beta \exp[-(t/\alpha)^\beta]$ (7)

CDF: $F(t) = 1 - \exp[-(t/\alpha)^\beta]$ (8)

- Where t = Random variable (e.g. life)
- β = Shape parameter (Weibull slope)
- α = Characteristic life ($F(\alpha) = 62.3\%$) (Ref: [20, 21])

Typical plots of PDF and CDF are shown in Figures 39 and 40, respectively.

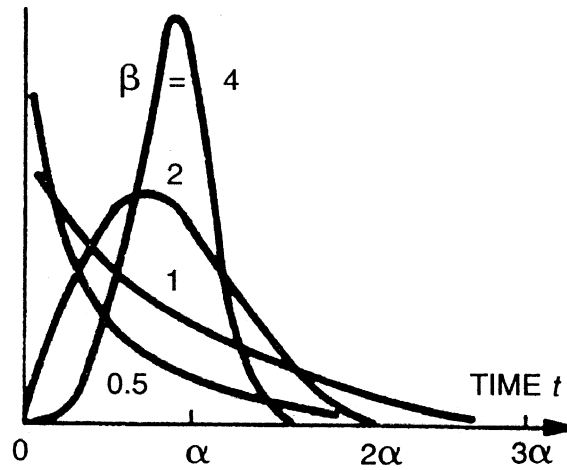


Figure 39. Probability Density Function $f(t)$ (Ref: [20], p. 194.)

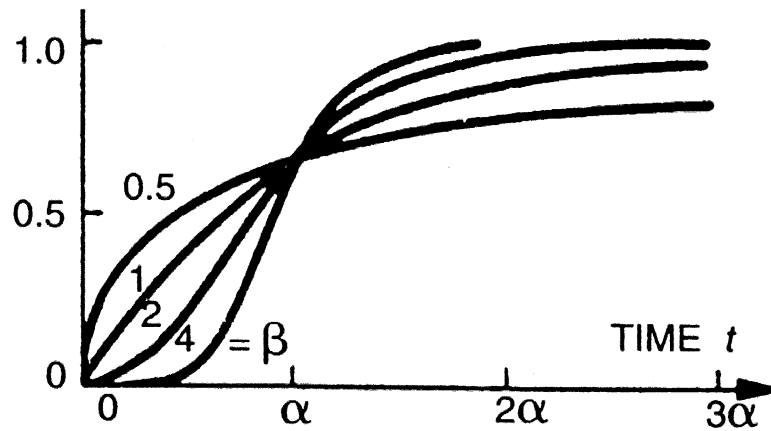


Figure 40. Cumulative Distribution Function $F(t)$ (Ref: [20], p. 194.)

In order to extract the reliability parameters (α , β) from the plot of the number of failures versus time (the number of failure cycles), mathematical manipulation of the Weibull function is necessary. By taking the natural logarithm of both sides of Equation (8), Equation (9) can be obtained:

$$\ln [1 - F(t)] = -(t/\alpha)^\beta \dots\dots\dots(9)$$

By taking natural logarithm of both sides of Equation (9), Equation (10) can be obtained:

$$\ln\{- \ln [1 - F(t)]\} = \beta \ln(t) - \beta \ln(\alpha) \dots\dots\dots (10)$$

When comparing Equation (10) with $Y = mX + b$, which represents the equation of a straight line,

$$Y = \ln\{- \ln [1 - F(t)]\}$$

$$X = \ln(t)$$

$$m = \beta$$

$$b = - \beta \ln(\alpha) \quad \Rightarrow \quad \alpha = e^{(-b/\beta)}$$

By plotting the $\ln\{- \ln [1 - F(t)]\}$ versus $\ln(t)$, α and β can be obtained from the slope and the intercept of the linear trendline [20].

From Figure 38, it can be seen that when the β is as high as 4, the PDF will be close to a normal distribution, which represents a consistent process. The higher the β value, the better the process. A wide and broad distribution of failures, characteristic of low β values, would be obtained if the process is not consistent.

3.4.7.2 One-way Analysis of Variance (One-way ANOVA)

ANOVA provides a test to determine whether to accept or reject the hypothesis that the means are all equal among different experimental groups [22]. One-way ANOVA was employed in the analysis of the mean values of shear strength for each of the designs.

3.4.8 Failure Analysis

For failure analysis, a cross-section was performed to understand the failure mechanism (crack) of the LLP solder joints. The information also allowed improvement of the reliability by changing the design geometry. A crack at the interface between the Cu-pad and the solder is shown in Figure 41.

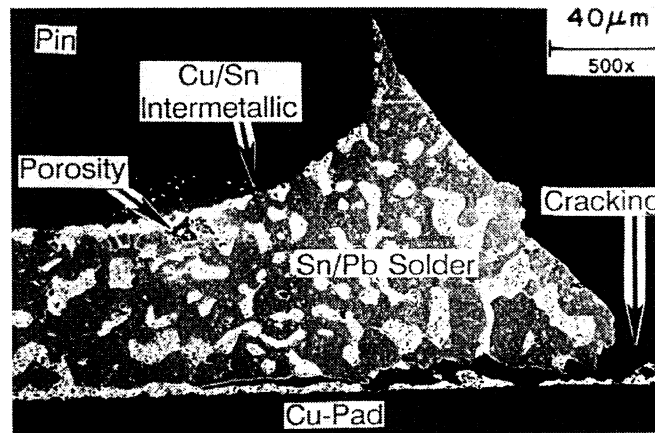


Figure 41. Cracks at the interface between Cu-pad and solder (Ref: [23], p. 78.).

3.5 Number of Parts and PCBs Needed for Experiment

All the parts and PCBs that were used in this study are listed in Table 5.

The number of parts needed in the DOE step was 240 units (20 x 6 x 2). The “20” represents 20 replications for each condition. The “6” represents the 6 trials (designs) in Table 5. The “2” represents 2 tests – the shear and temperature cycle tests. In addition, extra PCBs (8 boards) and LLPs (240 units) were prepared for backup purposes.

Fortunately, these backup units and PCBs were not needed in this experiment.

Table 5. Number of Parts and PCBs Needed in Experiment

Step	Lead Count	Parts	PCBs
DOE	44L	$20 \times 6 \times 2 = 240$	8
Backup	44L	$30 \times 8 = 240$	8
Total	44L	480	16

CHAPTER 4

RESULT AND DISCUSSION

The results of the Shear Test and Temperature Cycle Test, mentioned in Chapter 3, are presented in this chapter. This includes the experimental data and data analysis. Along with the experimental results, the validity of these results are also discussed at the end of each section.

4.1 Solder Joint Thickness

The nominal solder joint thickness was 2 mils, which is the general dimension for production units. The solder joint thickness is controlled by solder paste type, stencil design, and process control. All these factors can cause a variation in the solder joint thickness. Units were sampled for solder joint thickness measurement. The average solder joint thickness was found to be 2.39 mils, which is reasonably close to 2 mils, the nominal solder joint thickness. The measurement data and the statistical values, including the maximum, minimum, average and standard deviation of the solder joint thickness are shown in Appendix B.

4.2 Shear Test

A typical sheared surface of the solder joints of a 44L LLP is shown in Figure 42. The sheared surfaces of the solder joint formed by a single pin, on the PCB side and the package side, are shown in Figure 43. The measurement of shear forces, the sample

calculation of shear force to shear strength conversion, the table of nominal solder joint area for designs A to F, and the converted shear strength of each unit are shown in Appendix C-1, C-2, C-3, and C-4, respectively. The average shear strength, for each of the six designs, is summarized in Table 6, along with the predominant failure mode. Details of the failure mode of each sample is contained in Appendix D.

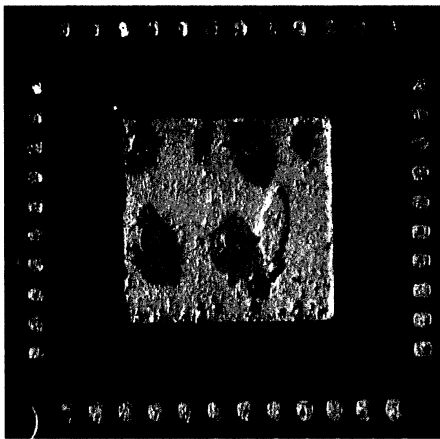


Fig. 42(a) Sheared surface of solder joint on PCB side (unit 1-B-3).

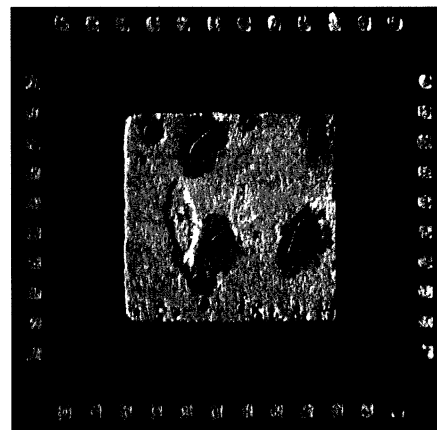


Fig. 42(b) Sheared surface of solder joint on package side (unit 1-B-3).

Figure 42. Sheared surface of solder joints of a 44L LLP.

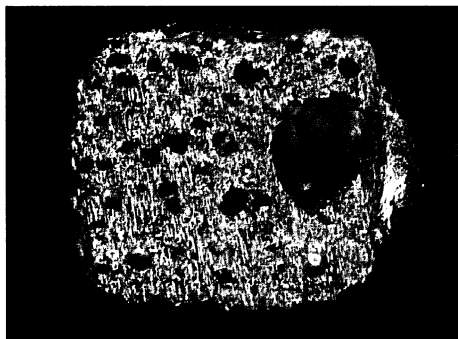


Fig. 43(a) Shear surface of pin 2 on PCB side (unit 1-A-2)

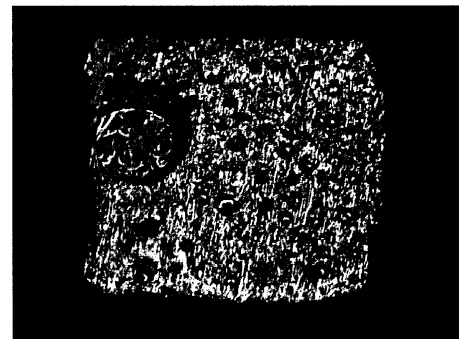


Fig. 43(b) Shear surface of pin 2 on package side (unit 1-A-2)

Figure 43. Sheared surfaces of solder joints on PCB and package sides.

Table 6. Predominant Failure Mode of Designs A to F

Design	Average Shear Strength (τ) (lb/mm ²)	Failure Mode*	
		Major	Minor
A	7.11 ± 0.78	3	4
B	7.67 ± 0.34	3	N/A
C	7.44 ± 0.14	3	4
D	8.33 ± 1.11	3	4
E	7.69 ± 0.49	3	4
F	7.77 ± 0.27	3	4

* Failure mode types according to Figure 37.

It can be seen that Mode 3 is the predominant failure mode, which means that most of the parts had been sheared through the solder joints, implying that the solder joints are the weakest part in the whole system. Improvements to the solder material's mechanical properties will contribute to improving solder joint strength, which in turn will help improve the reliability of this package/PCB system.

Design D had the highest shear strength. Analysis of Variance Test (ANOVA) was employed to test the significance of the data. Detailed calculations of ANOVA-single factor are shown in Appendix E-1 and E-2. The hypothesis of this test was that the mean shear strength is the same for all six designs. After analyzing the data, there is sufficient evidence to reject the hypothesis. At the 95% significance level, the expected shear strength of a package is not the same in the six designs. Thus, the average shear strength for each design in Table 6 is different. Although this result has been verified by statistical methods, it conflicts with the fact that if the same solder joint material, same

process conditions and same solder joint thicknesses are used, then the shear strength should be the same regardless of the area. This is because $\tau = F/A$. τ , F and A represent shear strength, shear force and solder joint area, respectively. The possible reason for this contradiction is that the effect of voids in the solder joints was not considered. From the X-ray micrographs for each design, several voids inside the solder joints were observed. These voids can also be seen in the micrograph of the sheared surfaces, as shown in Figure 42 and 43. The initiation mechanism of voids in surface mount techniques (SMT) was discussed in the Chapter 2. When calculating the shear strength, the nominal solder joint area, instead of the true solder joint area, was used. However, the extent of void formation differs from unit to unit. The existence of voids can reduce the shear force measured. The bigger the void volume, the lower the shear force. If the nominal solder joint area is used, then the lower shear strength can be obtained for those units with a lower shear force. To verify this assumption, the void volume of each unit needs to be estimated, and the true solder joint area for each unit can be determined. This can be done by photo scanning all the X-ray pictures into digital images, followed by estimation of the voiding area of each unit. Due to time limitations, this verification could not be completed during the course of this study.

The remnants of an unknown liquid inside a void is shown in Figure 44. The amount of this liquid was not sufficient for further analysis.

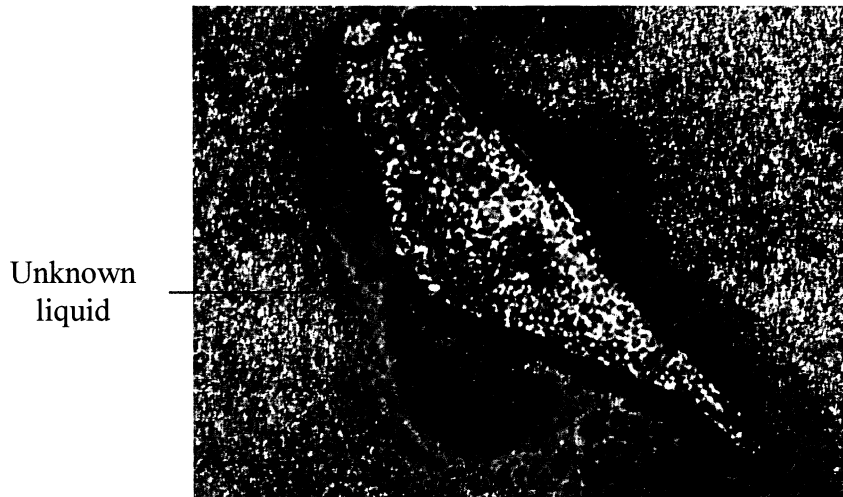


Figure 44. Unknown liquid inside the void of solder joint at DAP area.

Two “four-month-old units,” i.e., units that were surface mounted about four months earlier, with the same process conditions and materials were sheared and some tacky material was found inside the voids of the solder joint at the DAP area, as shown in Figure 45. The voids contained some tacky materials, indicating the presence of flux residues. If it was water, it should have vaporized or remained as a liquid and should not have displayed viscous behavior. This evidence also confirmed that flux entrapment is the major reason of void formation for this particular LLP package type/process sequence combination.

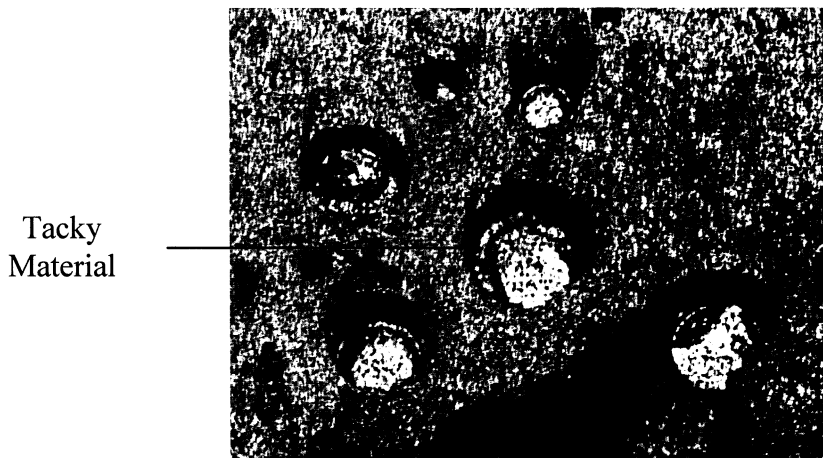


Figure 45. Tacky material inside the void of solder joint at DAP area for a four-month-old unit.

4.3 Temperature Cycling Test

The detailed measurements of the loop resistance are contained in Appendix F. The number of cycles to failure for each board and each part are presented in Table 7. A summary of the number of failures per design is shown in Table 8. The “first failed pin” stands for the first pin that was detected as being open during the loop resistance measurements. The location of the first failed pins for each part is shown in Figures 46 to 49. The number in brackets shows the number of cycles to failure; the units with no number indications are those units which had no failures after 3003 cycles, i.e., the “Good” units in the Table 7. The gray area in Figures 46 to 49 are schematic representations of the soldered DAP area.

Table 7. Number of Cycles to Failure of Each Board and Each Unit

Unit ID	# 5	# 6	# 7	# 8
A-1	409	223	267	267
B-1	2720	0	925	Good*
C-1	2627	1113	1555	2333
D-3	925	925	1414	877
E-3	1955	Good*	Good*	Good*
F-3	Good*	Good*	Good*	Good*
D-1	1414	502	737	643
E-1	Good*	2910	2910	Good*
F-1	Good*	Good*	2816	Good*
A-4	549	455	315	361
B-4	1294	2816	1461	Good*
C-4	2436	2051	1461	1767
A-2	502	168	315	223
B-2	Good*	1361	1294	2357
C-2	1511	1159	1555	1909
D-4	1064	502	737	361
E-4	Good*	Good*	2910	Good*
F-4	Good*	Good*	Good*	Good*
D-2	1652	549	691	1294
E-2	Good*	2357	Good*	Good*
F-2	Good*	Good*	Good*	Good*
A-5	502	409	267	223
B-5	1461	Good*	1361	2436
C-5	1909	2146	2051	1606
A-3	502	455	168	168
B-3	OK	1652	1511	2146
C-3	2720	1205	1767	1018
D-5	1205	1294	833	877
E-5	Good*	Good*	Good*	Good*
F-5	Good*	Good*	Good*	Good*

* The "Good" parts had no failures at 3003 cycles.

Table 8. Number of Failures Per Design at 3003 Cycles

Design	Number of Failures
A	20/20
B	14/19
C	20/20
D	20/20
E	5/20
F	1/20

First Failed Pins Board No. 5

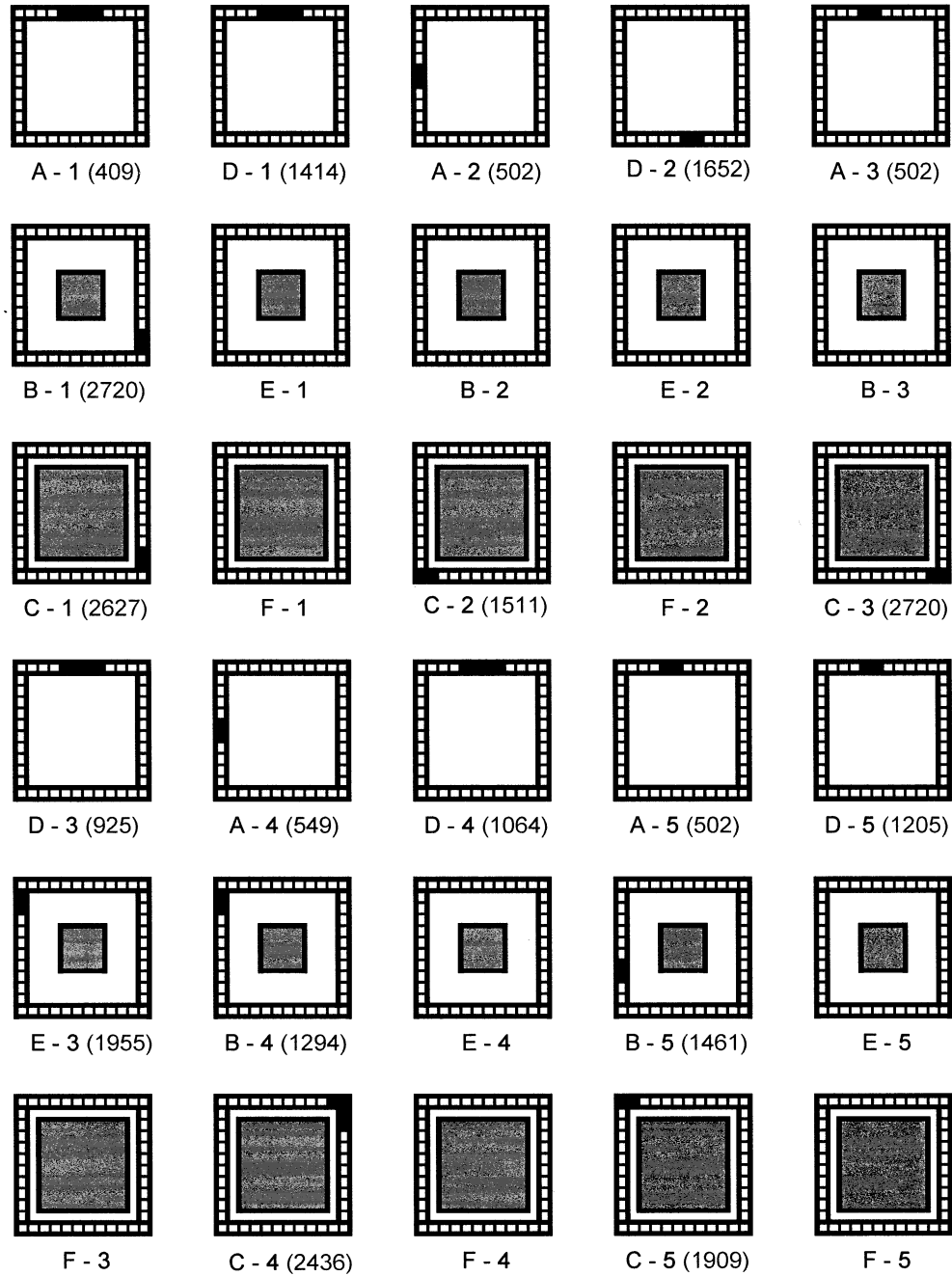


Figure 46. Indication of first failed pins for Board # 5 (the number in the brackets shows the number of cycles to failure; the units without number were still good after 3003 cycles).

First Failed Pins Board No. 6

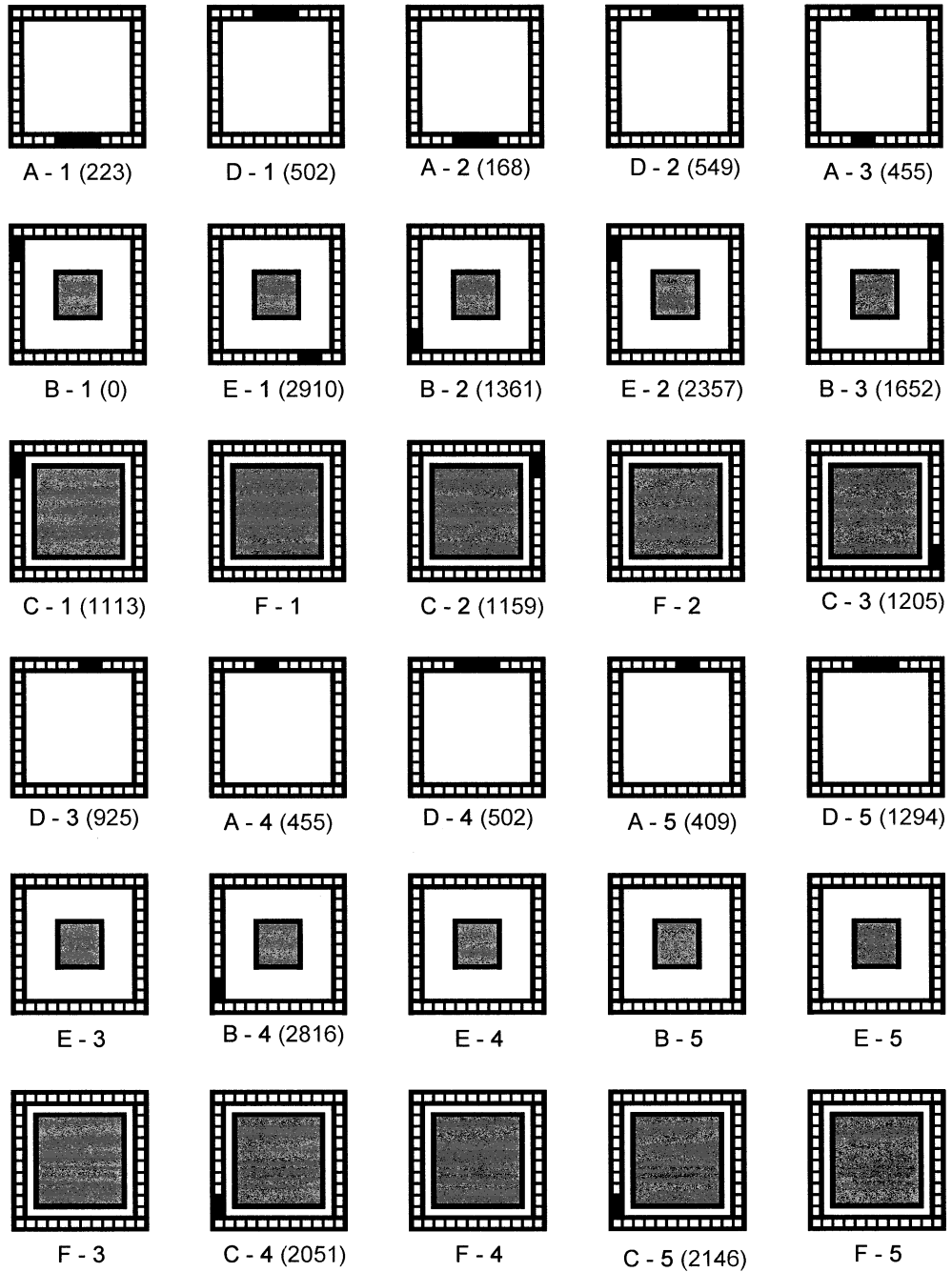


Figure 47. Indication of first failed pins for Board # 6 (the number in the brackets shows the number of cycles to failure; the units without number were still good after 3003 cycles).

First Failed Pins Board No. 7

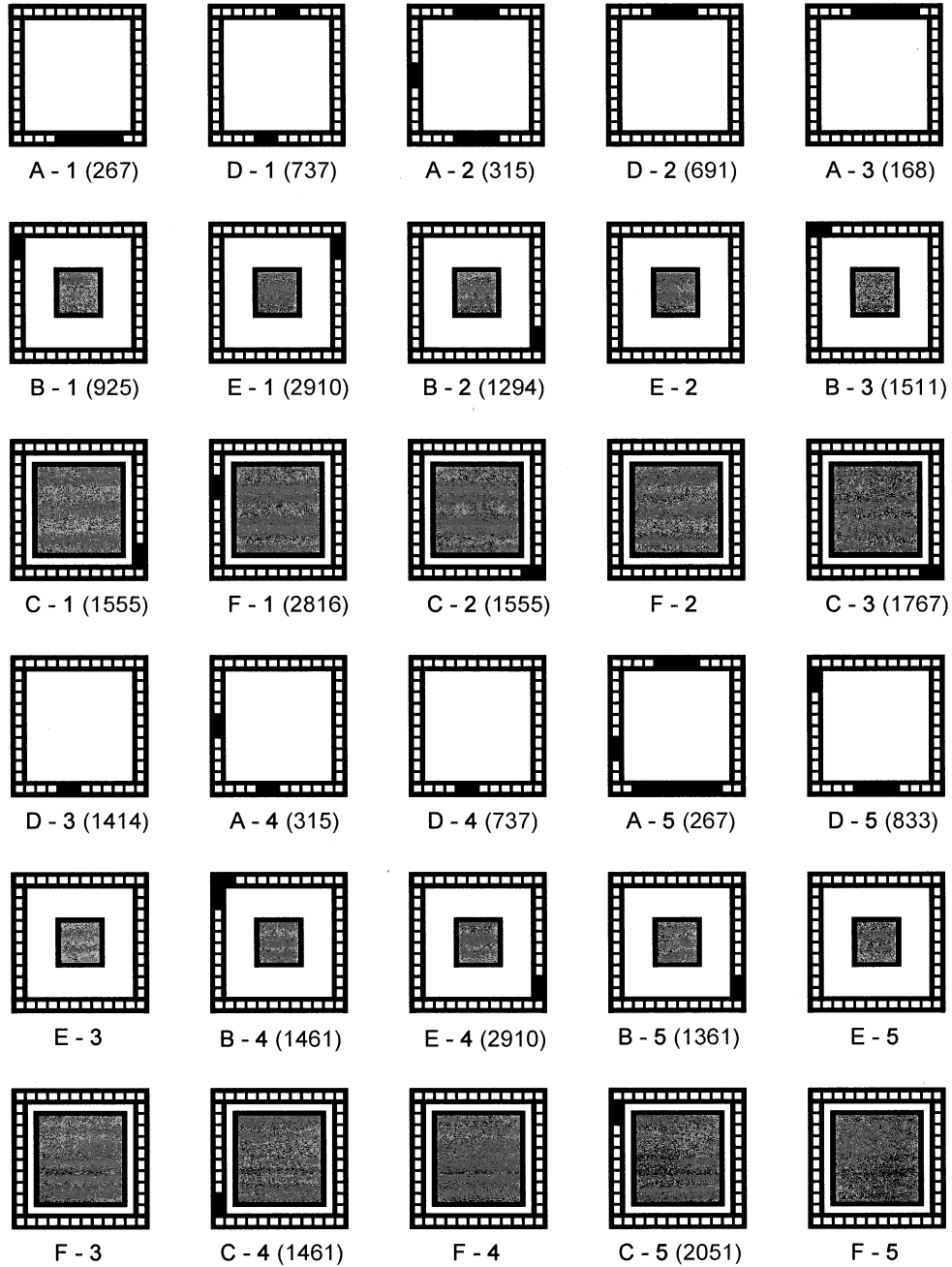


Figure 48. Indication of first failed pins for Board # 7 (the number in the brackets shows the number of cycles to failure; the units without number were still good after 3003 cycles).

First Failed Pins Board No. 8

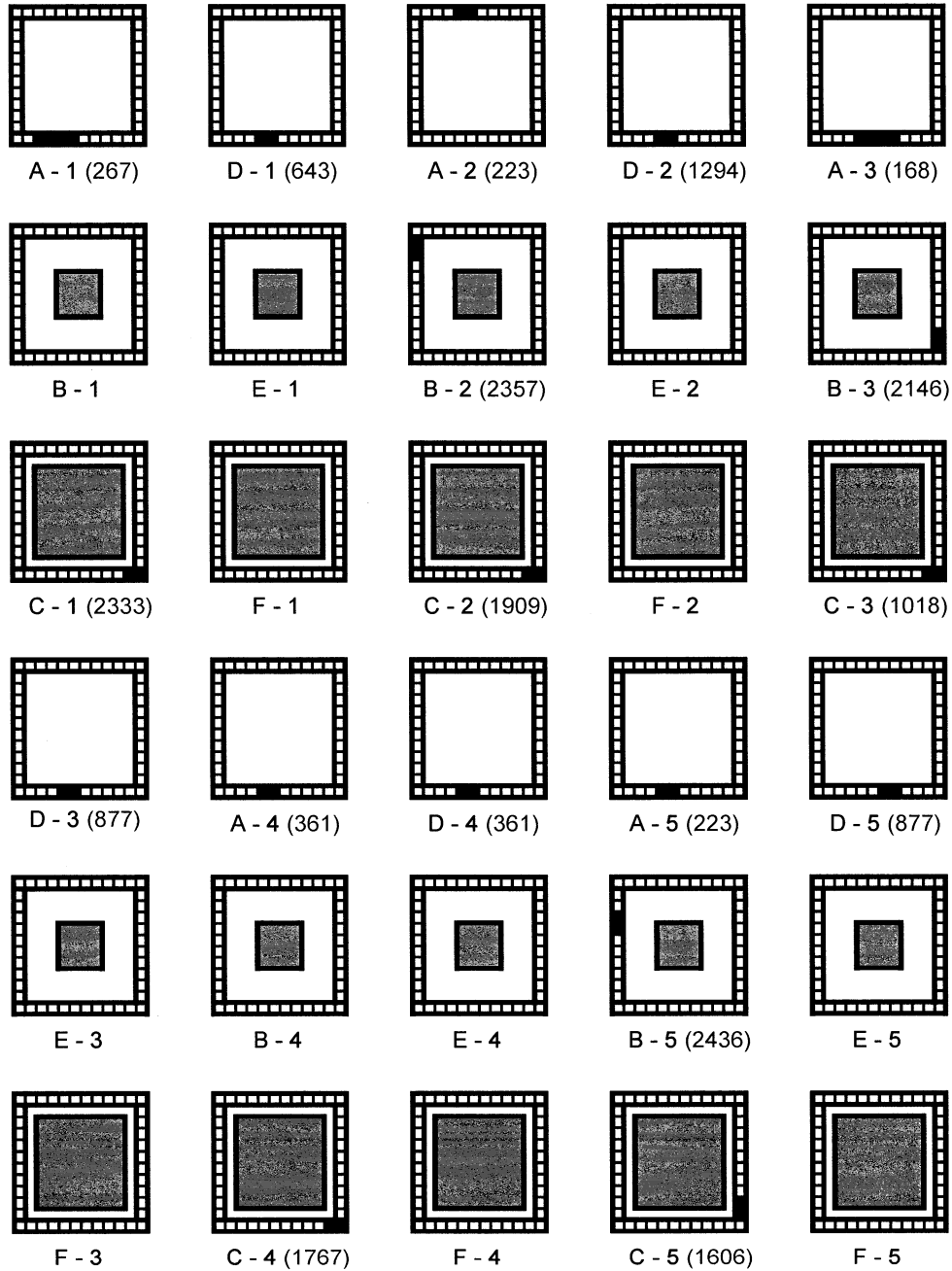


Figure 49. Indication of first failed pins for Board # 8 (the number in the brackets shows the number of cycles to failure; the units without number were still good after 3003 cycles).

From the results shown in Tables 7 and 8, Design E and F were found to survive longer than the other designs in the temperature cycle test. This leads to the conclusion that those parts with the DAP soldered down are better than the parts where the DAP was not soldered down. From Figures 44 to 47, it can be seen that most of the units failed at the corner pins, which matches the prediction that the stresses concentrate at the corner and therefore the corner pins fail first. However, this behavior was not observed for designs A and D. It was found that most of the first failed pins for designs A and D were observed at top and bottom rows of the pins. This is shown in Figure 50.

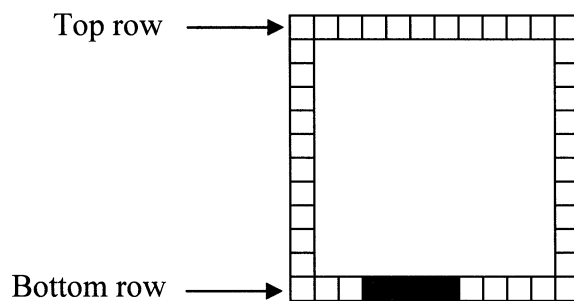


Figure 50. Indication of top and bottom rows of the pins (red color squares shows the first failed pins).

In order to explain this phenomenon, the “Scoop Effect” needs to be introduced. Before explaining the scoop effect, the surface mounting process needs to be understood better. First, a solder mask with a 1:1 ratio to the PCB was made for solder paste application. Second, the mask was aligned to the PCB pattern and solder paste was applied on the top of mask. Third, the solder paste was then transferred onto the PCB pattern by squeezing the solder paste through the mask with a squeegee. The squeegee is made of an elastic material. When squeezing through a mask, some solder paste will be “scooped” out of its

desired volume. This is the so-called “Scoop Effect”. When the long side of the aperture is perpendicular to the squeezing direction, the scoop effect is more obvious than when it is parallel in the squeezing direction. This is illustrated in the schematic drawing in Figure 51.

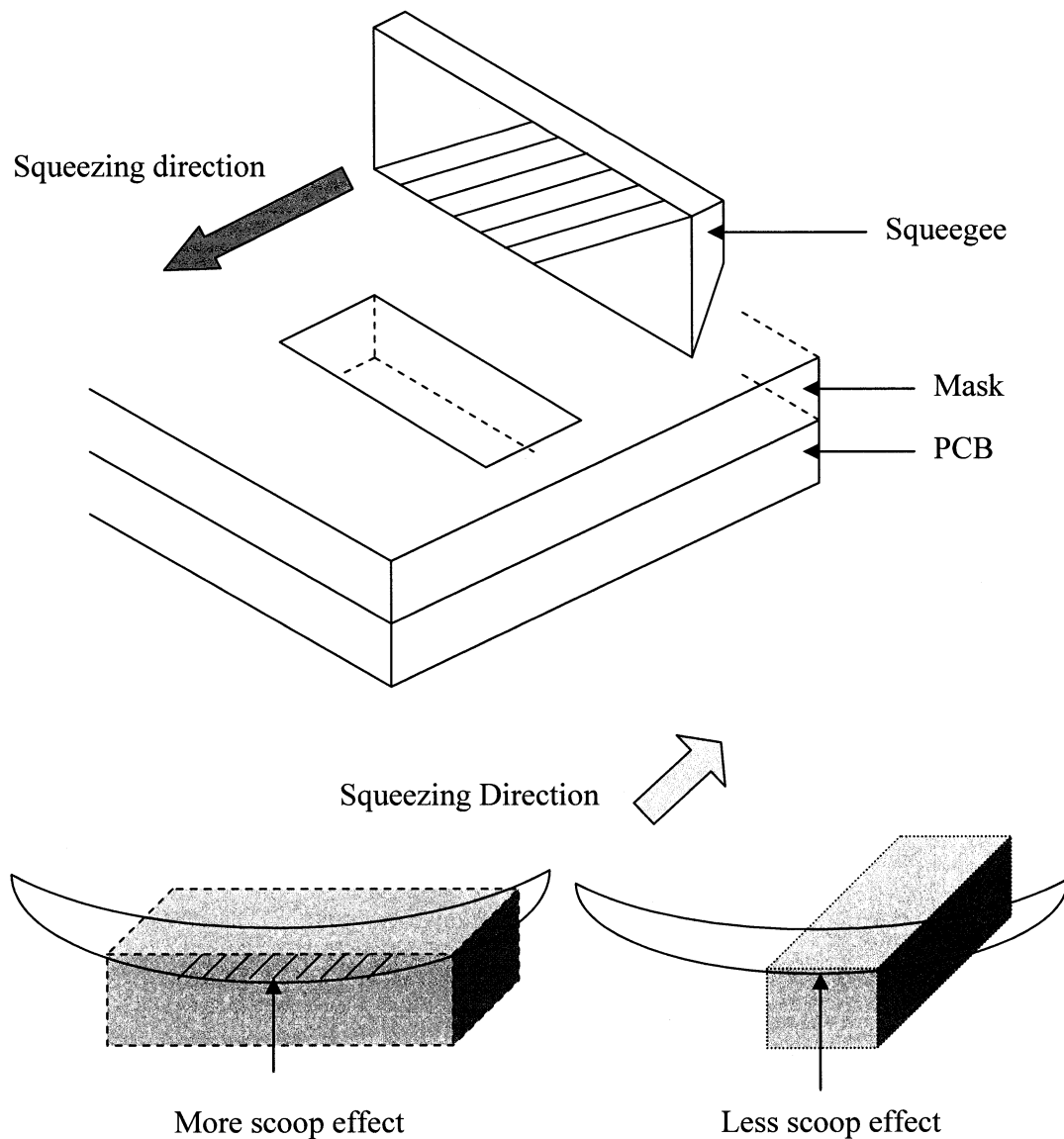


Figure 51. Schematic drawing of Scooping Effect.

For designs A and D, most of the pins that failed first were at the top and bottom rows, where the long side of the aperture of the pins was perpendicular to the travel direction of the squeegee. This may have caused an insufficient solder problem after the surface mount process. Those pins with insufficient solder may fail first during the temperature cycle test. This is a hypothesis at this time and needs verification. Most of the units of designs A and D “popped out”, which means all the solder joints completely cracked and lost their ability to hold the units onto the PCB during the temperature cycle test. Cross-sectioning was performed for those units still mounted on the PCBs.

The Weibull distribution of the cumulative failures for designs A to F is shown in Figure 52. The calculation of how to obtain these Weibull distributions is shown in Appendix G. From Figure 52, design A was found to have the shortest life, followed by design D. The longest life was found for design F, which had only one failure after 3000 cycles.

According to the result shown in Figure 52, the most important finding is that designs with large land areas were found to have longer life than designs with smaller land areas. This can easily be seen when the Weibull plot for each of the designs are compared. This is not surprising. When the solder joints area is larger, the ability for the solder joints to hold a LLP is better.

Designs with the DAP soldered down were also found to have a longer life than designs without the DAP soldered down. This can be obtained by comparing the results of designs A and D to those of designs B, C, E and F.

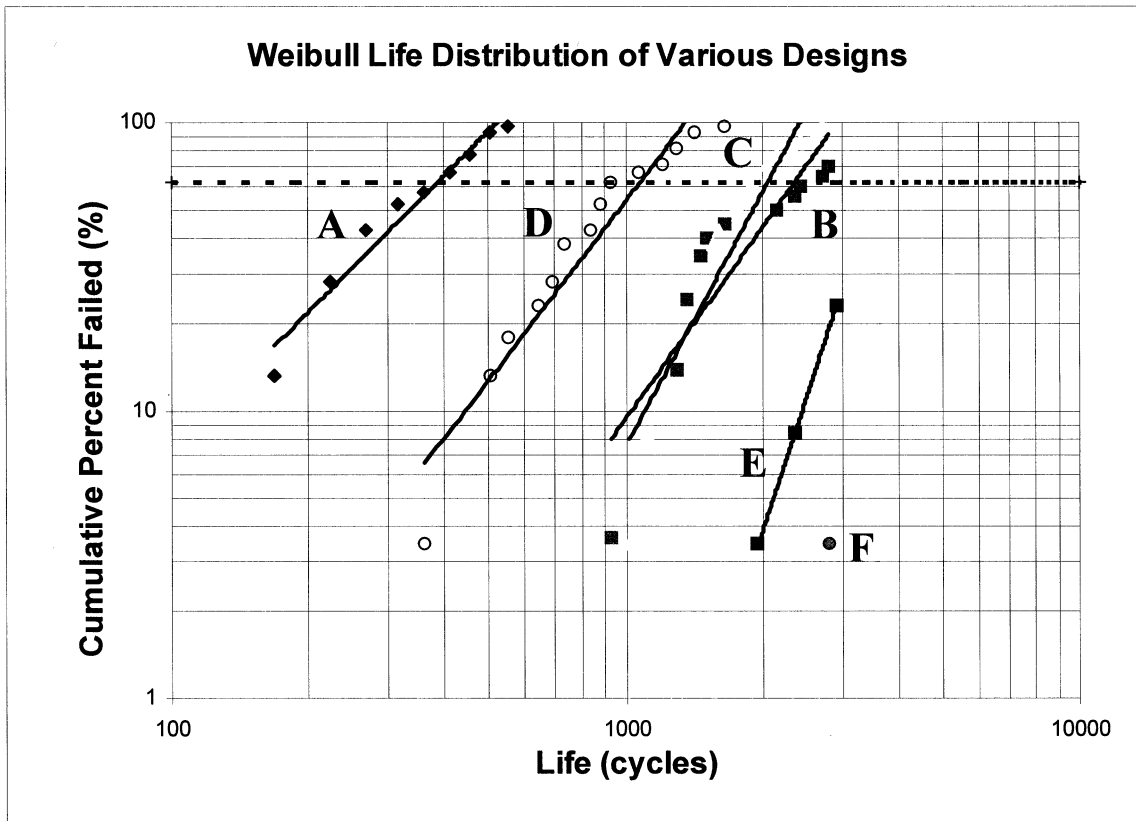


Figure 52. Weibull plots of the designs A to F.

This is because the LLPs with the DAP soldered down provide better support to holding the packages. However, when comparing the results of design B (small land area, 50 % DAP area) and design C (small land area, 100% DAP area), the two distributions cross each other. A similar comparison of designs E and F, which also have the same difference in the DAP soldered area, does not show the same trend. Conclusions regarding the effect of percentage DAP area soldered down cannot be drawn at this time, without further detailed investigations.

In order to understand the failure mechanism of the failed parts during the temperature cycling tests, the failed units were cross-sectioned after 3003 cycles. The different parts and materials in a LLP solder joint are shown in Figure 53. The cross-section pictures of first failure pins of each design are shown in Figure 54-59.

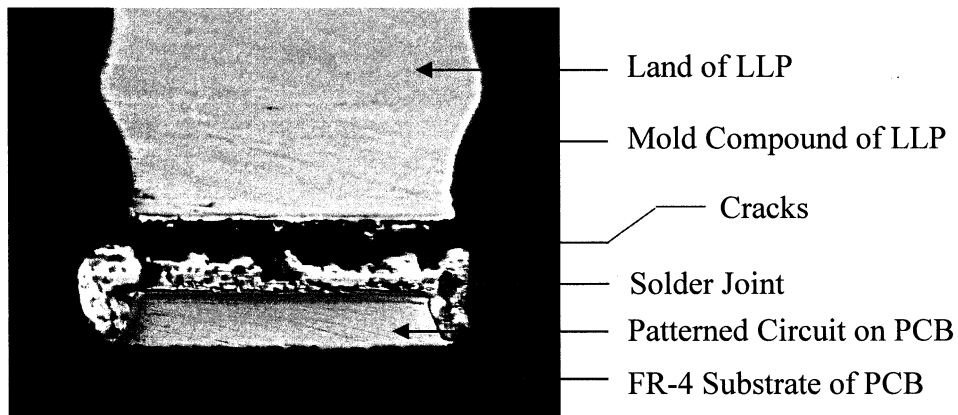


Figure 53. Indication of the cross-section pictures.

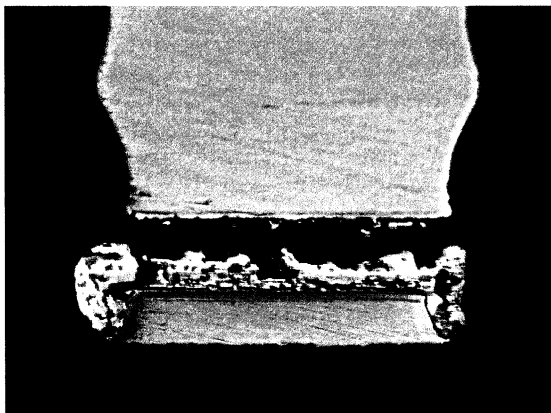


Fig. 54(a) A Design (5-A-2-Pin27)

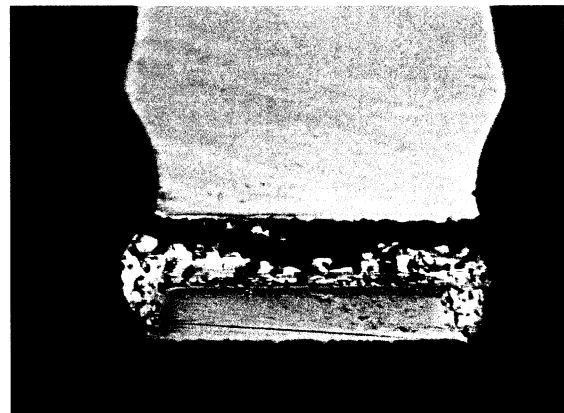


Fig. 54(b) A Design (5-A-2-Pin28)

Figure 54. Solder joints cross-section of design A.

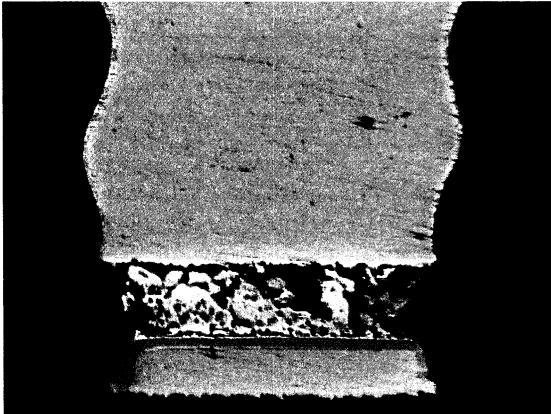


Fig. 55(a) B Design (5-B-1-Pin10)

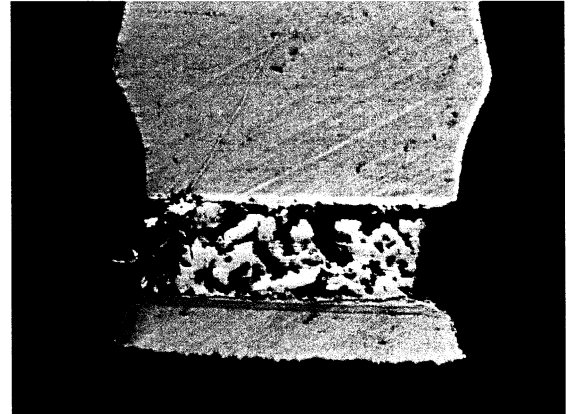


Fig. 55(b) B Design (5-B-5-Pin26)

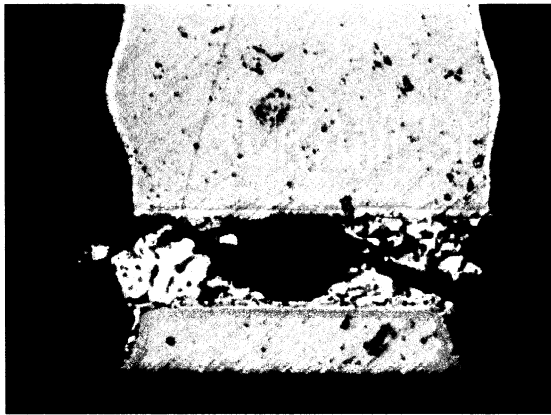


Fig. 55(c) B Design (7-B-3-Pin33)

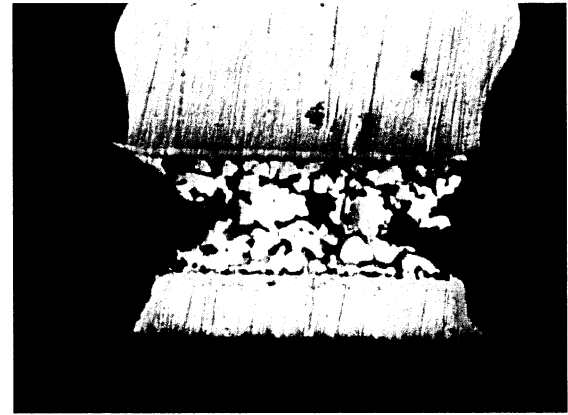


Fig. 55(d) B Design (8-B-2-Pin32)

Figure 55. Solder joints cross-section of design B.

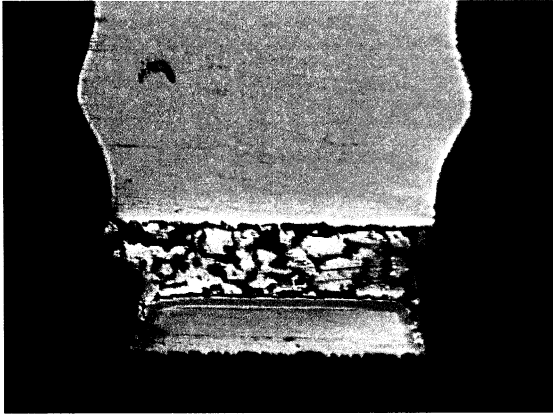


Fig. 56(a) C Design (5-C-2-Pin21)

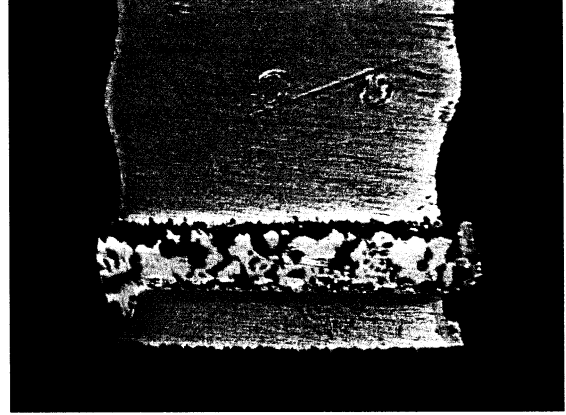


Fig. 56 (b) C Design (5-C-5-Pin 37)

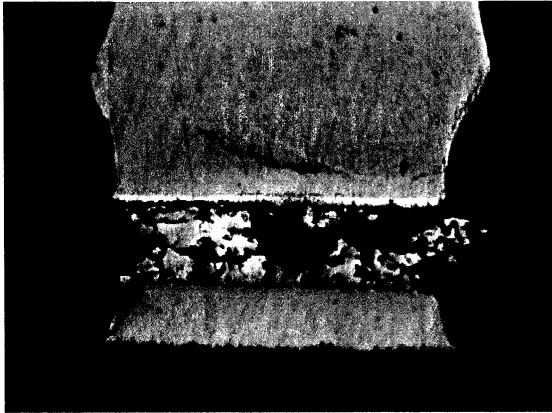


Fig. 56(c) C Design (7-C-4-Pin24)

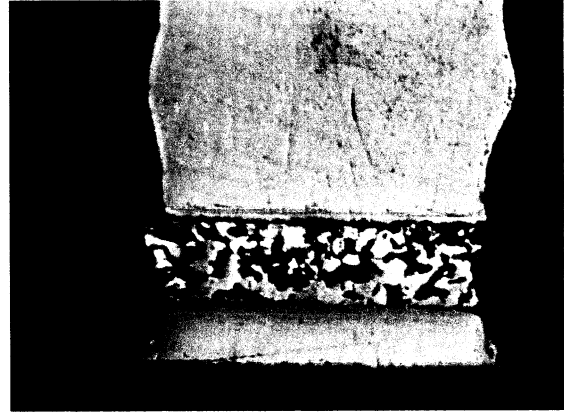


Fig. 56 (b) C Design (8-C-5-Pin 10)

Figure 56. Solder joints cross-section of design C.

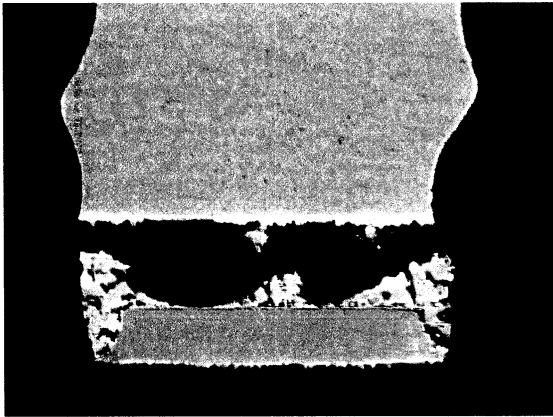


Fig. 57(a) **D** Design (5-D-5-Pin37)

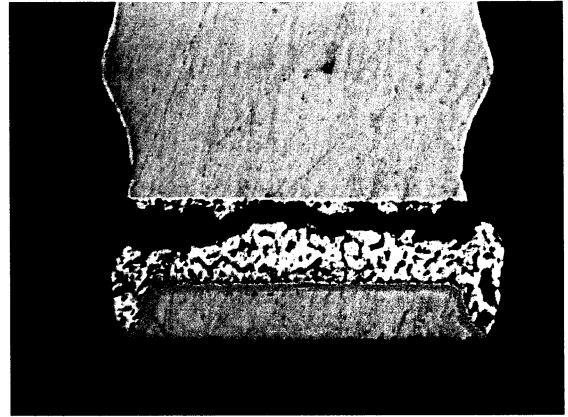


Fig. 57(b) **D** Design (6-D-2-Pin39)

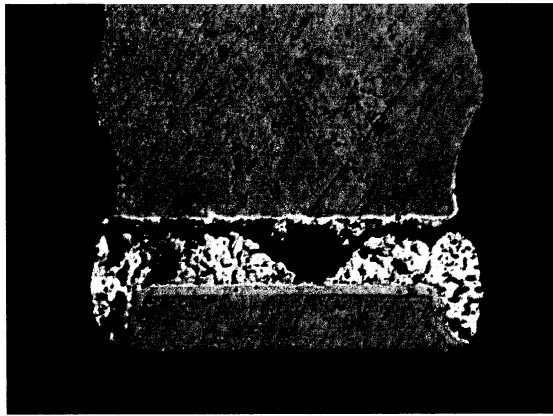


Fig. 57(c) **D** Design (7-D-1-Pin40)

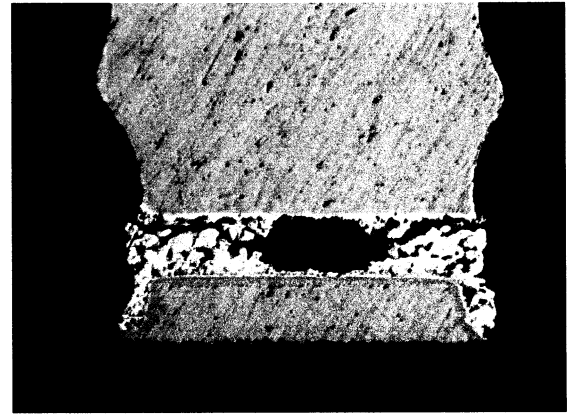


Fig. 57(d) **D** Design (7-D-2-Pin40)

Figure 57. Solder joints cross-section of design D.

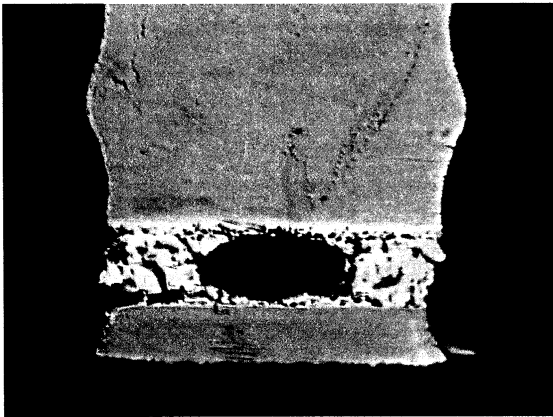


Fig. 58(a) E Design (6-E-1-Pin13)

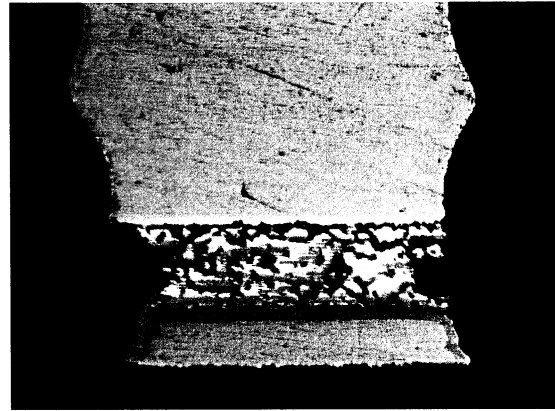


Fig. 58(b) E Design (5-E-3-Pin31)

Figure 58. Solder joints cross-section of design E.

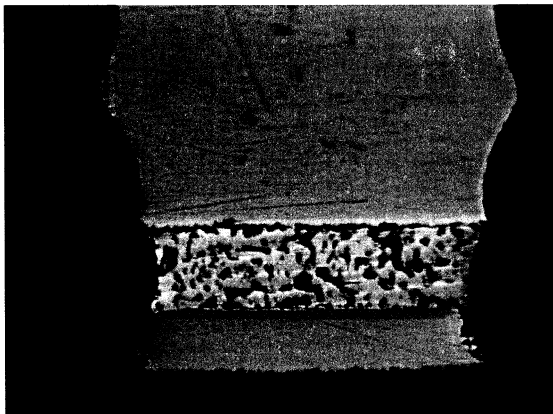


Fig. 59(a) F Design (7-F-1-Pin29)

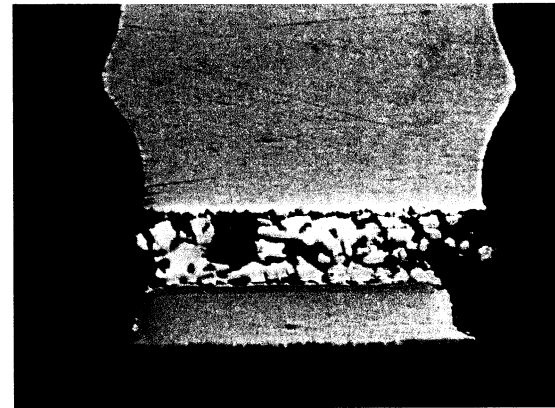


Fig. 59(b) F Design (7-F-1-Pin30)

Figure 59. Solder joints cross-section of design F.

It can be seen that the presence of voids may not be the reason for the failure of LLPs during the temperature cycling tests, unless if the voids are too big and result in insufficient solder for the solder joints. Stresses can be concentrated when a stress raiser exists. In this LLP solder joint system, two stress raisers, namely, sharp edges at interface and the voids, are shown in Figure 60.

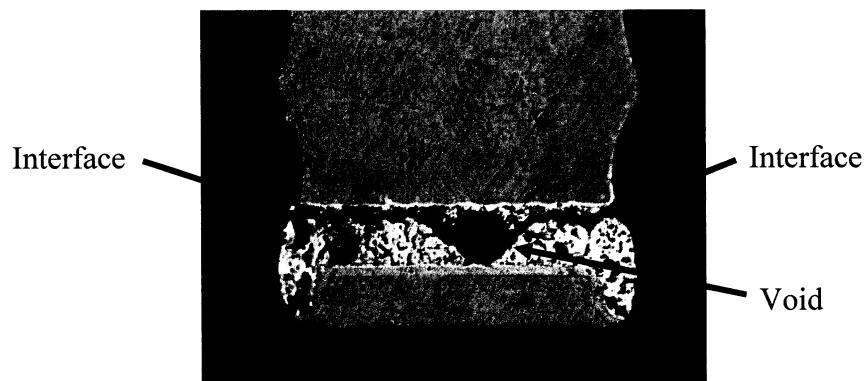


Figure 60. Stress raisers inside a LLP solder joint.

The place where a crack initiates and propagates depends on the presence of the critical stress required for that to happen. During the temperature cycle test, the highest stresses occurred at the interfaces between (a) the land and the solder and (b) the solder and copper circuit trace due to the coefficient of thermal expansion (CTE) mismatch between the constituents in each of these couples. In addition to the CTE mismatch, the formation of Sn-Cu intermetallic compound may cause interface embrittlement, thus increasing the crack propagation rate [23]. Once the cracks initiate, they will propagate through the path of least resistance during thermal cycling. According to the finite element models proposed by J. H. Lau et al [24], the magnitudes of the stresses and strains in a solder

joint with a void are larger than those in a void-free solder joint. Further, the stress and strain around the void is higher than at other places throughout the solder joint. This can explain why the cracks propagate through the voids inside the solder joints, as can be seen in figures 55(c), 56(c), 57(a)(c)(d), and 58(a).

From the results of shear testing, most of the parts had been sheared through the solder joints, which means the solder joints are the weakest part in the whole system. The tacky residue inside the voids was the evidence to confirm that flux entrapment is the major reason for void formation for this particular LLP package type/process combination. The void content inside the solder joints also needs to be estimated in order to obtain a correct value of the real shear stress.

From the temperature cycle test, the “Scoop Effect” was employed to explained the reason why most of the first failed pins were found at the top and bottom rows for designs A and D. After 3003 temperature cycles, the designs with large land areas were found to have a longer life than designs with smaller land area. Also, the designs with DAP soldered down were found to have a longer life than designs without DAP soldered down. However, the effect of the DAP soldered down area (50% vs. 100%) cannot be discerned since their Weibull Distribution Curves crossed each other.

From the failure analysis, most of the cracks were found to initiate near the edge of land/solder or solder/copper circuit trace interfaces. They then propagated through the voids inside the solder joints. The presence of voids, however, may not be the primary reason for failure during temperature cycle testing, unless if the void is too big and results in insufficient solder for the solder joints.

CHAPTER 5

CONCLUSION

The results presented in the previous chapter have led to several conclusions. Mode 3 failure, namely, failure through the solder metal was found to be the predominant failure mode during shear testing. In other words, the solder joints are the weakest part in the whole system. Improvements on the strength of the solder metal can help obtain higher reliability performance of the LLP/PCB system investigated.

A viscous liquid, identified as flux residue, was found inside the void. This flux residue confirmed that flux entrapment is the major reason for void formation.

From the results of temperature cycle testing it was found that (a) the designs with larger land areas had a longer life than designs with smaller land areas, and (b) designs with DAP soldered down had a longer live than designs without DAP soldered down. The effect of extent of DAP area soldered down, namely 50% or 100%, could not be determined.

Cracks leading to failure were found to initiate near the edge of the land/solder or solder/copper circuit trace interfaces, where the stresses are the highest due to the CTE mismatch. Once the cracks initiate, they propagate to the voids, where the stress and strain around the void is higher than at other places, before propagating through the entire solder joint.

CHAPTER 6

FUTURE WORK

Detailed investigation of the effect of percentage DAP area soldered down on failure rate during temperature cycling test needs to be done. In addition, interaction between land area and percent DAP area soldered down on reliability needs to be clarified. Furthermore, analysis of viscous residues in voids needs to be completed for accurate determination of the void formation mechanism. Finally, fractographic analysis of failed solder joints needs to be performed to accurately determine the fracture origin sites and propagation mechanism.

REFERENCES

1. J.H. Lau and Y.H. Pao, "Solder Joint Reliability of BGA, CSP, Flip Chip, and Fine Pitch SMT Assemblies," McGraw-Hill, (1996), p. 297.
2. P. Thompson, "Chip Scale Package Tutorial," Semiconductor Equipment and Materials International, (Semicon Taiwan, 1997), pp. 12-14.
3. National Semiconductor Corp. Official Web Site:
<http://www.national.com/packaging/llp>, "LLP Chip Scale Packaging".
4. M.G. Pecht, L.T. Nguyen and E.B. Hakim, "Plastic-Encapsulated Microelectronics," John Wiley & Sons, Inc., (1995), p. 261.
5. M.G. Pecht, L.T. Nguyen and E. B. Hakim, "Plastic-Encapsulated Microelectronics," John Wiley & Sons, Inc., (1995), p. 267.
6. J. H. Lau and Y.H. Pao, "Solder Joint Reliability of BGA, CSP, Flip Chip, and Fine Pitch SMT Assemblies," McGraw-Hill, (1996), pp. 59-63.
7. T.A. Krinke and D.K. Pai, "Factors Affecting Thermal Fatigue Life of LCCC Solder Joints," Welding Journal, v 67 n 10, Oct 1988, pp. 33-40.
8. Y.P. Wu and J.K.L. Lai, "Reliability Studies of Plastic Ball Grid Array Assemblies Reflowed in Nitrogen Ambient," Proceeding of Electronic Components and Technology Conference, 1998 IEEE, pp. 292-296.
9. J.H. Lau, G. Harkins, D. Rice, J. Kral and B. Wells, "Experimental & Statistical Analyses of Surface-Mount Technology PLCC Solder-Joint Reliability," IEEE Transactions on Reliability, v 37 n 5, Dec 1988, pp. 524-530.
10. M.G. Pecht, L.T. Nguyen and E. B. Hakim, "Plastic-Encapsulated Microelectronics," John Wiley & Sons, Inc., (1995), p. 169.
11. JEDEC STANDARD: J-STD-020, "Moisture/Reflow Sensitivity Classification for Nonhermetic Solid State Surface Mount Devices," April 1999.
12. M. Ohring, "Reliability and Failure of Electronic Materials and Devices," Academic Press, (1998), pp. 440-441.
13. W.B. Hance and N. Lee, "Formation and Control of Voiding in SMT," Int. Soc. Hybrid Microelectron (ISHM) Proceedings, 1992, pp. 535-542.

14. W.B. O'Hara and N. Lee, "*Voiding Mechanism in BGA Assembly*," The International Journal of Microcircuits and Electronic Packaging, v 19 n 3, 1996, pp. 190-198.
15. W.B. O'Hara and N. Lee, "*Controlling Solder Joint Voiding in BGA Assembly*," Surface Mount Technology, April 1998, pp. 68-72.
16. N. Lee, private communication, (August 2000).
17. D.V. Ragone, "*Thermodynamics of Materials - Volume I*," John Wiley & Sons, Inc., (1995), pp. 133-145.
18. P.W. Barnes, "*Pressure Variation Method for Fluxless, Void-free Ball/Chip Attach*," paper provided by National Semiconductor Corporation Library Services, unpublished.
19. IPC STANDARD: IPC-SM-785, "*Guidelines for Accelerated Reliability Testing of Surface Mount Attachments*," November 1992.
20. M. Ohring, "*Reliability and Failure of Electronic Materials and Devices*," Academic Press, (1998), pp. 193-202.
21. J.H. Lau and Y.H. Pao, "*Solder Joint Reliability of BGA, CSP, Flip Chip, and Fine Pitch SMT Assemblies*," McGraw-Hill, (1996), pp. 29-36.
22. K.N. Berk and P. Carey, "*Data Analysis with Microsoft Excel*," International Thomson Publishing Company, (1995), pp. 304-313.
23. J.H. Lau and Y.H. Pao, "*Solder Joint Reliability of BGA, CSP, Flip Chip, and Fine Pitch SMT Assemblies*," McGraw-Hill, (1997), pp. 75-80.
24. J.H. Lau and A.H. Jeans, "*Effects of Voids on SMT Solder Joint Reliability*," paper provided by National Semiconductor Corporation Library Services, unpublished.

APPENDIX A

Moisture Sensitivity Levels

Improper storage, handling, or assembly processes for plastic encapsulated microelectronic packages will allow the introduction of moisture into the device. The trapped moisture will cause damage during the surface mount process due to the moisture vaporizing and expanding. J-STD-020 defines a moisture sensitivity classification for the user to have a better idea about how to store and handle the device without damaging the device during the surface mounting and repairing processes. For example, for Level 1 sensitivity, the tested packages are soaked in an environmental chamber at 85°C/85% RH for 168 hours, followed by three passes of VPR or IR reflows. The samples are then inspected with a Scanning Acoustic Microscope to check if there are any delaminations or cracks. If a package type passes Level 1, the factory floor life will be unlimited for this specific package type.

Table A-1 Package Moisture Sensitivity Levels per J-STD-020

Level	Factory Floor Life		Soak Requirements (Preconditioning)			
	Conditions	Time	Time			Conditions
1	≤ 30°C/90% RH	Unlimited	168 hours			85°C/85% RH
2	≤ 30°C/60% RH	1 year	168 hours			85°C/60% RH
			Time (Hours)			
			X +	Y =	Z	
3	≤ 30°C/60% RH	168 hours	24	168	192	30°C/60% RH
4	≤ 30°C/60% RH	72 hours	24	72	96	30°C/60% RH
5	≤ 30°C/60% RH	24 / 28 hours	24	24 / 28	48 / 72	30°C/60% RH
6	≤ 30°C/60% RH	6 hours	0	6	6	30°C/60% RH

APPENDIX B

Solder Joint Thickness Measurement and Statistical Values

24 units (12 units/PCB) were sampled for solder joint thickness measurement. The thickness for every unit is shown in Table B-1. The maximum, minimum, average and standard deviation values are also shown in Table B-1.

Table B-1 Solder Joint Thickness

Board No.	Unit ID	Thickness (mil)	Statistical Data
1	A-1	2.10	Ave. = 2.39 Min. = 1.40 Max. = 3.00 Std Dev. = 0.38 Range = 1.60
	B-1	2.30	
	C-1	2.30	
	D-1	2.40	
	E-1	2.50	
	F-1	2.40	
	A-5	1.80	
	B-5	2.90	
	C-5	2.60	
	D-5	2.40	
	E-5	2.60	
	F-5	2.70	
5	A-1	1.80	
	B-1	2.50	
	C-1	2.50	
	D-1	2.60	
	E-1	3.00	
	F-1	2.70	
	A-5	1.40	
	B-5	2.20	
	C-5	2.40	
	D-5	1.90	
	E-5	2.60	
	F-5	2.80	

APPENDIX C

Shear Force Measurement and Shear Strength Determinations

Shear force measurement and determination of shear strength are demonstrated in Appendix C. Appendix C-1 shows the shear force for each unit. Appendix C-2 is a demonstration of how to determine the shear strength from shear force. Appendix C-3 is the nominal solder joint area for designs A to F. The shear strength and averaged shear strength for designs A to F are shown in Appendix C-4.

APPENDIX C-1

Records of Shear Force Measurement for Designs A to F

Table C-1 Records of Shear Force Measurement for Design A to F

Unit ID	Shear Force (lb)			
	Board 1	Board 2	Board 3	Board 4
A-1	20	26	-	23
A-2	24	27	21	17
A-3	24	28	24	26
A-4	22	23	20	28
A-5	23	24	20	26
B-1	133	111	113	120
B-2	138	123	127	123
B-3	133	127	108	110
B-4	123	112	124	110
B-5	130	111	127	131
C-1	242	225	210	216
C-2	226	210	217	216
C-3	211	-	229	226
C-4	218	180*	242	232
C-5	219	250	241	230
D-1	42	52	-	42
D-2	53	53	52	39
D-3	31	50	43	47
D-4	50	45	47	46
D-5	51	38	48	41
E-1	152	147	146	132
E-2	142	115**	146	150
E-3	140	151	150	149
E-4	131	143	129	131
E-5	100	136	120	145
F-1	247	266	250	219
F-2	258	258	254	252
F-3	218	279	255	233
F-4	257	278	268	251
F-5	233	271	250	260

P.S. * = Sample moved during shear test. Package crack. Data invalid.
 ** = Package crack. Data invalid.

APPENDIX C-2

Shear Strength Determinations

Design A

Board No.	Unit ID	Shear Force (lb)	Nominal Soldered Area	Shear Strength (lb/mm ²)
1	A-1	20	3.30 mm ²	6.06
	A-2	24		7.27
	A-3	24		7.27
	A-4	22		6.67
	A-5	23		6.97
2	A-1	26		7.88
	A-2	27		8.18
	A-3	28		8.48
	A-4	23		6.97
	A-5	24		7.27
3	A-1	-		-
	A-2	21		6.36
	A-3	24		7.27
	A-4	20		6.06
	A-5	20		6.06
4	A-1	23		6.97
	A-2	17		5.15
	A-3	26		7.88
	A-4	28		8.48
	A-5	26		7.88

Shear Strength = Shear Force/Nominal Soldered Area

For example, for Unit A-1, Shear Strength = 20 (lb)/3.30mm² = 6.06 lb/mm².

APPENDIX C-3

Nominal Solder Joint Area for Designs A to F

Nominal Solder Joint Area (mm²) for Design A to F

Design A	Design B	Design C	Design D	Design E	Design F
3.30	15.87	30.34	5.50	18.07	32.54

The nominal solder joint area was obtained from the Pb/Sn plated area in the Package Outline Drawing.

APPENDIX C-4

Shear Strengths Converted from Shear Forces for Designs A to F

Unit ID	Shear Strength (lb/mm ²)				Average Shear Strength (lb/mm ²)
	Board 1	Board 2	Board 3	Board 4	
A-1	6.06	7.88	-	6.97	7.11
A-2	7.27	8.18	6.36	5.15	
A-3	7.27	8.48	7.27	7.88	
A-4	6.67	6.97	6.06	8.48	
A-5	6.97	7.27	6.06	7.88	
B-1	8.38	6.99	7.12	7.56	7.67
B-2	8.70	7.75	8.00	7.75	
B-3	8.38	8.00	6.81	6.93	
B-4	7.75	7.06	7.81	6.93	
B-5	8.19	6.99	8.00	8.25	
C-1	7.98	7.42	6.92	7.12	7.44
C-2	7.45	6.92	7.15	7.12	
C-3	6.95	-	7.55	7.45	
C-4	7.19	-	7.98	7.65	
C-5	7.22	8.24	7.94	7.58	
D-1	7.64	9.45	-	7.64	8.33
D-2	9.64	9.64	9.45	7.09	
D-3	5.64	9.09	7.82	8.55	
D-4	9.09	8.18	8.55	8.36	
D-5	9.27	6.91	8.73	7.45	
E-1	8.41	8.14	8.08	7.30	7.69
E-2	7.86	-	8.08	8.30	
E-3	7.75	8.36	8.30	8.25	
E-4	7.25	7.91	7.14	7.25	
E-5	5.53	7.53	6.64	8.02	
F-1	7.59	8.17	7.68	6.73	7.77
F-2	7.93	7.93	7.81	7.74	
F-3	6.70	8.57	7.84	7.16	
F-4	7.90	8.54	8.24	7.71	
F-5	7.16	8.33	7.68	7.99	

Note: Valid data were not available in a few cases. These are denoted by “-“.

APPENDIX D

Failure Mode for Designs A to F

The shear failure modes were divided into 5 categories. Mode 3 and 4 demonstrate that the failures are sheared through solder joint and sheared at the interface between solder joint and PCB trace, respectively.

Table D-1 Failure Mode of Each Unit for Designs A to F

Unit ID	Failure Mode				Predominant Failure Mode
	Board 1	Board 2	Board 3	Board 4	
A-1	3	3	-	3	3
A-2	3	3	3	3	
A-3	3	3	3	3/4	
A-4	3	3	3/4	3/4	
A-5	3	3	3/4	3/4	
B-1	3	3	3	3	3
B-2	3	3	3	3	
B-3	3	3	3	3	
B-4	3	3	3	3	
B-5	3	3	3	3	
C-1	3/4	3	3	3/4	3
C-2	3/4	3	3/4	3/4	
C-3	3	-	3/4	3/4	
C-4	3	-	3/4	3	
C-5	3/4	3	3/4	3/4	
D-1	3	3/4	-	3	3
D-2	3	3	3	3	
D-3	3	3	3/4	3/4	
D-4	3	3	3/4	3	
D-5	3	3	3/4	3	
E-1	3	3	3/4	3	3
E-2	3	-	3/4	3	
E-3	3	3	3/4	3	
E-4	3	3	3	3	
E-5	3	3	3	3	
F-1	3	3	3/4	3/4	3
F-2	3/4	3	3/4	3/4	
F-3	3/4	3/4	3/4	3	
F-4	3/4	3	3/4	3/4	
F-5	3	3/4	3/4	3/4	

Note: When Mode 4 failure did occur, it did so only in a small area – at one or two pins. The failure mode for the other pins and DAPs in the same unit was Mode 3.

APPENDIX E

Shear Strength Data and ANOVA

To analyze the significance of the shear strength data, ANOVA single factor was used here. The rearranged shear strength data is shown in Appendix E-1 and the detailed calculation of ANOVA-single factor is shown in Appendix E-2.

APPENDIX E-1

Shear Strength Data for Designs A to F

Table E-1 Shear Strength Data for All Six Designs

A	B	C	D	E	F
6.06	8.38	7.98	7.64	8.41	7.59
7.27	8.70	7.45	9.64	7.86	7.93
7.27	8.38	6.95	5.64	7.75	6.7
6.67	7.75	7.19	9.09	7.25	7.9
6.97	8.19	7.22	9.27	5.53	7.16
7.88	6.99	7.42	9.45	8.14	8.17
8.18	7.75	6.92	9.64	8.36	7.93
8.48	8.00	8.24	9.09	7.91	8.57
6.97	7.06	6.92	8.18	7.53	8.54
7.27	6.99	7.15	6.91	8.08	8.33
6.36	7.12	7.55	9.45	8.08	7.68
7.27	8.00	7.98	7.82	8.3	7.81
6.06	6.81	7.94	8.55	7.14	7.84
6.06	7.81	7.12	8.73	6.64	8.24
6.97	8.00	7.12	7.64	7.3	7.68
5.15	7.56	7.45	7.09	8.3	6.73
7.88	7.75	7.65	8.55	8.25	7.74
8.48	6.93	7.58	8.36	7.25	7.16
7.88	6.93	7.44	7.45	8.02	7.71
7.11	8.25	7.44	8.33	7.69	7.99

Note: In order to use ANOVA analysis in Excel software, the number of data in each design should be equal. For some parts, the valid shear stress was not obtained. Thus, the average value of each design was employed to replace those invalid data as shown in the shaded box.

APPENDIX E-2

ANOVA – Single Factor for Shear Strength Data

Anova: Single Factor

SUMMARY

Groups	Count	Sum	Average	Variance
A	20	142.24	7.11	0.78
B	20	153.35	7.67	0.34
C	20	148.71	7.44	0.14
D	20	166.52	8.33	1.11
E	20	153.79	7.69	0.49
F	20	155.40	7.77	0.27

ANOVA

Source of Variation	SS	df	MS	F	P-value	F crit
Between Groups	16.14	5	3.23	6.19	4.09E-05	2.29
Within Groups	59.43	114	0.52			
Total	75.57	119				

SS: sum of square

Df: degree of freedom

MS: mean square

F: F value

P-value:

Fcrit: critical F value

Hypothesis:

Ho: The true shear strength means are the same for all six designs.

Ha: The six means are not all the same.

Because of following facts, the conclusion can be obtained.

1. $MS_{\text{between}} > MS_{\text{within}}$
2. $F_{\text{test}} = 6.19 > F_{\text{critical}} = 2.29$
3. $P\text{-value} = 4.09 \times 10^{-5} \ll 0.05$

Conclusion: Sufficient evidence to reject the Ho. At the 95% significance level, the expected shear strength of a package is not the same in the six designs.

APPENDIX F

Loop Resistance of PCB # 5 ~ # 8 from 0 Cycles to 3003 Cycles

Loop resistance was measured for approximate every 100 cycles during the temperature cycling test. The detailed measurements of the loop resistance for PCB #5, #6, #7 and # 8 from 0 cycles to 3003 cycles are shown in Table F-1, F-2, F-3 and F-4, respectively.

Table F-1-1 Board # 5: 0 cycle to 549 cycles

Cycles	0	168	223	267	315	361	409	455	502	549
Board No.	# 5	# 5	# 5	# 5	# 5	# 5	# 5	# 5	# 5	# 5
A-1	3.02	3.38	3.39	3.35	3.35	3.42	78.2K	OPEN	OPEN	OPEN
B-1	2.84	3.21	3.22	3.17	3.17	3.20	3.18	3.18	3.07	3.07
C-1	2.62	2.21	2.23	2.19	2.18	2.22	2.20	2.19	2.18	2.23
D-3	2.41	2.78	2.79	2.76	2.75	2.78	2.74	2.75	2.71	2.69
E-3	2.26	2.67	2.68	2.65	2.64	2.68	2.64	2.64	2.62	2.63
F-3	2.05	2.50	2.50	2.46	2.46	2.48	2.42	2.41	2.31	2.23
D-1	2.97	3.33	3.33	3.29	3.29	3.31	3.18	3.19	3.11	3.03
E-1	2.77	3.13	3.13	3.09	3.08	3.11	3.05	3.06	3.01	2.99
F-1	2.54	2.39	2.37	2.34	2.34	2.35	2.30	2.30	2.27	2.21
A-4	2.36	2.73	2.74	2.70	2.70	2.73	2.68	2.72	2.70	OPEN
B-4	2.18	2.59	2.59	2.56	2.55	2.57	2.55	2.56	2.53	2.54
C-4	1.97	1.59	1.59	1.57	1.56	1.58	1.58	1.59	1.64	1.69
A-2	2.93	3.27	3.28	3.24	3.24	3.26	3.15	3.15	OPEN	OPEN
B-2	2.67	3.01	3.01	2.98	2.97	2.99	2.94	2.94	2.90	2.87
C-2	2.47	2.20	2.21	2.18	2.17	2.19	2.17	2.18	2.16	2.19
D-4	2.22	2.56	2.56	2.53	2.52	2.55	2.51	2.52	2.45	2.41
E-4	2.06	2.44	2.44	2.41	2.41	2.43	2.40	2.40	2.38	2.39
F-4	1.86	1.58	1.58	1.56	1.56	1.58	1.58	1.58	1.62	1.66
D-2	2.66	2.92	2.92	2.89	2.89	2.91	2.81	2.81	2.67	2.67
E-2	2.44	2.70	2.70	2.67	2.66	2.68	2.63	2.63	2.55	2.56
F-2	2.24	2.05	2.05	2.03	2.02	2.05	2.02	2.02	2.00	2.02
A-5	2.03	2.31	2.31	2.28	2.28	2.30	2.27	2.27	OPEN	OPEN
B-5	1.85	2.15	2.15	2.13	2.12	2.14	2.12	2.12	2.10	2.11
C-5	1.66	2.29	2.29	2.26	2.25	2.27	2.21	2.21	2.07	2.05
A-3	2.55	2.73	2.73	2.70	2.70	2.72	2.64	2.65	OPEN	OPEN
B-3	2.35	2.54	2.55	2.51	2.51	2.53	2.48	2.48	2.40	2.41
C-3	2.11	2.12	2.12	2.09	2.09	2.10	2.06	2.07	1.98	1.95
D-5	1.89	2.10	2.10	2.07	2.07	2.08	2.06	2.06	2.01	1.99
E-5	1.75	1.99	2.00	1.97	1.96	1.98	1.96	1.96	1.94	1.95
F-5	1.54	1.52	1.52	1.50	1.49	1.50	1.50	1.50	1.52	1.54

Table F-1-2 Board # 5: 549 cycles to 1018 cycles

Cycles	597	643	691	737	784	833	877	925	968	1018
Board No.	# 5	# 5	# 5	# 5	# 5	# 5	# 5	# 5	# 5	# 5
A-1	OPEN	OPEN	OPEN	OPEN	OPEN	OPEN	OPEN	OPEN	OPEN	OPEN
B-1	3.08	3.05	3.07	2.87	2.89	2.86	2.89	2.87	2.87	2.87
C-1	2.22	2.20	2.21	2.64	2.66	2.63	2.66	2.64	2.65	2.64
D-3	2.70	2.60	2.31	2.44	2.45	2.43	2.47	2.91	OPEN	OPEN
E-3	2.63	2.61	2.62	2.28	2.30	2.28	2.31	2.28	2.30	2.28
F-3	2.24	2.22	2.23	2.07	2.08	2.06	2.10	2.07	2.09	2.06
D-1	3.03	3.02	3.04	3.01	3.03	3.00	3.03	3.00	3.01	3.00
E-1	2.99	2.98	2.99	2.80	2.81	2.79	2.82	2.78	2.80	2.79
F-1	2.22	2.15	2.20	2.57	2.58	2.56	2.59	2.56	2.57	2.56
A-4	OPEN	OPEN	OPEN	OPEN	OPEN	OPEN	OPEN	OPEN	OPEN	OPEN
B-4	2.54	2.53	2.53	2.20	2.22	2.20	2.23	2.20	2.22	2.21
C-4	1.69	1.67	1.68	1.99	2.01	1.99	2.01	1.98	2.00	1.99
A-2	OPEN	OPEN	OPEN	OPEN	OPEN	OPEN	OPEN	OPEN	OPEN	OPEN
B-2	2.88	2.86	2.88	2.70	2.72	2.70	2.72	2.69	2.70	2.70
C-2	2.19	2.17	2.18	2.50	2.51	2.49	2.52	2.49	2.50	2.50
D-4	2.41	2.39	2.40	2.24	2.26	2.25	2.27	2.24	2.25	2.26
E-4	2.39	2.38	2.39	2.08	2.10	2.09	2.11	2.08	2.09	2.08
F-4	1.67	1.65	1.66	1.88	1.89	1.88	1.90	1.87	1.88	1.87
D-2	2.68	2.66	2.68	2.70	2.71	2.69	2.71	2.69	2.69	2.69
E-2	2.57	2.54	2.56	2.46	2.48	2.46	2.48	2.46	2.46	2.46
F-2	2.02	2.00	2.01	2.26	2.28	2.26	2.28	2.26	2.26	2.26
A-5	OPEN	OPEN	OPEN	OPEN	OPEN	OPEN	OPEN	OPEN	OPEN	OPEN
B-5	2.11	2.09	2.10	1.87	1.91	1.87	1.88	1.86	1.87	1.87
C-5	2.06	2.03	2.04	1.68	1.69	1.68	1.69	1.67	1.67	1.67
A-3	OPEN	OPEN	OPEN	OPEN	OPEN	OPEN	OPEN	OPEN	OPEN	OPEN
B-3	2.41	2.40	2.40	2.37	2.39	2.38	2.40	2.37	2.38	2.37
C-3	1.96	1.94	1.95	2.13	2.15	2.13	2.16	2.12	2.13	2.13
D-5	2.02	1.99	1.99	1.91	1.93	1.91	1.93	1.91	1.92	1.91
E-5	1.95	1.94	1.94	1.77	1.78	1.77	1.80	1.76	1.77	1.77
F-5	1.55	1.53	1.54	1.55	1.57	1.56	1.57	1.55	1.56	1.55

Table F-1-3 Board # 5:1018 cycles to 1511 cycles

Cycles	1064	1113	1159	1205	1294	1340	1361	1414	1461	1511
Board No.	# 5	# 5	# 5	# 5	# 5	# 5	# 5	# 5	# 5	# 5
A-1	OPEN	OPEN	OPEN	OPEN	OPEN	OPEN	OPEN	OPEN	OPEN	OPEN
B-1	2.85	2.86	2.88	2.85	2.86	2.85	2.87	2.84	2.85	2.86
C-1	2.62	2.64	2.65	2.62	2.64	2.64	2.64	2.62	2.62	2.64
D-3	OPEN	OPEN	OPEN	OPEN	OPEN	OPEN	OPEN	OPEN	OPEN	OPEN
E-3	2.27	2.27	2.29	2.26	2.28	2.28	2.28	2.27	2.27	2.28
F-3	2.06	2.05	2.07	2.04	2.07	2.06	2.06	2.05	2.05	2.07
D-1	2.99	2.99	3.01	2.99	3.01	3.00	3.01	OPEN	OPEN	OPEN
E-1	2.77	2.79	2.80	2.77	2.79	2.78	2.78	2.76	2.77	2.78
F-1	2.55	2.56	2.57	2.54	2.56	2.55	2.55	2.53	2.54	2.56
A-4	OPEN	OPEN	OPEN	OPEN	OPEN	OPEN	OPEN	OPEN	OPEN	OPEN
B-4	2.21	2.23	2.31	2.38	2.67	2.81	3.37	0.2G	OPEN	OPEN
C-4	1.98	1.98	1.99	1.97	2.00	1.98	1.99	1.97	1.98	1.99
A-2	OPEN	OPEN	OPEN	OPEN	OPEN	OPEN	OPEN	OPEN	OPEN	OPEN
B-2	2.68	2.71	2.70	2.67	2.70	2.69	2.68	2.69	2.68	2.69
C-2	2.48	2.49	2.51	2.48	2.51	2.50	2.50	2.53	2.61	2.78
D-4	OPEN	OPEN	OPEN	OPEN	OPEN	OPEN	OPEN	OPEN	OPEN	OPEN
E-4	2.07	2.09	2.08	2.06	2.09	2.08	2.08	2.08	2.07	2.08
F-4	1.87	1.88	1.87	1.85	1.88	1.87	1.87	1.87	1.86	1.87
D-2	2.69	2.69	2.69	2.67	2.69	2.68	2.68	2.68	2.67	2.68
E-2	2.46	2.46	2.46	2.44	2.46	2.45	2.45	2.45	2.44	2.45
F-2	2.26	2.25	2.26	2.24	2.27	2.25	2.25	2.26	2.24	2.26
A-5	OPEN	OPEN	OPEN	OPEN	OPEN	OPEN	OPEN	OPEN	OPEN	OPEN
B-5	1.87	1.86	1.87	1.86	1.89	1.87	1.87	1.92	4.21	5.24
C-5	1.67	1.66	1.67	1.66	1.69	1.67	1.66	1.67	1.66	1.67
A-3	OPEN	OPEN	OPEN	OPEN	OPEN	OPEN	OPEN	OPEN	OPEN	OPEN
B-3	2.37	2.38	2.37	2.35	2.40	2.38	2.36	2.37	2.35	2.37
C-3	2.13	2.12	2.13	2.11	2.15	2.13	2.12	2.13	2.12	2.13
D-5	1.92	1.90	1.96	15M	OPEN	OPEN	OPEN	OPEN	OPEN	OPEN
E-5	1.77	1.75	1.76	1.75	1.78	1.77	1.76	1.76	1.75	1.76
F-5	1.55	1.54	1.55	1.54	1.57	1.56	1.55	1.55	1.54	1.55

Table F-1-4 Board # 5: 1511 cycles to 2100 cycles

Cycles	1555	1606	1652	1696	1767	1814	1909	1955	2051	2100
Board No.	# 5	# 5	# 5	# 5	# 5	# 5	# 5	# 5	# 5	# 5
A-1	OPEN	OPEN	OPEN	OPEN	OPEN	OPEN	OPEN	OPEN	OPEN	OPEN
B-1	2.85	2.84	2.83	2.81	2.86	2.86	2.85	2.83	2.88	2.85
C-1	2.62	2.62	2.61	2.59	2.64	2.63	2.62	2.61	2.64	2.63
D-3	OPEN	OPEN	OPEN	OPEN	OPEN	OPEN	OPEN	OPEN	OPEN	OPEN
E-3	2.27	2.27	2.26	2.25	2.30	2.32	2.48	2.50	2.59	2.61
F-3	2.05	2.05	2.04	2.03	2.05	2.06	2.05	2.03	2.06	2.05
D-1	OPEN	OPEN	OPEN	OPEN	OPEN	OPEN	OPEN	OPEN	OPEN	OPEN
E-1	2.77	2.77	2.75	2.73	2.77	2.78	2.77	2.75	2.78	2.76
F-1	2.54	2.54	2.53	2.51	2.55	2.55	2.55	2.53	2.56	2.54
A-4	OPEN	OPEN	OPEN	OPEN	OPEN	OPEN	OPEN	OPEN	OPEN	OPEN
B-4	OPEN	OPEN	OPEN	OPEN	OPEN	OPEN	OPEN	OPEN	OPEN	OPEN
C-4	1.98	1.98	1.97	1.96	1.99	1.99	2.00	1.99	2.03	2.02
A-2	OPEN	OPEN	OPEN	OPEN	OPEN	OPEN	OPEN	OPEN	OPEN	OPEN
B-2	2.68	2.67	2.66	2.64	2.69	2.68	2.68	2.67	2.69	2.67
C-2	4.99	11.81	OPEN	OPEN	OPEN	OPEN	OPEN	OPEN	OPEN	OPEN
D-4	OPEN	OPEN	OPEN	OPEN	OPEN	OPEN	OPEN	OPEN	OPEN	OPEN
E-4	2.07	2.06	2.05	2.04	2.07	2.07	2.07	2.06	2.08	2.06
F-4	1.86	1.85	1.85	1.84	1.86	1.86	1.87	1.85	1.87	1.86
D-2	2.68	2.75	3.47	OPEN	OPEN	OPEN	OPEN	OPEN	OPEN	OPEN
E-2	2.45	2.44	2.43	2.41	2.44	2.44	2.45	2.43	2.45	2.43
F-2	2.25	2.24	2.23	2.22	2.25	2.25	2.25	2.23	2.25	2.24
A-5	OPEN	OPEN	OPEN	OPEN	OPEN	OPEN	OPEN	OPEN	OPEN	OPEN
B-5	5.24	5.24	OPEN	OPEN	OPEN	OPEN	OPEN	OPEN	OPEN	OPEN
C-5	1.66	1.66	2.67	1.67	1.74	1.78	1.85	2.11	2.70	2.99
A-3	OPEN	OPEN	OPEN	OPEN	OPEN	OPEN	OPEN	OPEN	OPEN	OPEN
B-3	2.36	2.35	2.35	2.33	2.35	2.35	2.36	2.35	2.37	2.35
C-3	2.12	2.11	2.12	2.10	2.12	2.12	2.13	2.12	2.13	2.12
D-5	OPEN	OPEN	OPEN	OPEN	OPEN	OPEN	OPEN	OPEN	OPEN	OPEN
E-5	1.75	1.75	1.74	1.73	1.75	1.76	1.76	1.75	1.76	1.75
F-5	1.54	1.53	1.53	1.52	1.54	1.54	1.55	1.54	1.55	1.54

Table F-1-5 Board # 5: 2100 cycles to 2720 cycles

Cycles	2146	2192	2241	2285	2333	2357	2436	2530	2627	2720
Board No.	# 5	# 5	# 5	# 5	# 5	# 5	# 5	# 5	# 5	# 5
A-1	OPEN	OPEN	OPEN	OPEN	OPEN	OPEN	OPEN	OPEN	OPEN	OPEN
B-1	2.83	2.85	2.87	2.85	2.89	2.90	2.92	2.90	2.94	3.15
C-1	2.61	2.62	2.64	2.61	2.64	2.66	2.71	2.80	7.91	OPEN
D-3	OPEN	OPEN	OPEN	OPEN	OPEN	OPEN	OPEN	OPEN	OPEN	OPEN
E-3	2.90	2.95	2.98	2.97	3.03	3.10	3.24	7.14	OPEN	OPEN
F-3	2.04	2.05	2.05	2.03	2.34	2.05	2.06	2.06	2.06	2.03
D-1	OPEN	OPEN	OPEN	OPEN	OPEN	OPEN	OPEN	OPEN	OPEN	OPEN
E-1	2.76	2.76	2.77	2.74	2.76	2.77	2.77	2.78	2.77	2.75
F-1	2.54	2.54	2.55	2.52	2.54	2.54	2.55	2.55	2.54	2.52
A-4	OPEN	OPEN	OPEN	OPEN	OPEN	OPEN	OPEN	OPEN	OPEN	OPEN
B-4	OPEN	OPEN	OPEN	OPEN	OPEN	OPEN	OPEN	OPEN	OPEN	OPEN
C-4	2.03	2.04	2.06	2.05	2.08	2.13	2.22	2.42	13.03	7.36
A-2	OPEN	OPEN	OPEN	OPEN	OPEN	OPEN	OPEN	OPEN	OPEN	OPEN
B-2	2.67	2.67	2.67	2.64	2.67	2.67	2.68	2.69	2.67	2.66
C-2	OPEN	OPEN	OPEN	OPEN	OPEN	OPEN	OPEN	OPEN	OPEN	OPEN
D-4	OPEN	OPEN	OPEN	OPEN	OPEN	OPEN	OPEN	OPEN	OPEN	OPEN
E-4	2.07	2.06	2.06	2.04	2.06	2.06	2.07	2.08	2.06	2.05
F-4	1.86	1.86	1.86	1.84	1.86	1.86	1.87	1.87	1.86	1.85
D-2	OPEN	OPEN	OPEN	OPEN	OPEN	OPEN	OPEN	OPEN	OPEN	OPEN
E-2	2.43	2.43	2.44	2.41	2.43	2.43	2.44	2.45	2.44	2.42
F-2	2.23	2.24	2.24	2.22	2.23	2.24	2.25	2.25	2.24	2.22
A-5	OPEN	OPEN	OPEN	OPEN	OPEN	OPEN	OPEN	OPEN	OPEN	OPEN
B-5	OPEN	OPEN	OPEN	OPEN	OPEN	OPEN	OPEN	OPEN	OPEN	OPEN
C-5	OPEN	OPEN	OPEN	OPEN	OPEN	OPEN	OPEN	OPEN	OPEN	OPEN
A-3	OPEN	OPEN	OPEN	OPEN	OPEN	OPEN	OPEN	OPEN	OPEN	OPEN
B-3	2.34	2.35	2.35	2.33	2.35	2.35	2.36	2.36	2.36	2.37
C-3	2.11	2.12	2.12	2.10	2.12	2.13	2.14	2.15	2.16	2.49
D-5	OPEN	OPEN	OPEN	OPEN	OPEN	OPEN	OPEN	OPEN	OPEN	OPEN
E-5	1.75	1.75	1.75	1.73	1.74	1.75	1.75	1.76	1.75	1.74
F-5	1.53	1.54	1.54	1.52	1.53	1.53	1.54	1.55	1.53	1.53

Table F-1-6 Board # 5: 2720 cycles to 3003 cycles

Cycles	2816	2910	3003		
Board No.	# 5	# 5	# 5	10%	Failure Cycles
A-1	OPEN	OPEN	OPEN	3.322	409
B-1	OPEN	4.58	OPEN	3.124	2720
C-1	OPEN	OPEN	OPEN	2.882	2627
D-3	OPEN	OPEN	OPEN	2.651	925
E-3	OPEN	OPEN	OPEN	2.486	1955
F-3	2.05	2.05	2.07	2.255	OK
D-1	OPEN	OPEN	OPEN	3.267	1414
E-1	2.78	2.77	2.80	3.047	OK
F-1	2.56	2.55	2.58	2.794	OK
A-4	OPEN	OPEN	OPEN	2.596	549
B-4	OPEN	OPEN	OPEN	2.398	1294
C-4	7.36	OPEN	OPEN	2.167	2436
A-2	OPEN	OPEN	OPEN	3.223	502
B-2	2.68	2.68	2.70	2.937	OK
C-2	OPEN	OPEN	OPEN	2.717	1511
D-4	OPEN	OPEN	OPEN	2.442	1064
E-4	2.08	2.07	2.09	2.266	OK
F-4	1.86	1.86	1.88	2.046	OK
D-2	OPEN	OPEN	OPEN	2.926	1652
E-2	2.45	2.44	2.46	2.684	OK
F-2	2.25	2.24	2.26	2.464	OK
A-5	OPEN	OPEN	OPEN	2.233	502
B-5	OPEN	OPEN	OPEN	2.035	1461
C-5	OPEN	OPEN	OPEN	1.826	1909
A-3	OPEN	OPEN	OPEN	2.805	502
B-3	2.39	2.40	2.53	2.585	OK
C-3	3.05	3.41	4.39	2.321	2720
D-5	OPEN	OPEN	OPEN	2.079	1205
E-5	1.75	1.75	1.77	1.925	OK
F-5	1.54	1.54	1.56	1.694	OK

Note 1: 10% means the value of the loop resistance increased by 10 %.

Note 2: “Failure cycles” means the number of cycles at which the part was found to have more than 10% increase in the loop resistance; this was defined as an open circuit.

Note 3: “OK” means the increase of loop resistance of the part was still within 10 %.

Table F-2-1 Board # 6: 0 cycle to 549 cycles

Cycles	0	168	223	267	315	361	409	455	502	549
Board No.	# 6	# 6	# 6	# 6	# 6	# 6	# 6	# 6	# 6	# 6
A-1	3.33	3.55	OPEN	OPEN	OPEN	OPEN	OPEN	OPEN	OPEN	OPEN
B-1	OPEN	OPEN	OPEN	OPEN	OPEN	OPEN	OPEN	OPEN	OPEN	OPEN
C-1	2.83	2.41	2.39	2.36	2.36	2.38	2.36	2.37	2.36	2.41
D-3	2.63	3.01	2.98	2.95	2.94	2.96	2.95	2.94	2.79	2.77
E-3	2.42	2.87	2.84	2.80	2.81	2.82	2.80	2.81	2.75	2.81
F-3	2.14	2.49	2.43	2.39	2.39	2.41	2.34	2.18	2.12	2.12
D-1	3.16	3.44	3.25	3.20	3.21	3.23	3.21	3.14	OPEN	OPEN
E-1	2.89	3.23	3.06	3.11	3.02	3.04	3.01	2.97	2.90	2.90
F-1	2.69	2.39	2.34	2.30	2.30	2.31	2.29	2.26	2.18	2.18
A-4	2.48	2.86	2.82	2.77	2.78	2.80	2.78	77K	OPEN	OPEN
B-4	2.30	2.74	2.71	2.67	2.67	2.69	2.66	2.65	2.62	2.65
C-4	2.04	1.71	1.71	1.68	1.68	1.69	1.72	1.78	1.78	1.84
A-2	3.03	OPEN	OPEN	OPEN	OPEN	OPEN	OPEN	OPEN	OPEN	OPEN
B-2	2.77	2.99	2.94	2.89	2.90	2.91	2.89	2.86	2.80	2.77
C-2	2.69	2.24	2.23	2.19	2.19	2.21	2.20	2.21	2.19	2.20
D-4	2.48	2.66	2.64	2.59	2.60	2.61	2.59	2.60	OPEN	OPEN
E-4	2.30	2.55	2.54	2.50	2.50	2.51	2.48	2.48	2.45	2.49
F-4	2.04	1.66	1.67	1.97	1.63	1.65	1.67	1.71	1.72	1.78
D-2	2.80	2.94	2.85	2.80	2.81	2.83	2.81	2.82	3.30	OPEN
E-2	2.54	2.69	2.64	2.60	2.60	2.62	2.56	2.55	2.50	2.50
F-2	2.32	2.09	2.07	1.76	2.04	2.06	2.03	2.03	2.02	2.05
A-5	2.11	2.37	2.35	2.31	2.31	2.33	77K	OPEN	OPEN	OPEN
B-5	1.92	2.24	2.23	2.19	2.19	2.21	2.18	2.17	2.15	2.18
C-5	1.66	2.23	2.19	2.15	2.15	2.16	2.05	1.96	1.91	1.90
A-3	2.70	2.80	2.73	2.69	2.70	2.72	2.74	OPEN	OPEN	OPEN
B-3	2.46	2.57	2.54	2.49	2.50	2.51	2.49	2.44	2.39	2.38
C-3	2.24	2.14	2.11	2.08	2.08	2.09	2.04	1.93	1.91	1.91
D-5	2.01	2.22	2.20	2.17	2.17	2.18	2.14	2.07	2.05	2.06
E-5	1.83	2.08	2.07	2.04	2.04	2.05	2.03	2.01	2.00	2.02
F-5	1.58	1.57	1.57	1.55	1.55	1.56	1.56	1.58	1.58	1.61

Table F-2-2 Board # 6: 549 cycles to 1018 cycles

Cycles	597	643	691	737	784	833	877	925	968	1018
Board No.	# 6	# 6	# 6	# 6	# 6	# 6	# 6	# 6	# 6	# 6
A-1	OPEN	OPEN	OPEN	OPEN	OPEN	OPEN	OPEN	OPEN	OPEN	OPEN
B-1	OPEN	OPEN	OPEN	OPEN	OPEN	OPEN	OPEN	OPEN	OPEN	OPEN
C-1	2.39	2.38	2.39	2.85	2.87	2.86	2.88	2.86	2.88	2.91
D-3	2.73	2.72	2.74	2.65	2.67	2.66	2.68	8.41	OPEN	OPEN
E-3	2.77	2.76	2.78	2.44	2.45	2.44	2.45	2.43	2.44	2.44
F-3	2.10	2.09	2.12	2.16	2.17	2.16	2.17	2.15	2.16	2.16
D-1	OPEN	OPEN	OPEN	OPEN	OPEN	OPEN	OPEN	OPEN	OPEN	OPEN
E-1	2.89	2.88	2.95	2.91	2.93	2.91	2.93	2.91	2.91	2.91
F-1	2.12	2.11	2.18	2.70	2.73	2.71	2.72	2.71	2.71	2.70
A-4	OPEN	OPEN	OPEN	OPEN	OPEN	OPEN	OPEN	OPEN	OPEN	OPEN
B-4	2.64	2.62	2.65	2.31	2.33	2.32	2.33	2.31	2.32	2.31
C-4	1.82	1.81	1.83	2.03	2.07	2.06	2.07	2.05	2.03	2.06
A-2	OPEN	OPEN	OPEN	OPEN	OPEN	OPEN	OPEN	OPEN	OPEN	OPEN
B-2	2.77	2.76	2.78	2.79	2.81	2.80	2.81	2.80	2.80	2.80
C-2	2.20	2.19	2.21	2.56	2.59	2.57	2.59	2.57	2.58	2.58
D-4	OPEN	OPEN	OPEN	OPEN	OPEN	OPEN	OPEN	OPEN	OPEN	OPEN
E-4	2.47	2.45	2.48	2.18	2.19	2.18	2.19	2.17	2.18	2.17
F-4	1.75	1.75	1.76	1.91	1.92	1.92	1.93	1.91	1.91	1.91
D-2	OPEN	OPEN	OPEN	OPEN	OPEN	OPEN	OPEN	OPEN	OPEN	OPEN
E-2	2.47	2.45	2.48	2.55	2.57	2.56	2.57	2.58	2.56	2.55
F-2	2.03	2.02	2.03	2.33	2.35	2.34	2.35	2.33	2.34	2.33
A-5	OPEN	OPEN	OPEN	OPEN	OPEN	OPEN	OPEN	OPEN	OPEN	OPEN
B-5	2.16	2.15	2.17	1.94	1.96	1.95	1.96	1.94	1.95	1.94
C-5	1.88	1.87	1.89	1.67	1.68	1.68	1.69	1.67	1.68	1.67
A-3	OPEN	OPEN	OPEN	OPEN	OPEN	OPEN	OPEN	OPEN	OPEN	OPEN
B-3	2.37	2.36	2.38	2.48	2.50	2.49	2.50	2.48	2.49	2.48
C-3	1.90	1.89	1.90	2.26	2.28	2.27	2.28	2.26	2.27	2.27
D-5	2.05	2.04	2.06	2.03	2.05	2.04	2.05	2.03	2.04	2.03
E-5	2.00	1.99	2.01	1.84	1.86	1.85	1.86	1.84	1.85	1.84
F-5	1.60	1.59	1.60	1.59	1.61	1.60	1.61	1.59	1.61	1.59

Table F-2-3 Board # 6:1018 cycles to 1511 cycles

Cycles	1064	1113	1159	1205	1294	1340	1361	1414	1461	1511
Board No.	# 6	# 6	# 6	# 6	# 6	# 6	# 6	# 6	# 6	# 6
A-1	OPEN	OPEN	OPEN	OPEN	OPEN	OPEN	OPEN	OPEN	OPEN	OPEN
B-1	OPEN	OPEN	OPEN	OPEN	OPEN	OPEN	OPEN	OPEN	OPEN	OPEN
C-1	3.01	3.25	3.55	3.68	6.72	21.9M	OPEN	6.75	OPEN	10.61
D-3	OPEN	OPEN	OPEN	OPEN	OPEN	OPEN	OPEN	OPEN	OPEN	OPEN
E-3	2.44	2.43	2.45	2.44	2.46	2.44	2.44	2.44	2.43	2.44
F-3	2.16	2.15	2.16	2.16	2.18	2.17	2.16	2.16	2.15	2.16
D-1	OPEN	OPEN	OPEN	OPEN	OPEN	OPEN	OPEN	OPEN	OPEN	OPEN
E-1	2.91	2.90	2.92	2.90	2.90	2.91	2.90	2.90	2.91	2.90
F-1	2.70	2.70	2.71	2.70	2.72	2.71	2.70	2.70	2.70	2.70
A-4	OPEN	OPEN	OPEN	OPEN	OPEN	OPEN	OPEN	OPEN	OPEN	OPEN
B-4	2.31	2.30	2.32	2.32	2.33	2.32	2.31	2.31	2.31	2.31
C-4	2.06	2.05	2.06	2.06	2.08	2.07	2.07	2.07	2.08	2.08
A-2	OPEN	OPEN	OPEN	OPEN	OPEN	OPEN	OPEN	OPEN	OPEN	OPEN
B-2	2.80	2.80	2.85	2.85	2.90	2.93	17.22	3.50	3.99	6.81
C-2	2.59	2.88	14.90	6.51	150.00	6.16	3.68	OPEN	30.30	9.05
D-4	OPEN	OPEN	OPEN	OPEN	OPEN	OPEN	OPEN	OPEN	OPEN	OPEN
E-4	2.17	2.16	2.18	2.17	2.19	2.18	2.17	2.17	2.17	2.17
F-4	1.91	1.90	1.91	1.91	1.93	1.91	1.91	1.91	1.91	1.91
D-2	OPEN	OPEN	OPEN	OPEN	OPEN	OPEN	OPEN	OPEN	OPEN	OPEN
E-2	2.56	2.54	2.56	2.55	2.55	2.56	2.56	2.55	2.55	2.55
F-2	2.33	2.32	2.35	2.33	2.35	2.34	2.33	2.33	2.33	2.33
A-5	OPEN	OPEN	OPEN	OPEN	OPEN	OPEN	OPEN	OPEN	OPEN	OPEN
B-5	1.95	1.93	1.95	1.94	1.96	1.95	1.94	1.94	1.94	1.94
C-5	1.67	1.66	1.68	1.68	1.69	1.68	1.67	1.67	1.67	1.67
A-3	OPEN	OPEN	OPEN	OPEN	OPEN	OPEN	OPEN	OPEN	OPEN	OPEN
B-3	2.48	2.48	2.50	2.48	2.50	2.49	2.48	2.48	2.49	2.50
C-3	2.28	2.28	2.33	2.49	6.85	OPEN	OPEN	OPEN	OPEN	OPEN
D-5	2.04	2.02	2.05	2.06	OPEN	OPEN	OPEN	OPEN	OPEN	OPEN
E-5	1.85	1.83	1.85	1.84	1.86	1.85	1.84	1.84	1.84	1.84
F-5	1.60	1.58	1.60	1.59	1.61	1.60	1.59	1.59	1.59	1.59

Table F-2-4 Board # 6: 1511 cycles to 2100 cycles

Cycles	1555	1606	1652	1696	1767	1814	1909	1955	2051	2100
Board No.	# 6	# 6	# 6	# 6	# 6	# 6	# 6	# 6	# 6	# 6
A-1	OPEN	OPEN	OPEN	OPEN	OPEN	OPEN	OPEN	OPEN	OPEN	OPEN
B-1	OPEN	OPEN	OPEN	OPEN	OPEN	OPEN	OPEN	OPEN	OPEN	OPEN
C-1	18.90	OPEN	OPEN	OPEN	OPEN	OPEN	OPEN	OPEN	OPEN	OPEN
D-3	OPEN	OPEN	OPEN	OPEN	OPEN	OPEN	OPEN	OPEN	OPEN	OPEN
E-3	2.43	2.43	2.42	2.41	2.42	2.44	2.45	2.42	2.43	2.42
F-3	2.15	2.15	2.14	2.13	2.14	2.16	2.17	2.12	2.15	2.14
D-1	OPEN	OPEN	OPEN	OPEN	OPEN	OPEN	OPEN	OPEN	OPEN	OPEN
E-1	2.91	2.91	2.88	2.91	2.89	2.91	2.92	2.91	2.90	2.92
F-1	2.69	2.70	2.68	2.68	2.69	2.70	2.72	2.68	2.71	2.69
A-4	OPEN	OPEN	OPEN	OPEN	OPEN	OPEN	OPEN	OPEN	OPEN	OPEN
B-4	2.30	2.31	2.29	2.29	2.30	2.31	2.33	2.30	2.32	2.30
C-4	2.08	2.09	2.09	2.09	2.12	2.14	2.19	2.18	2.26	2.27
A-2	OPEN	OPEN	OPEN	OPEN	OPEN	OPEN	OPEN	OPEN	OPEN	OPEN
B-2	OPEN	OPEN	OPEN	OPEN	OPEN	OPEN	OPEN	OPEN	OPEN	OPEN
C-2	5.45	OPEN	OPEN	OPEN	OPEN	OPEN	OPEN	OPEN	OPEN	OPEN
D-4	OPEN	OPEN	OPEN	OPEN	OPEN	OPEN	OPEN	OPEN	OPEN	OPEN
E-4	2.16	2.17	2.15	2.15	2.16	2.17	2.18	2.15	2.17	2.16
F-4	1.90	1.90	1.89	1.89	1.89	1.91	1.92	1.89	1.90	1.89
D-2	OPEN	OPEN	OPEN	OPEN	OPEN	OPEN	OPEN	OPEN	OPEN	OPEN
E-2	2.55	2.55	2.55	2.53	2.55	2.57	2.57	2.54	2.57	2.56
F-2	2.32	2.33	2.31	2.31	2.32	2.33	2.34	2.31	2.33	2.32
A-5	OPEN	OPEN	OPEN	OPEN	OPEN	OPEN	OPEN	OPEN	OPEN	OPEN
B-5	1.93	1.93	1.92	1.92	1.92	1.94	1.95	1.92	1.93	1.92
C-5	1.67	1.67	1.66	1.66	1.68	1.69	1.72	1.71	1.78	1.81
A-3	OPEN	OPEN	OPEN	OPEN	OPEN	OPEN	OPEN	OPEN	OPEN	OPEN
B-3	2.52	2.64	2.86	3.28	3.68	7.84	OPEN	OPEN	OPEN	OPEN
C-3	OPEN	OPEN	OPEN	OPEN	OPEN	OPEN	OPEN	OPEN	OPEN	OPEN
D-5	OPEN	OPEN	OPEN	OPEN	OPEN	OPEN	OPEN	OPEN	OPEN	OPEN
E-5	1.83	1.84	1.82	1.82	1.83	1.84	1.85	1.82	1.84	1.82
F-5	1.59	1.59	1.58	1.57	1.58	1.68	1.60	1.58	1.59	1.58

Table F-2-5 Board # 6: 2100 cycles to 2720 cycles

Cycles	2146	2192	2241	2285	2333	2357	2436	2530	2627	2720
Board No.	# 6	# 6	# 6	# 6	# 6	# 6	# 6	# 6	# 6	# 6
A-1	OPEN	OPEN	OPEN	OPEN	OPEN	OPEN	OPEN	OPEN	OPEN	OPEN
B-1	OPEN	OPEN	OPEN	OPEN	OPEN	OPEN	OPEN	OPEN	OPEN	OPEN
C-1	OPEN	OPEN	OPEN	OPEN	OPEN	OPEN	OPEN	OPEN	OPEN	OPEN
D-3	OPEN	OPEN	OPEN	OPEN	OPEN	OPEN	OPEN	OPEN	OPEN	OPEN
E-3	2.42	2.41	2.42	2.40	2.41	2.43	2.43	2.43	2.43	2.41
F-3	2.14	2.14	2.14	2.13	2.13	2.15	2.15	2.15	2.14	2.13
D-1	OPEN	OPEN	OPEN	OPEN	OPEN	OPEN	OPEN	OPEN	OPEN	OPEN
E-1	2.92	2.90	2.93	2.91	2.89	2.90	2.90	2.92	2.91	2.93
F-1	2.69	2.68	2.69	2.67	2.68	2.70	2.70	2.71	2.70	2.69
A-4	OPEN	OPEN	OPEN	OPEN	OPEN	OPEN	OPEN	OPEN	OPEN	OPEN
B-4	2.30	2.30	2.31	2.30	2.31	2.33	2.34	2.35	2.38	2.43
C-4	2.35	2.39	2.47	2.55	2.74	5.46	3.82	4.03	OPEN	OPEN
A-2	OPEN	OPEN	OPEN	OPEN	OPEN	OPEN	OPEN	OPEN	OPEN	OPEN
B-2	OPEN	OPEN	OPEN	OPEN	OPEN	OPEN	OPEN	OPEN	OPEN	OPEN
C-2	OPEN	OPEN	OPEN	OPEN	OPEN	OPEN	OPEN	OPEN	OPEN	OPEN
D-4	OPEN	OPEN	OPEN	OPEN	OPEN	OPEN	OPEN	OPEN	OPEN	OPEN
E-4	2.16	2.15	2.16	2.14	2.15	2.16	2.16	2.15	2.16	2.15
F-4	1.89	1.89	1.90	1.88	1.89	1.90	1.90	1.89	1.90	1.89
D-2	OPEN	OPEN	OPEN	OPEN	OPEN	OPEN	OPEN	OPEN	OPEN	OPEN
E-2	2.56	2.57	2.60	2.65	2.64	4.85	11.65	5.15	5.16	6.36
F-2	2.32	2.31	2.32	2.31	2.31	2.32	2.33	2.32	2.32	2.31
A-5	OPEN	OPEN	OPEN	OPEN	OPEN	OPEN	OPEN	OPEN	OPEN	OPEN
B-5	1.93	1.92	1.93	1.91	1.92	1.93	1.94	1.93	1.94	1.95
C-5	1.87	1.89	1.97	2.05	2.42	6.45	OPEN	21.70	OPEN	OPEN
A-3	OPEN	OPEN	OPEN	OPEN	OPEN	OPEN	OPEN	OPEN	OPEN	OPEN
B-3	OPEN	OPEN	OPEN	OPEN	OPEN	OPEN	OPEN	OPEN	OPEN	OPEN
C-3	OPEN	OPEN	OPEN	OPEN	OPEN	OPEN	OPEN	OPEN	OPEN	OPEN
D-5	OPEN	OPEN	OPEN	OPEN	OPEN	OPEN	OPEN	OPEN	OPEN	OPEN
E-5	1.83	1.82	1.83	1.81	1.82	1.83	1.83	1.82	1.82	1.82
F-5	1.58	1.58	1.58	1.57	1.58	1.58	1.59	1.58	1.58	1.58

Table F-2-6 Board # 6: 2720 cycles to 3003 cycles

Cycles	2816	2910	3003		
Board No.	# 6	# 6	# 6	10%	Failure Cycles
A-1	OPEN	OPEN	OPEN	3.663	223
B-1	OPEN	OPEN	OPEN	Open	0
C-1	OPEN	OPEN	OPEN	3.113	1113
D-3	OPEN	OPEN	OPEN	2.893	925
E-3	2.43	2.43	2.44	2.662	OK
F-3	2.15	2.15	2.16	2.354	OK
D-1	OPEN	OPEN	OPEN	3.476	502
E-1	3.03	OPEN	OPEN	3.179	2910
F-1	2.73	2.74	2.84	2.959	OK
A-4	OPEN	OPEN	OPEN	2.728	455
B-4	2.57	24.10	OPEN	2.53	2816
C-4	OPEN	OPEN	OPEN	2.244	2051
A-2	OPEN	OPEN	OPEN	3.333	168
B-2	OPEN	OPEN	OPEN	3.047	1361
C-2	OPEN	OPEN	OPEN	2.959	1159
D-4	OPEN	OPEN	OPEN	2.728	502
E-4	2.17	2.17	2.17	2.53	OK
F-4	1.91	1.90	1.92	2.244	OK
D-2	OPEN	OPEN	OPEN	3.08	549
E-2	7.24	OPEN	OPEN	2.794	2357
F-2	2.33	2.33	2.34	2.552	OK
A-5	OPEN	OPEN	OPEN	2.321	409
B-5	1.98	2.01	2.05	2.112	OK
C-5	OPEN	OPEN	OPEN	1.826	2146
A-3	OPEN	OPEN	OPEN	2.97	455
B-3	OPEN	OPEN	OPEN	2.706	1652
C-3	OPEN	OPEN	OPEN	2.464	1205
D-5	OPEN	OPEN	OPEN	2.211	1294
E-5	1.83	1.83	1.84	2.013	OK
F-5	1.59	1.59	1.60	1.738	OK

Note 1: 10% means the value of the loop resistance increased by 10 %.

Note 2: “Failure cycles” means the number of cycles at which the part was found to have more than 10% increase in the loop resistance; this was defined as an open circuit.

Note 3: “OK” means the increase of loop resistance of the part was still within 10 %.

Table F-3-1 Board # 7: 0 cycle to 549 cycles

Cycles	0	168	223	267	315	361	409	455	502	549
Board No.	# 7	# 7	# 7	# 7	# 7	# 7	# 7	# 7	# 7	# 7
A-1	2.69	2.44	2.14	5.86K	OPEN	OPEN	OPEN	OPEN	OPEN	OPEN
B-1	2.54	2.34	2.26	2.23	2.30	2.31	2.28	2.29	2.27	2.37
C-1	2.36	1.71	1.74	1.75	1.70	1.75	1.73	1.73	1.74	1.83
D-3	2.15	2.15	2.13	2.12	2.09	2.12	2.08	2.04	2.05	2.09
E-3	1.96	2.15	2.13	2.11	2.11	1.95	1.92	2.11	2.09	1.96
F-3	1.79	2.10	2.09	2.07	2.07	2.08	2.07	2.07	2.06	2.10
D-1	2.63	2.36	1.80	2.20	2.26	2.25	2.24	2.21	2.19	2.21
E-1	2.48	2.24	2.09	2.20	2.19	2.25	2.23	2.21	2.19	2.24
F-1	2.29	1.49	1.65	1.68	1.70	1.59	1.56	1.53	1.52	1.60
A-4	2.08	2.06	2.05	2.05	OPEN	OPEN	OPEN	OPEN	OPEN	OPEN
B-4	1.89	2.05	2.04	2.03	2.03	2.00	1.95	2.02	2.01	2.05
C-4	1.70	1.99	1.99	1.97	1.97	1.98	1.95	1.96	1.95	1.99
A-2	2.51	2.22	1.87	2.28	OPEN	OPEN	OPEN	OPEN	OPEN	OPEN
B-2	2.39	2.14	2.16	2.10	2.11	2.13	2.13	2.11	2.12	2.17
C-2	2.19	1.51	1.59	1.51	1.56	1.58	1.59	1.56	1.44	1.60
D-4	2.00	1.95	1.93	1.92	1.86	1.91	1.86	1.86	1.73	1.90
E-4	1.83	1.98	1.97	1.95	1.95	1.93	1.90	1.95	1.90	1.94
F-4	1.60	1.87	1.86	1.84	1.84	1.81	1.83	1.84	1.83	1.87
D-2	2.38	2.02	1.49	1.90	1.96	2.01	1.94	1.93	1.91	1.98
E-2	2.22	1.90	1.90	1.90	1.91	1.92	1.89	1.87	1.86	1.93
F-2	2.02	1.28	1.34	1.30	1.39	1.38	1.37	1.34	1.33	1.54
A-5	1.83	1.83	2.40	OPEN	OPEN	OPEN	OPEN	OPEN	OPEN	OPEN
B-5	1.64	1.73	1.72	1.70	1.68	1.69	1.67	1.70	1.69	1.71
C-5	1.43	1.63	1.63	1.61	1.61	1.62	1.61	1.61	1.60	1.64
A-3	2.31	24.70	27.30	24.30	64.70	64.70	64.30	67.20	67.00	67.10
B-3	2.12	1.72	1.63	1.70	1.74	1.74	1.73	1.71	1.70	1.76
C-3	1.95	-	-	-	-	-	-	-	-	-
D-5	1.71	1.55	1.52	1.51	1.51	1.51	1.50	1.49	1.49	1.53
E-5	1.50	1.51	1.51	1.50	1.49	1.49	1.48	1.49	1.49	1.51
F-5	1.31	1.46	1.46	1.45	1.44	1.45	1.44	1.44	1.44	1.47

Table F-3-2 Board # 7: 549 cycles to 1018 cycles

Cycles	597	643	691	737	784	833	877	925	968	1018
Board No.	# 7	# 7	# 7	# 7	# 7	# 7	# 7	# 7	# 7	# 7
A-1	OPEN	OPEN	OPEN	OPEN	OPEN	OPEN	OPEN	OPEN	OPEN	OPEN
B-1	2.32	2.34	2.47	2.57	2.58	2.59	2.62	OPEN	OPEN	OPEN
C-1	1.79	1.80	1.89	2.38	2.38	2.39	2.40	2.37	2.39	2.39
D-3	2.06	2.06	1.95	2.17	2.17	2.18	2.19	2.17	2.18	2.18
E-3	2.14	1.93	2.13	1.98	1.99	1.99	1.99	1.98	1.98	1.98
F-3	2.09	2.08	2.08	1.81	1.81	1.82	1.83	1.81	1.81	1.81
D-1	2.24	2.25	2.30	OPEN	OPEN	OPEN	OPEN	OPEN	OPEN	OPEN
E-1	2.23	2.24	2.32	2.50	2.51	2.51	2.52	2.50	2.50	2.50
F-1	1.57	1.76	1.95	2.32	2.32	2.32	2.33	2.31	2.31	2.31
A-4	OPEN	OPEN	OPEN	OPEN	OPEN	OPEN	OPEN	OPEN	OPEN	OPEN
B-4	2.04	1.98	2.04	1.91	1.91	1.91	1.92	1.90	1.91	1.91
C-4	1.99	1.97	1.98	1.72	1.73	1.73	1.74	1.72	1.73	1.73
A-2	OPEN	OPEN	OPEN	OPEN	OPEN	OPEN	OPEN	OPEN	OPEN	OPEN
B-2	2.13	2.14	2.22	2.42	2.42	2.43	2.44	2.42	2.42	2.43
C-2	1.59	1.61	1.83	2.22	2.22	2.22	2.23	2.21	2.21	2.21
D-4	1.88	1.88	1.79	OPEN	OPEN	OPEN	OPEN	OPEN	OPEN	OPEN
E-4	1.97	1.91	1.93	1.85	1.85	1.86	1.86	1.84	1.85	1.85
F-4	1.86	1.84	1.85	1.63	1.62	1.64	1.64	1.62	1.63	1.62
D-2	1.98	2.01	567.00	OPEN	OPEN	OPEN	OPEN	OPEN	OPEN	OPEN
E-2	1.91	1.91	2.00	2.26	2.25	2.25	2.26	2.23	2.24	2.24
F-2	1.53	1.52	1.59	2.04	2.04	2.04	2.05	2.03	2.03	2.04
A-5	OPEN	OPEN	OPEN	OPEN	OPEN	OPEN	OPEN	OPEN	OPEN	OPEN
B-5	1.70	1.69	1.69	1.66	1.66	1.67	1.67	1.65	1.66	1.66
C-5	1.63	1.62	1.62	1.45	1.45	1.46	1.46	1.44	1.44	1.44
A-3	69.90	66.90	47.30	OPEN	OPEN	OPEN	OPEN	OPEN	OPEN	OPEN
B-3	1.72	1.74	1.91	2.14	2.14	2.15	2.17	2.14	2.14	2.14
C-3	-	-	-	1.97	1.97	1.98	2.00	1.97	1.98	1.98
D-5	1.51	1.51	1.53	1.75	1.74	2.75	22.80	OPEN	OPEN	OPEN
E-5	1.51	1.49	1.51	1.52	1.52	1.53	1.53	1.51	1.52	1.51
F-5	1.46	1.45	1.45	1.33	1.33	1.34	1.34	1.32	1.33	1.33

Table F-3-3 Board # 7:1018 cycles to 1511 cycles

Cycles	1064	1113	1159	1205	1294	1340	1361	1414	1461	1511
Board No.	# 7	# 7	# 7	# 7	# 7	# 7	# 7	# 7	# 7	# 7
A-1	OPEN	OPEN	OPEN	OPEN	OPEN	OPEN	OPEN	OPEN	OPEN	OPEN
B-1	OPEN	OPEN	OPEN	OPEN	OPEN	OPEN	OPEN	OPEN	OPEN	OPEN
C-1	2.39	2.38	2.40	2.38	2.40	2.40	2.40	2.42	2.44	2.56
D-3	2.18	2.16	2.19	2.17	2.19	2.19	2.20	0.3G	OPEN	OPEN
E-3	1.99	1.97	1.99	1.98	1.99	1.99	1.99	1.98	1.97	1.98
F-3	1.82	1.80	1.83	1.81	1.82	1.82	1.82	1.81	1.80	1.81
D-1	OPEN	OPEN	OPEN	OPEN	OPEN	OPEN	OPEN	OPEN	OPEN	OPEN
E-1	2.52	2.50	2.52	2.50	2.52	2.51	2.51	2.51	2.50	2.50
F-1	2.32	2.30	2.32	2.31	2.33	2.32	2.32	2.32	2.30	2.31
A-4	OPEN	OPEN	OPEN	OPEN	OPEN	OPEN	OPEN	OPEN	OPEN	OPEN
B-4	1.92	1.90	1.92	1.91	1.94	1.95	1.95	2.01	2.56	15.05
C-4	1.75	1.73	1.76	1.76	1.82	1.84	1.87	1.87	2.14	32.80
A-2	OPEN	OPEN	OPEN	OPEN	OPEN	OPEN	OPEN	OPEN	OPEN	OPEN
B-2	2.45	2.44	2.48	2.51	6.97	21.40	OPEN	OPEN	OPEN	OPEN
C-2	2.22	2.20	2.23	2.21	2.23	2.23	2.23	2.25	2.28	2.31
D-4	OPEN	OPEN	OPEN	OPEN	OPEN	OPEN	OPEN	OPEN	OPEN	OPEN
E-4	1.86	1.84	1.86	1.84	1.86	1.85	1.85	1.85	1.84	1.85
F-4	1.63	1.61	1.63	1.62	1.63	1.63	1.62	1.62	1.62	1.62
D-2	OPEN	OPEN	OPEN	OPEN	OPEN	OPEN	OPEN	OPEN	OPEN	OPEN
E-2	2.25	2.23	2.25	2.24	2.25	2.25	2.24	2.24	2.23	2.24
F-2	2.04	2.02	2.05	2.03	2.04	2.04	2.04	2.04	2.03	2.03
A-5	OPEN	OPEN	OPEN	OPEN	OPEN	OPEN	OPEN	OPEN	OPEN	OPEN
B-5	1.67	1.65	1.67	1.66	1.69	1.71	1.84	2.53	OPEN	OPEN
C-5	1.45	1.43	1.45	1.44	1.45	1.45	1.45	1.45	1.44	1.45
A-3	OPEN	OPEN	OPEN	OPEN	OPEN	OPEN	OPEN	OPEN	OPEN	OPEN
B-3	2.16	2.13	2.15	2.14	2.16	2.15	2.15	2.15	2.18	10.32
C-3	1.99	1.97	1.99	1.98	2.00	1.99	1.99	2.00	2.00	2.03
D-5	OPEN	OPEN	OPEN	OPEN	OPEN	OPEN	OPEN	OPEN	OPEN	OPEN
E-5	1.52	1.50	1.52	1.51	1.52	1.52	1.52	1.51	1.51	1.51
F-5	1.34	1.32	1.34	1.32	1.34	1.33	1.33	1.33	1.32	1.33

Table F-3-4 Board # 7: 1511 cycles to 2100 cycles

Cycles	1555	1606	1652	1696	1767	1814	1909	1955	2051	2100
Board No.	# 7	# 7	# 7	# 7	# 7	# 7	# 7	# 7	# 7	# 7
A-1	OPEN	OPEN	OPEN	OPEN	OPEN	OPEN	OPEN	OPEN	OPEN	OPEN
B-1	OPEN	OPEN	OPEN	OPEN	OPEN	OPEN	OPEN	OPEN	OPEN	OPEN
C-1	2.78	2.90	3.02	3.40	OPEN	OPEN	OPEN	OPEN	OPEN	OPEN
D-3	OPEN	OPEN	OPEN	OPEN	OPEN	OPEN	OPEN	OPEN	OPEN	OPEN
E-3	1.96	1.97	1.96	1.96	1.97	1.97	1.98	1.98	1.97	1.96
F-3	1.80	1.80	1.79	1.79	1.80	1.80	1.81	1.81	1.80	1.79
D-1	OPEN	OPEN	OPEN	OPEN	OPEN	OPEN	OPEN	OPEN	OPEN	OPEN
E-1	2.49	2.50	2.49	2.49	2.50	2.50	2.51	2.51	2.51	2.51
F-1	2.30	2.30	2.29	2.29	2.30	2.30	2.31	2.31	2.31	2.33
A-4	OPEN	OPEN	OPEN	OPEN	OPEN	OPEN	OPEN	OPEN	OPEN	OPEN
B-4	OPEN	OPEN	OPEN	OPEN	OPEN	OPEN	OPEN	OPEN	OPEN	OPEN
C-4	OPEN	OPEN	OPEN	OPEN	OPEN	OPEN	OPEN	OPEN	OPEN	OPEN
A-2	OPEN	OPEN	OPEN	OPEN	OPEN	OPEN	OPEN	OPEN	OPEN	OPEN
B-2	OPEN	OPEN	OPEN	OPEN	OPEN	OPEN	OPEN	OPEN	OPEN	OPEN
C-2	4.63	11.74	OPEN	OPEN	OPEN	OPEN	OPEN	OPEN	OPEN	OPEN
D-4	OPEN	OPEN	OPEN	OPEN	OPEN	OPEN	OPEN	OPEN	OPEN	OPEN
E-4	1.83	1.84	1.83	1.83	1.83	1.84	1.84	1.84	1.84	1.83
F-4	1.61	1.67	1.60	1.60	1.61	1.61	1.62	1.62	1.61	1.60
D-2	OPEN	OPEN	OPEN	OPEN	OPEN	OPEN	OPEN	OPEN	OPEN	OPEN
E-2	2.23	2.23	2.22	2.22	2.23	2.23	2.23	2.23	2.23	2.22
F-2	2.03	2.02	2.01	2.01	2.02	2.03	2.03	2.03	2.03	2.02
A-5	OPEN	OPEN	OPEN	OPEN	OPEN	OPEN	OPEN	OPEN	OPEN	OPEN
B-5	OPEN	OPEN	OPEN	OPEN	OPEN	OPEN	OPEN	OPEN	OPEN	OPEN
C-5	1.44	1.45	1.44	1.45	1.46	1.48	1.48	1.48	1.64	1.86
A-3	OPEN	OPEN	OPEN	OPEN	OPEN	OPEN	OPEN	OPEN	OPEN	OPEN
B-3	OPEN	OPEN	OPEN	OPEN	OPEN	OPEN	OPEN	OPEN	OPEN	OPEN
C-3	2.04	2.06	2.09	2.11	2.50	2.50	2.50	OPEN	2.50	2.50
D-5	OPEN	OPEN	OPEN	OPEN	OPEN	OPEN	OPEN	OPEN	OPEN	OPEN
E-5	1.50	1.50	1.50	1.50	1.50	1.51	1.51	1.51	1.51	1.50
F-5	1.32	1.32	1.31	1.31	1.32	1.33	1.33	1.33	1.33	1.32

Table F-3-5 Board # 7: 2100 cycles to 2720 cycles

Cycles	2146	2192	2241	2285	2333	2357	2436	2530	2627	2720
Board No.	# 7	# 7	# 7	# 7	# 7	# 7	# 7	# 7	# 7	# 7
A-1	OPEN	OPEN	OPEN	OPEN	OPEN	OPEN	OPEN	OPEN	OPEN	OPEN
B-1	OPEN	OPEN	OPEN	OPEN	OPEN	OPEN	OPEN	OPEN	OPEN	OPEN
C-1	OPEN	OPEN	OPEN	OPEN	OPEN	OPEN	OPEN	OPEN	OPEN	OPEN
D-3	OPEN	OPEN	OPEN	OPEN	OPEN	OPEN	OPEN	OPEN	OPEN	OPEN
E-3	1.96	1.97	1.98	1.95	1.95	1.96	1.98	1.96	1.97	1.96
F-3	1.79	1.80	1.81	1.79	1.79	1.79	1.81	1.79	1.80	1.79
D-1	OPEN	OPEN	OPEN	OPEN	OPEN	OPEN	OPEN	OPEN	OPEN	OPEN
E-1	2.52	2.53	2.56	2.53	2.53	2.54	2.55	2.56	2.56	2.57
F-1	2.31	2.33	2.33	2.30	2.32	2.31	2.31	2.31	2.33	2.42
A-4	OPEN	OPEN	OPEN	OPEN	OPEN	OPEN	OPEN	OPEN	OPEN	OPEN
B-4	OPEN	OPEN	OPEN	OPEN	OPEN	OPEN	OPEN	OPEN	OPEN	OPEN
C-4	OPEN	OPEN	OPEN	OPEN	OPEN	OPEN	OPEN	OPEN	OPEN	OPEN
A-2	OPEN	OPEN	OPEN	OPEN	OPEN	OPEN	OPEN	OPEN	OPEN	OPEN
B-2	OPEN	OPEN	OPEN	OPEN	OPEN	OPEN	OPEN	OPEN	OPEN	OPEN
C-2	OPEN	OPEN	OPEN	OPEN	OPEN	OPEN	OPEN	OPEN	OPEN	OPEN
D-4	OPEN	OPEN	OPEN	OPEN	OPEN	OPEN	OPEN	OPEN	OPEN	OPEN
E-4	1.83	1.84	1.84	1.82	1.82	1.83	1.85	1.85	1.93	1.95
F-4	1.61	1.61	1.61	1.60	1.60	1.60	1.61	1.60	1.61	1.60
D-2	OPEN	OPEN	OPEN	OPEN	OPEN	OPEN	OPEN	OPEN	OPEN	OPEN
E-2	2.23	2.25	2.24	2.22	2.22	2.23	2.23	2.27	2.24	2.23
F-2	2.03	2.04	2.03	2.02	2.03	2.02	2.04	2.02	2.03	2.03
A-5	OPEN	OPEN	OPEN	OPEN	OPEN	OPEN	OPEN	OPEN	OPEN	OPEN
B-5	OPEN	OPEN	OPEN	OPEN	OPEN	OPEN	OPEN	OPEN	OPEN	OPEN
C-5	2.49	2.49	OPEN	OPEN	OPEN	OPEN	OPEN	OPEN	OPEN	OPEN
A-3	OPEN	OPEN	OPEN	OPEN	OPEN	OPEN	OPEN	OPEN	OPEN	OPEN
B-3	OPEN	OPEN	OPEN	OPEN	OPEN	OPEN	OPEN	OPEN	OPEN	OPEN
C-3	2.50	2.50	OPEN	OPEN	OPEN	OPEN	OPEN	OPEN	OPEN	OPEN
D-5	OPEN	OPEN	OPEN	OPEN	OPEN	OPEN	OPEN	OPEN	OPEN	OPEN
E-5	1.50	1.51	1.51	1.50	1.49	1.50	1.50	1.50	1.50	1.50
F-5	1.32	1.33	1.33	1.31	1.31	1.32	1.32	1.32	1.32	1.32

Table F-3-6 Board # 7: 2720 cycles to 3003 cycles

Cycles	2816	2910	3003		
Board No.	# 7	# 7	# 7	10%	Failure Cycles
A-1	OPEN	OPEN	OPEN	2.959	267
B-1	OPEN	OPEN	OPEN	2.794	925
C-1	OPEN	OPEN	OPEN	2.596	1555
D-3	OPEN	OPEN	OPEN	2.365	1414
E-3	1.97	1.97	1.99	2.156	OK
F-3	1.81	1.80	1.82	1.969	OK
D-1	OPEN	OPEN	OPEN	2.893	737
E-1	2.62	OPEN	OPEN	2.728	2910
F-1	6.56	9.27	20.56	2.519	2816
A-4	OPEN	OPEN	OPEN	2.288	315
B-4	OPEN	OPEN	OPEN	2.079	1461
C-4	OPEN	OPEN	OPEN	1.87	1461
A-2	OPEN	OPEN	OPEN	2.761	315
B-2	OPEN	OPEN	OPEN	2.629	1294
C-2	OPEN	OPEN	OPEN	2.409	1555
D-4	OPEN	OPEN	OPEN	2.2	737
E-4	2.09	2.27	4.89	2.013	2910
F-4	1.62	1.61	1.63	1.76	OK
D-2	OPEN	OPEN	OPEN	2.618	691
E-2	2.25	2.27	2.30	2.442	OK
F-2	2.05	2.02	2.04	2.222	OK
A-5	OPEN	OPEN	OPEN	2.013	267
B-5	OPEN	OPEN	OPEN	1.804	1361
C-5	OPEN	OPEN	OPEN	1.573	2051
A-3	OPEN	OPEN	OPEN	2.541	168
B-3	OPEN	OPEN	OPEN	2.332	1511
C-3	OPEN	OPEN	OPEN	2.145	1767
D-5	OPEN	OPEN	OPEN	1.881	833
E-5	1.51	1.50	1.53	1.65	OK
F-5	1.33	1.33	1.36	1.441	OK

Note 1: 10% means the value of the loop resistance increased by 10 %.

Note 2: “Failure cycles” means the number of cycles at which the part was found to have more than 10% increase in the loop resistance; this was defined as an open circuit.

Note 3: “OK” means the increase of loop resistance of the part was still within 10 %.

Table F-4-1 Board # 8: 0 cycle to 549 cycles

Cycles	0	168	223	267	315	361	409	455	502	549
Board No.	# 8	# 8	# 8	# 8	# 8	# 8	# 8	# 8	# 8	# 8
A-1	3.01	2.10	2.60	73.30	OPEN	OPEN	OPEN	OPEN	OPEN	OPEN
B-1	2.78	2.29	2.46	2.60	2.42	2.51	2.24	2.43	2.45	2.43
C-1	2.57	2.04	1.90	2.20	1.95	2.00	1.91	1.97	1.97	2.07
D-3	2.38	2.33	2.32	2.16	2.23	2.16	2.25	2.16	2.16	2.22
E-3	2.14	2.31	2.30	2.27	2.25	2.29	2.27	2.26	2.27	2.31
F-3	1.94	2.26	2.25	2.23	2.21	2.23	2.22	2.21	2.22	2.24
D-1	2.86	1.97	2.11	2.55	2.49	2.42	2.52	2.37	2.11	2.35
E-1	2.66	2.18	2.36	2.52	2.38	2.39	2.48	2.36	2.32	2.38
F-1	2.46	1.95	1.82	2.15	1.86	2.12	2.29	1.92	1.84	1.97
A-4	2.27	2.22	2.21	2.03	2.13	3.84	60.00	OPEN	OPEN	OPEN
B-4	2.01	2.17	2.16	2.13	2.12	2.15	2.13	2.13	2.13	2.15
C-4	1.82	2.13	2.12	2.10	2.08	2.11	2.09	2.09	2.09	1.93
A-2	2.63	1.78	OPEN	OPEN	OPEN	OPEN	OPEN	OPEN	OPEN	OPEN
B-2	2.45	2.00	2.17	2.11	2.18	2.18	2.22	2.13	2.13	2.15
C-2	2.30	1.81	1.64	1.63	1.75	1.76	1.85	1.67	1.69	1.71
D-4	2.11	2.08	2.04	2.00	1.93	OPEN	OPEN	OPEN	OPEN	OPEN
E-4	1.85	2.02	1.98	1.95	1.94	1.96	1.95	1.94	1.95	1.98
F-4	1.65	1.96	1.93	1.89	1.88	1.91	1.89	1.89	1.89	1.91
D-2	2.46	1.54	2.03	2.01	1.98	2.02	2.07	1.98	1.62	1.63
E-2	2.26	1.74	1.91	1.86	1.91	1.93	1.98	1.89	1.88	1.88
F-2	2.10	1.55	1.38	1.45	1.68	1.51	1.60	1.44	1.44	1.46
A-5	1.89	1.80	OPEN	OPEN	OPEN	OPEN	OPEN	OPEN	OPEN	OPEN
B-5	1.65	1.77	1.74	1.71	1.70	1.72	1.71	1.71	1.71	1.73
C-5	1.53	1.78	1.76	1.73	1.72	1.74	1.72	1.72	1.73	1.75
A-3	2.35	24.30	26.50	62.50	51.70	65.50	53.40	64.00	60.00	60.00
B-3	2.12	1.55	1.75	1.76	1.84	1.76	1.82	1.77	1.73	1.75
C-3	1.94	-	-	-	-	-	-	-	-	-
D-5	1.74	1.59	1.55	1.85	1.20	1.36	2.22	1.50	1.50	1.52
E-5	1.54	1.60	1.58	1.55	1.54	1.56	1.55	1.55	1.55	1.57
F-5	1.39	1.58	1.56	1.53	1.52	1.54	1.53	1.53	1.53	1.55

Table F-4-2 Board # 8: 549 cycles to 1018 cycles

Cycles	597	643	691	737	784	833	877	925	968	1018
Board No.	# 8	# 8	# 8	# 8	# 8	# 8	# 8	# 8	# 8	# 8
A-1	OPEN	OPEN	OPEN	OPEN	OPEN	OPEN	OPEN	OPEN	OPEN	OPEN
B-1	2.46	2.43	2.44	2.81	2.81	2.82	2.83	2.79	2.80	2.81
C-1	1.97	1.97	1.97	2.59	2.59	2.60	2.61	2.57	2.58	2.59
D-3	2.22	2.17	2.15	2.41	2.41	2.42	OPEN	OPEN	OPEN	OPEN
E-3	2.28	2.28	2.29	2.16	2.16	2.17	2.18	2.15	2.16	2.17
F-3	2.23	2.23	2.24	1.96	1.96	1.96	1.98	1.94	1.95	1.96
D-1	2.40	OPEN	OPEN	OPEN	OPEN	OPEN	OPEN	OPEN	OPEN	OPEN
E-1	2.36	2.34	2.36	2.68	2.69	2.71	2.71	2.71	2.68	2.68
F-1	1.86	2.04	1.87	2.48	2.48	2.49	2.51	2.47	2.48	2.48
A-4	OPEN	OPEN	OPEN	OPEN	OPEN	OPEN	OPEN	OPEN	OPEN	OPEN
B-4	2.14	2.13	2.15	2.03	2.02	2.03	2.05	2.01	2.02	2.02
C-4	2.11	2.10	2.11	1.84	1.84	1.84	1.86	1.83	1.84	1.84
A-2	OPEN	OPEN	OPEN	OPEN	OPEN	OPEN	OPEN	OPEN	OPEN	OPEN
B-2	2.14	2.08	2.18	2.47	2.48	2.48	2.50	2.46	2.47	2.47
C-2	1.71	1.71	1.78	2.32	2.33	2.33	2.35	2.32	2.32	2.33
D-4	OPEN	OPEN	OPEN	OPEN	OPEN	OPEN	OPEN	OPEN	OPEN	OPEN
E-4	1.96	1.95	1.97	1.87	1.87	1.89	1.89	1.86	1.86	1.86
F-4	1.90	1.90	1.91	1.67	1.67	1.67	1.69	1.66	1.67	1.67
D-2	1.82	1.93	1.97	2.48	2.48	2.49	2.50	2.47	2.48	2.48
E-2	1.90	1.85	1.92	2.28	2.28	2.29	2.30	2.27	2.28	2.28
F-2	1.45	1.48	1.51	2.12	2.12	2.13	2.14	2.11	2.12	2.12
A-5	OPEN	OPEN	OPEN	OPEN	OPEN	OPEN	OPEN	OPEN	OPEN	OPEN
B-5	1.72	1.71	1.72	1.67	1.67	1.68	1.69	1.66	1.67	1.67
C-5	1.74	1.73	1.74	1.55	1.54	1.55	1.56	1.53	1.54	1.54
A-3	60.00	66.00	34.50	OPEN	OPEN	OPEN	OPEN	OPEN	OPEN	OPEN
B-3	1.74	1.69	1.87	2.14	2.15	2.15	2.17	2.14	2.15	2.14
C-3	-	-	-	1.95	1.97	1.98	2.00	2.00	2.06	2.36
D-5	1.51	1.51	1.69	1.75	1.76	1.76	218.70	60.90	OPEN	OPEN
E-5	1.56	1.56	1.57	1.56	1.56	1.57	1.58	1.55	1.56	1.56
F-5	1.54	1.53	1.55	1.40	1.41	1.41	1.42	1.39	1.40	1.40

Table F-4-3 Board # 8:1018 cycles to 1511 cycles

Cycles	1064	1113	1159	1205	1294	1340	1361	1414	1461	1511
Board No.	# 8	# 8	# 8	# 8	# 8	# 8	# 8	# 8	# 8	# 8
A-1	OPEN	OPEN	OPEN	OPEN	OPEN	OPEN	OPEN	OPEN	OPEN	OPEN
B-1	2.82	2.81	2.83	2.80	2.83	2.82	2.81	2.81	2.80	2.81
C-1	2.60	2.59	2.61	2.58	2.61	2.60	2.60	2.60	2.58	2.59
D-3	OPEN	OPEN	OPEN	OPEN	OPEN	OPEN	OPEN	OPEN	OPEN	OPEN
E-3	2.18	2.15	2.17	2.16	2.18	2.17	2.70	2.17	2.15	2.17
F-3	1.97	1.95	1.97	1.95	1.97	1.97	1.96	1.96	1.95	1.96
D-1	OPEN	OPEN	OPEN	OPEN	OPEN	OPEN	OPEN	OPEN	OPEN	OPEN
E-1	2.70	2.70	2.69	2.68	2.70	2.69	2.68	2.69	2.67	2.68
F-1	2.50	2.47	2.49	2.48	2.50	2.49	2.49	2.49	2.47	2.48
A-4	OPEN	OPEN	OPEN	OPEN	OPEN	OPEN	OPEN	OPEN	OPEN	OPEN
B-4	2.04	2.01	2.03	2.02	2.04	2.03	2.03	2.03	2.03	2.03
C-4	1.86	1.83	1.85	1.83	1.85	1.85	1.85	1.85	1.84	1.85
A-2	OPEN	OPEN	OPEN	OPEN	OPEN	OPEN	OPEN	OPEN	OPEN	OPEN
B-2	2.49	2.46	2.48	2.47	2.48	2.48	2.47	2.48	2.46	2.47
C-2	2.34	2.31	2.33	2.32	2.34	2.34	2.33	2.33	2.32	2.34
D-4	OPEN	OPEN	OPEN	OPEN	OPEN	OPEN	OPEN	OPEN	OPEN	OPEN
E-4	1.88	1.85	1.87	1.86	1.88	1.87	1.87	1.87	1.86	1.87
F-4	1.68	1.65	1.67	1.66	1.68	1.68	1.67	1.67	1.66	1.67
D-2	2.50	2.47	2.49	2.59	22.40	OPEN	OPEN	OPEN	OPEN	OPEN
E-2	2.29	2.27	2.29	2.28	2.30	2.29	2.28	2.28	2.27	2.28
F-2	2.13	2.11	2.13	2.11	2.13	2.13	2.12	2.12	2.11	2.12
A-5	OPEN	OPEN	OPEN	OPEN	OPEN	OPEN	OPEN	OPEN	OPEN	OPEN
B-5	1.69	1.66	1.68	1.66	1.68	1.68	1.67	1.67	1.67	1.68
C-5	1.56	1.53	1.55	1.54	1.56	1.56	1.55	1.56	1.56	1.58
A-3	OPEN	OPEN	OPEN	OPEN	OPEN	OPEN	OPEN	OPEN	OPEN	OPEN
B-3	2.16	2.13	2.15	2.14	2.16	2.16	2.15	2.15	2.14	2.15
C-3	2.48	3.60	3.81	4.23	10.50	15.30	14.59	OPEN	16.32	OPEN
D-5	OPEN	OPEN	OPEN	OPEN	OPEN	OPEN	OPEN	OPEN	OPEN	OPEN
E-5	1.58	1.55	1.57	1.56	1.57	1.57	1.56	1.56	1.56	1.57
F-5	1.42	1.39	1.41	1.40	1.41	1.41	1.40	1.40	1.40	1.41

Table F-4-4 Board # 8: 1511 cycles to 2100 cycles

Cycles	1555	1606	1652	1696	1767	1814	1909	1955	2051	2100
Board No.	# 8	# 8	# 8	# 8	# 8	# 8	# 8	# 8	# 8	# 8
A-1	OPEN	OPEN	OPEN	OPEN	OPEN	OPEN	OPEN	OPEN	OPEN	OPEN
B-1	2.79	2.79	2.78	2.78	2.79	2.80	2.82	2.78	2.80	2.79
C-1	2.57	2.80	2.57	2.56	2.58	2.59	2.61	2.57	2.59	2.58
D-3	OPEN	OPEN	OPEN	OPEN	OPEN	OPEN	OPEN	OPEN	OPEN	OPEN
E-3	2.15	2.16	2.14	2.14	2.15	2.16	2.18	2.14	2.15	2.15
F-3	1.94	1.95	1.94	1.94	1.95	1.96	1.98	1.94	1.95	1.94
D-1	OPEN	OPEN	OPEN	OPEN	OPEN	OPEN	OPEN	OPEN	OPEN	OPEN
E-1	2.66	2.67	2.66	2.65	2.67	2.67	2.69	2.66	2.67	2.66
F-1	2.47	2.47	2.46	2.45	2.47	2.48	2.49	2.46	2.47	2.46
A-4	OPEN	OPEN	OPEN	OPEN	OPEN	OPEN	OPEN	OPEN	OPEN	OPEN
B-4	2.01	2.01	2.01	2.00	2.01	2.02	2.04	2.01	2.01	2.01
C-4	1.84	1.85	1.86	1.89	2.31	OPEN	OPEN	OPEN	OPEN	OPEN
A-2	OPEN	OPEN	OPEN	OPEN	OPEN	OPEN	OPEN	OPEN	OPEN	OPEN
B-2	2.46	2.46	2.45	2.45	2.46	2.47	2.48	2.45	2.48	2.50
C-2	2.32	2.34	2.34	2.37	2.45	2.47	2.56	2.57	5.10	OPEN
D-4	OPEN	OPEN	OPEN	OPEN	OPEN	OPEN	OPEN	OPEN	OPEN	OPEN
E-4	1.85	1.85	1.85	1.84	1.86	1.86	1.88	1.85	1.86	1.85
F-4	1.65	1.66	1.65	1.65	1.66	1.67	1.68	1.65	1.66	1.65
D-2	OPEN	OPEN	OPEN	OPEN	OPEN	OPEN	OPEN	OPEN	OPEN	OPEN
E-2	2.27	2.27	2.26	2.26	2.27	2.28	2.29	2.26	2.31	2.26
F-2	2.10	2.11	2.10	2.10	2.11	2.12	2.13	2.10	2.15	2.10
A-5	OPEN	OPEN	OPEN	OPEN	OPEN	OPEN	OPEN	OPEN	OPEN	OPEN
B-5	1.66	1.66	1.66	1.65	1.67	1.67	1.69	1.66	1.70	1.66
C-5	1.58	1.70	1.84	3.33	4.37	8.10	OPEN	OPEN	OPEN	OPEN
A-3	OPEN	OPEN	OPEN	OPEN	OPEN	OPEN	OPEN	OPEN	OPEN	OPEN
B-3	2.13	2.14	2.13	2.13	2.14	2.15	2.18	2.17	2.29	2.33
C-3	OPEN	OPEN	OPEN	OPEN	OPEN	OPEN	OPEN	OPEN	OPEN	OPEN
D-5	OPEN	OPEN	OPEN	OPEN	OPEN	OPEN	OPEN	OPEN	OPEN	OPEN
E-5	1.55	1.55	1.54	1.54	1.55	1.56	1.57	1.55	1.59	1.55
F-5	1.39	1.39	1.38	1.38	1.40	1.40	1.42	1.39	1.43	1.39

Table F-4-5 Board # 8: 2100 cycles to 2720 cycles

Cycles	2146	2192	2241	2285	2333	2357	2436	2530	2627	2720
Board No.	# 8	# 8	# 8	# 8	# 8	# 8	# 8	# 8	# 8	# 8
A-1	OPEN	OPEN	OPEN	OPEN	OPEN	OPEN	OPEN	OPEN	OPEN	OPEN
B-1	2.78	2.79	2.79	2.77	2.78	2.79	2.79	2.78	2.79	2.78
C-1	2.58	2.59	2.61	2.71	2.86	4.35	4.44	5.02	OPEN	3.34
D-3	OPEN	OPEN	OPEN	OPEN	OPEN	OPEN	OPEN	OPEN	OPEN	OPEN
E-3	2.14	2.15	2.15	2.14	2.14	2.15	2.15	2.14	2.15	2.14
F-3	1.94	1.95	1.95	1.94	1.94	1.95	1.95	1.94	1.95	1.94
D-1	OPEN	OPEN	OPEN	OPEN	OPEN	OPEN	OPEN	OPEN	OPEN	OPEN
E-1	2.66	2.66	2.67	2.65	2.65	2.67	2.66	2.66	2.66	2.66
F-1	2.46	2.47	2.47	2.45	2.46	2.47	2.47	2.46	2.47	2.46
A-4	OPEN	OPEN	OPEN	OPEN	OPEN	OPEN	OPEN	OPEN	OPEN	OPEN
B-4	2.01	2.01	2.01	2.00	2.00	2.01	2.01	2.01	2.01	2.01
C-4	2.79	6.67	2.78	4.58	3.65	OPEN	7.45	14.53	OPEN	OPEN
A-2	OPEN	OPEN	OPEN	OPEN	OPEN	OPEN	OPEN	OPEN	OPEN	OPEN
B-2	2.54	2.60	2.64	2.65	2.68	OPEN	OPEN	OPEN	OPEN	OPEN
C-2	6.81	7.36	8.42	OPEN	OPEN	OPEN	OPEN	OPEN	OPEN	OPEN
D-4	OPEN	OPEN	OPEN	OPEN	OPEN	OPEN	OPEN	OPEN	OPEN	OPEN
E-4	1.85	1.85	1.85	1.84	1.84	1.85	1.85	1.85	1.85	1.85
F-4	1.65	1.66	1.66	1.65	1.65	1.65	1.66	1.65	1.65	1.65
D-2	OPEN	OPEN	OPEN	OPEN	OPEN	OPEN	OPEN	OPEN	OPEN	OPEN
E-2	2.26	2.27	2.27	2.26	2.25	2.27	2.26	2.26	2.26	2.26
F-2	2.10	2.11	2.11	2.10	2.09	2.11	2.11	2.10	2.10	2.10
A-5	OPEN	OPEN	OPEN	OPEN	OPEN	OPEN	OPEN	OPEN	OPEN	OPEN
B-5	1.66	1.67	1.68	1.67	1.67	1.71	OPEN	OPEN	OPEN	OPEN
C-5	OPEN	OPEN	OPEN	OPEN	OPEN	OPEN	OPEN	OPEN	OPEN	OPEN
A-3	OPEN	OPEN	OPEN	OPEN	OPEN	OPEN	OPEN	OPEN	OPEN	OPEN
B-3	2.42	2.50	2.60	2.72	OPEN	21.20	22.90	22.90	22.90	22.90
C-3	OPEN	OPEN	OPEN	OPEN	OPEN	OPEN	OPEN	OPEN	OPEN	OPEN
D-5	OPEN	OPEN	OPEN	OPEN	OPEN	OPEN	OPEN	OPEN	OPEN	OPEN
E-5	1.55	1.55	1.55	1.54	1.54	1.55	1.55	1.55	1.55	1.55
F-5	1.39	1.39	1.40	1.38	1.38	1.39	1.39	1.39	1.39	1.39

Table F-4-6 Board # 8: 2720 cycles to 3003 cycles

Cycles	2816	2910	3003		
Board No.	# 8	# 8	# 8	10%	Failure Cycles
A-1	OPEN	OPEN	OPEN	3.311	267
B-1	2.81	2.80	2.85	3.058	OK
C-1	18.54	18.54	18.54	2.827	2333
D-3	OPEN	OPEN	OPEN	2.618	877
E-3	2.15	2.14	2.16	2.354	OK
F-3	1.95	1.94	1.96	2.134	OK
D-1	OPEN	OPEN	OPEN	3.146	643
E-1	2.67	2.66	2.68	2.926	OK
F-1	2.47	2.46	2.48	2.706	OK
A-4	OPEN	OPEN	OPEN	2.497	361
B-4	2.02	2.02	2.04	2.211	OK
C-4	OPEN	OPEN	OPEN	2.002	1767
A-2	OPEN	OPEN	OPEN	2.893	223
B-2	OPEN	OPEN	OPEN	2.695	2357
C-2	OPEN	OPEN	OPEN	2.53	1909
D-4	OPEN	OPEN	OPEN	2.321	361
E-4	1.86	1.85	1.86	2.035	OK
F-4	1.66	1.65	1.67	1.815	OK
D-2	OPEN	OPEN	OPEN	2.706	1294
E-2	2.27	2.26	2.28	2.486	OK
F-2	2.11	2.10	2.12	2.31	OK
A-5	OPEN	OPEN	OPEN	2.079	223
B-5	OPEN	OPEN	OPEN	1.815	2436
C-5	OPEN	OPEN	OPEN	1.683	1606
A-3	OPEN	OPEN	OPEN	2.585	168
B-3	22.90	22.90	22.90	2.332	2146
C-3	OPEN	OPEN	OPEN	2.134	1018
D-5	OPEN	OPEN	OPEN	1.914	877
E-5	1.55	1.55	1.57	1.694	OK
F-5	1.39	1.39	1.41	1.529	OK

Note 1: 10% means the value of the loop resistance increased by 10 %.

Note 2: “Failure cycles” means the number of cycles at which the part was found to have more than 10% increase in the loop resistance; this was defined as an open circuit.

Note 3: “OK” means the increase of loop resistance of the part was still within 10 %.

APPENDIX G

Calculation of Weibull Distribution

The x-axis and y-axis of Weibull distribution are failure cycles (life) and cumulative percent failed, respectively. The detailed data points of Weibull distribution, shape parameter, and characteristic life for designs A, B, C, D, E and F are shown in Table G-1, G-2, G-3, G-4, G-5 and G-6, respectively.

$$F(t) = 1 - \exp[-(t/\alpha)^\beta] \dots \text{Weibull Distribution Function}$$

$$\ln [1-F(t)] = - (t/\alpha)^\beta$$

$$\ln \{- \ln [1-F(t)]\} = \beta \ln(t) - \beta \ln(\alpha)$$

Compare with $Y = mX + q$

$$\rightarrow m = \beta \quad \rightarrow q = - \beta \ln(\alpha) \quad \rightarrow \alpha = \exp[q/(-\beta)]$$

β : Shape parameter (Weibull slope)

α : Characteristic life ($F(\alpha) = 62.3\%$)

Table G-1 Design A

Failure Time	Failure Count	Median Rank	Weibull Transformation	ln(Weibull Trans)	ln(Cycle)
168	3	0.132	0.142	-1.952	5.124
223	6	0.279	0.328	-1.116	5.407
267	9	0.426	0.556	-0.587	5.587
315	11	0.525	0.743	-0.297	5.753
361	12	0.574	0.852	-0.160	5.889
409	14	0.672	1.113	0.107	6.014
455	16	0.770	1.468	0.384	6.120
502	19	0.917	2.485	0.910	6.219
549	20	0.966	3.372	1.216	6.308

$$y = 2.465x - 14.523$$

$$\beta : 2.465$$

$$\alpha : 362$$

$$R^2 : 0.977$$

Table G-2 Design B

Failure Time	Failure Count	Median Rank	Weibull Transformation	ln(Weibull Trans)	ln(Cycle)
925	1	0.036	0.037	-3.304	6.830
1294	3	0.139	0.150	-1.898	7.165
1361	5	0.242	0.277	-1.282	7.216
1461	7	0.345	0.424	-0.859	7.287
1511	8	0.397	0.506	-0.682	7.321
1652	9	0.448	0.595	-0.519	7.410
2146	10	0.500	0.693	-0.367	7.671
2357	11	0.552	0.802	-0.221	7.765
2436	12	0.603	0.924	-0.079	7.798
2720	13	0.655	1.063	0.061	7.908
2816	14	0.706	1.225	0.203	7.943

$$y = 2.652x - 20.622$$

β : 2.652
 α : 2383
 R^2 : 0.848

Table G-3 Design C

Failure Time	Failure Count	Median Rank	Weibull Transformation	ln(Weibull Trans)	ln(Cycle)
1018	1	0.034	0.035	-3.355	6.926
1113	2	0.083	0.087	-2.442	7.015
1159	3	0.132	0.142	-1.952	7.055
1205	4	0.181	0.200	-1.609	7.094
1461	5	0.230	0.262	-1.340	7.287
1511	6	0.279	0.328	-1.116	7.321
1555	8	0.377	0.474	-0.747	7.349
1606	9	0.426	0.556	-0.587	7.382
1767	11	0.525	0.743	-0.297	7.477
1909	13	0.623	0.974	-0.026	7.554
2051	15	0.721	1.275	0.243	7.626
2146	16	0.770	1.468	0.384	7.671
2333	17	0.819	1.707	0.535	7.755
2436	18	0.868	2.022	0.704	7.798
2627	19	0.917	2.485	0.910	7.874
2720	20	0.966	3.372	1.216	7.908

$$y = 4.033x - 30.609$$

β : 4.033
 α : 1978
 R^2 : 0.963

Table G-4 Design D

Failure Time	Failure Count	Median Rank	Weibull Transformation	ln(Weibull Trans)	ln(Cycle)
361	1	0.034	0.035	-3.355	5.889
502	3	0.132	0.142	-1.952	6.219
549	4	0.181	0.200	-1.609	6.308
643	5	0.230	0.262	-1.340	6.466
691	6	0.279	0.328	-1.116	6.538
737	8	0.377	0.474	-0.747	6.603
833	9	0.426	0.556	-0.587	6.725
877	11	0.525	0.743	-0.297	6.777
925	13	0.623	0.974	-0.026	6.830
1064	14	0.672	1.113	0.107	6.970
1205	15	0.721	1.275	0.243	7.094
1294	17	0.819	1.707	0.535	7.165
1414	19	0.917	2.485	0.910	7.254
1652	20	0.966	3.372	1.216	7.410

$$y = 2.841x - 19.699$$

$$\begin{aligned} \beta &: 2.841 \\ \alpha &: 1026 \\ R^2 &: 0.980 \end{aligned}$$

Table G-5 Design E

Failure Time	Failure Count	Median Rank	Weibull Transformation	ln(Weibull Trans)	ln(Cycle)
1955	1	0.034	0.035	-3.355	7.578
2357	2	0.083	0.087	-2.442	7.765
2910	5	0.230	0.262	-1.340	7.976

$$y = 5.069 - 41.781$$

$$\begin{aligned} \beta &: 5.069 \\ \alpha &: 3799 \\ R^2 &: 1.000 \end{aligned}$$

Table G-6 Design F

Failure Time	Failure Count	Median Rank	Weibull Transformation	Ln(Weibull Trans)	Ln(Cycle)
2816	1	0.034	0.035	-3.355	7.943